

การสังเคราะห์และพิสูจน์เอกลักษณ์ของโครงโลหะ-อินทรีย์ฐาน 1,3-แอลเทอร์เนตคาลิกซ์[4]เอรีน

นายศุภชัย กระจ่างศรี

วิทยานิพนธ์นี้เป็นส่วนหนึ่งของการศึกษาตามหลักสูตรปริญญาวิทยาศาสตรมหาบัณฑิต

สาขาวิชาเคมี ภาควิชาเคมี

คณะวิทยาศาสตร์ จุฬาลงกรณ์มหาวิทยาลัย

ปีการศึกษา 2555

ลิขสิทธิ์ของจุฬาลงกรณ์มหาวิทยาลัย

บทคัดย่อและเพิ่มข้อมูลฉบับเต็มของวิทยานิพนธ์ตั้งแต่ปีการศึกษา 2554 ที่ให้บริการในคลังปัญญาจุฬาฯ (CUIR)

เป็นเพิ่มข้อมูลของนิสิตเจ้าของวิทยานิพนธ์ที่ส่งผ่านทางบัณฑิตวิทยาลัย

The abstract and full text of theses from the academic year 2011 in Chulalongkorn University Intellectual Repository (CUIR) are the thesis authors' files submitted through the Graduate School.

SYNTHESIS AND CHARACTERIZATION OF 1,3-ALTERNATE  
CALIX[4]ARENE-BASED METAL-ORGANIC FRAMEWORKS

Mr. Suppachai Krajangsri

A Thesis Submitted in Partial Fulfillment of the Requirements  
for the Degree of Master of Science in Chemistry

Department of Chemistry

Faculty of Science

Chulalongkorn University

Academic Year 2012

Copyright of Chulalongkorn University

Thesis Title                   SYNTHESIS AND CHARACTERIZATION OF 1,3-  
ALTERNATE CALIX[4]ARENE-BASED METAL-  
ORGANIC FRAMEWORKS

By                               Mr. Suppachai Krajangsri

Field of Study                Chemistry

Thesis Advisor               Associate Professor Buncha Pulpoka, Ph.D.

---

Accepted by the Faculty of Science, Chulalongkorn University in  
Partial Fulfillment of the Requirements for the Master's Degree

..... Dean of the Faculty of  
Science  
(Professor Supot Hannongbua, Dr.rer.nat.)

#### THESIS COMMITTEE

.....Chairman  
(Assistant Professor Warinthorn Chavasiri, Ph.D.)

.....Thesis Advisor  
(Associate Professor Buncha Pulpoka, Ph.D.)

.....Examiner  
(Associate Professor Nuanphun Chantarasiri, Ph.D.)

.....Examiner  
(Associate Professor Nongnuj Muangsin, Ph.D.)

.....External Examiner  
(Assistant Professor Apirat Laobuthee, Ph.D.)

ศุภชัย กระจ่างศรี: การสังเคราะห์และพิสูจน์เอกลักษณ์ของโครง โลหะ-อินทรีย์ฐาน 1,3-แอลเทอร์เนตคาลิกซ์ [4]เอรีน. (SYNTHESIS AND CHARACTERIZATION OF 1,3-ALTERNATE CALIX[4]ARENE-BASED METAL-ORGANIC FRAMEWORKS) อ. ที่ปรึกษาวิทยานิพนธ์หลัก: รศ. ดร. บัญชา พูลโกศา, 129 หน้า.

ในงานวิจัยนี้เป็นการสังเคราะห์อนุพันธ์ 1,3-อัลเทอร์เนตคาลิกซ์ [4]เอรีน เพื่อนำไปใช้เป็นสารเชื่อมอินทรีย์ในการสังเคราะห์โครงโลหะ-อินทรีย์ ได้แก่ 1,3-alternate calix[4]arene tetra-*p*-benzoic acid (3A) และ 1,3-alternate calix[4]arene tetra-*m*-benzoic acid (3B) ที่เป็นไอโซเมอร์เชิงโครงสร้างกัน โดยมีหมู่คาร์บอกซิลอยู่ที่ตำแหน่งพาราและเมตา ตามลำดับ สารเชื่อมอินทรีย์ 3A และ 3B ถูกสังเคราะห์ผ่าน 3 ขั้นตอน ด้ ร้อยละผลิตภัณฑ์โดยรวมเป็น 38 เปอร์เซ็นต์ และ 34 เปอร์เซ็นต์ตามลำดับ เมื่อนำสารเชื่อมอินทรีย์ที่สังเคราะห์ได้ไปใช้สังเคราะห์โครงโลหะ-อินทรีย์ กับไอออนโลหะชนิดต่างๆ ในตัวทำละลายไดเมทิลฟอรัมาไมด์ ด้วยวิธีสังเคราะห์แบบโซลโวเทอร์มัล แล้วได้ทำการพิสูจน์เอกลักษณ์และทดสอบสมบัติในการดูดซับแก๊สของโครงโลหะ-อินทรีย์ฐาน 1,3-อัลเทอร์เนตคาลิกซ์[4]เอรีนที่สังเคราะห์ได้ จากการพิสูจน์ทราบด้านสัณฐานวิทยาของโครงโลหะ-อินทรีย์ที่พบว่าโครงโลหะ-อินทรีย์นี้มีขนาดอนุภาคในช่วงไมครอน มีหลายรูปร่าง เช่น ทรงรูปเข็ม ลูกบาศก์ เก็ดและแผ่น ไอโซเทอร์มของการดูดซับแก๊สไนโตรเจนเป็นแบบที่ 3 ซึ่งแสดงให้เห็นว่าวัสดุนี้ไม่มีรูพรุนและมีพื้นที่ผิวน้อย ทั้งนี้อาจเป็นเพราะโครงสร้างของ สารเชื่อมอินทรีย์มีขนาดที่ใหญ่อาจจะทำให้ไม่เกิดโพรงที่มีลักษณะเชื่อมต่อกัน เมื่อนำผลึกเดี่ยวของโครงโลหะ-อินทรีย์ฐาน 1,3-อัลเทอร์เนตคาลิกซ์[4]เอรีนที่เตรียมได้มาวิเคราะห์ด้วยเทคนิค sc-XRD ของผลึกเดี่ยวพบว่าโครงโลหะ-อินทรีย์ที่สังเคราะห์จากสารเชื่อมอินทรีย์ 3A และไอออนซิงค์ (II) ได้โครงสร้างสามมิติที่เกิดจากการจัดเรียงตัวของสายโคออดิเนชันพอลิเมอร์แบบใช้ตรง ในกรณีของโครงโลหะ-อินทรีย์ที่สังเคราะห์จาก 3B และไอออนซิงค์(II) การเกิดพันธะระหว่างสารเชื่อมอินทรีย์และไอออนโลหะนี้เกิดเป็นสายโซ่พอลิเมอร์แบบซิกแซกและสายโซ่จัดเรียงตัวได้เป็นโครงสร้างสามมิติเช่นกัน นอกจากนี้โครงโลหะ-อินทรีย์ที่เตรียมจากลิแกนด์ 3B และไอออนแคดเมียม (II) พบว่าเกิดผลึกเดี่ยวที่มีโครงสร้างต่างกันสองแบบ โดยมียูนิตเซลล์เป็น โมโนคลินิก และออร์โธโรมบิกและทั้งสองตัวเป็นโครงสร้างสามมิติ นอกจากสมบัติในการดูดซับแก๊สแล้ว ยังได้ทดสอบสมบัติตัวเร่งปฏิกิริยาสำหรับปฏิกิริยาฟรีเดล-คราฟต์เบื้องต้นของโครงโลหะ-อินทรีย์ที่สังเคราะห์จากสารอนุพันธ์ 1,3-อัลเทอร์เนตคาลิกซ์ [4]เอรีนซึ่งพบว่าโครงโลหะ-อินทรีย์ไม่เหมาะสมที่จะนำมาใช้กับปฏิกิริยาดังกล่าว

สาขาวิชา..เคมี.....ลายมือชื่อ.....  
 สาขาวิชา ..เคมี.....ลายมือชื่อ.....  
 ปีการศึกษา.....2555.....

## 5372475023: MAJOR CHEMISTRY

KEYWORDS: 1,3-ALTERNATE CALIX[4]ARENE/ METAL-ORGANIC FRAMEWORKS

SUPPACHAIKRAJANGSRI: SYNTHESIS AND CHARACTERIZATION OF 1,3-ALTERNATE CALIX[4]ARENE-BASED METAL-ORGANIC FRAMEWORKS. ADVISOR: ASSOC. PROF. BUNCHA PULPOKA, Ph.D., 129 pp.

This research involves the syntheses of 1,3-alternate calix[4]arene derivatives to use as organic linkers in the construction of calix[4]arene-based metal-organic frameworks (MOFs). These organic linkers, 1,3-alternate calix[4]arene tetra-*p*-benzoic acid (**3A**) and 1,3-alternate calix[4]arene tetra-*m*-benzoic acid (**3B**) are structural isomers which the carboxylic acid groups are at *para* and *meta* positions of phenyl substituent units, respectively. Each of organic linkers was synthesized in 3 steps with total yields of 38 % for **3A** and 34 % for **3B**. The obtained organic linkers were employed in synthesis of metal-organic frameworks with various metal ions in dimethylformamide solvent by solvothermal syntheses methods in various containers; round-bottom flask, sealed tube, auto clave and the obtained 1,3-alternate calix[4]arene-based MOFs were investigated their morphologies and gas adsorption properties for the potential use in gas storage. Morphologies of obtained MOFs as micro-particles of MOFs were found in various forms, such as needle-like, cubic, rod and platelet shapes. The nitrogen adsorption-desorption isotherms featured as type III adsorption isotherm which was typical for nonporous materials. Fortunately, the single-crystals of both organic linkers and 1,3-alternate calix[4]arene-based MOFs were obtained which have been characterized by sc-XRD technique. The single-crystal structures of MOF prepared by using **3A** and Zn(II) ion (named, **CU-SCRU1**) exhibited as three dimension structure *via* the arrangement of the polymeric coordinated linear chain. In the case of MOF that synthesized by using **3B** and Zn(II) ion (named, **CU-SCRU2**), the coordinated bond between organic linker, **3B** and Zn(II) ion formed to be a zig-zag polymeric chain and extended by intermolecular interaction to provide the three dimension frameworks. Moreover, in the reaction of **3B** and Cd(II) ion yielded two different single-crystal structures. Their single-crystal X-ray diffraction study revealed that they were three dimensional framework, crystallizing in monoclinic (named, **CU-SCRU3**) and orthrorombic (named, **CU-SCRU4**). Apart from their gas adsorption property of 1,3-alternate calix[4]arene-based MOFs, their catalytic property were preliminary investigated but it was revealed that they were not suitable for using as catalyzing in Friedel-Craft alkylation reaction.

Program :.....CHEMISTRY .....Student's Signature.....

Field of Study :....CHEMISTRY .....Advisor's Signature.....

Academic Year :.....2012.....

## ACKNOWLEDGEMENTS

I would like to express appreciation to my thesis advisor, Associate Professor Buncha Pulpoka, for the generous encouragement, help and provision to work and study in his laboratory. I would like to thank Assistant Professor Dr. Warinthorn Chavasiri, for serving as the chairman, Associate Professor Dr. Nuanphan Chantarasiri, Associate Professor Dr. Nongnuj Muangsin and Associate Professor Dr. Apirat Laobuthee for serving as the members of my thesis committee. respectively, for their valuable suggestion and comments. Furthermore, I am grateful to Associate Professor Dr. Nongnuj Muangsin for teaching to determine X-ray crystal structure of my synthesized compound.

I would like to thank The National Center of Excellence for Petroleum, Petrochemicals and Advanced Materials (NCE-PPAM) for partial financial support.

I also thank Professor Dr. Thawatchai Tuntulani and Supramolecular Chemistry Research Unit (SCRU), for warm welcome into their family, great experience and laboratory facilities.

I would like to thank my family for their love, encouragement, and financial support throughout my life. Finally, I would like to thank my friends, especially Salinthip Laokroekkiat, Nutthaporn Labeung, Preecha Thiampunya, Preeyanut Duanglaor and Yanisa Sanguantap for their love, understanding and great encouragement the entire course of my study.

# CONTENTS

	<b>Page</b>
<b>ABSTRACT (THAI)</b> .....	iv
<b>ABSTRACT (ENGLISH)</b> .....	v
<b>ACKNOWLEDGEMENTS</b> .....	vi
<b>CONTENTS</b> .....	vii
<b>LIST OF TABLES</b> .....	xi
<b>LIST OF FIGURES</b> .....	xii
<b>LIST OF SCHEMES</b> .....	xvii
<b>LIST OF ABBREVIATIONS</b> .....	xix
<b>CHAPTER I INTRODUCTION</b> .....	1
1.1 Objectives.....	2
1.2 Scope of Research.....	3
<b>CHAPTER II BACKGROUND AND LITERATURE REVIEWS</b> .....	4
2.1 An overview of metal-organic frameworks.....	4
2.2 Factors influencing on topologies and properties of metal-organic frameworks.....	4
2.2.1 Metal centers.....	5
2.2.1.1 Single metal ions.....	5
2.2.1.2 Secondary building units.....	6
2.2.2 Organic linkers.....	9
2.2.2.1 Carboxylate organic linkers.....	9
2.2.2.2 N-donor organic linkers.....	11
2.3 The effect of reaction condition on the topologies and properties of metal-organic frameworks.....	14
2.3.1 Counter anions of metal salt.....	15
2.3.2 Concentration.....	16
2.3.3 Metal-ligand ratio.....	17
2.3.4 Solvents.....	18

	<b>Page</b>
2.3.5 Temperature.....	19
2.3.6 pHs.....	20
2.4 Synthetic methods of metal-organic frameworks.....	20
2.4.1 Hydrothermal/solvothermal synthesis.....	20
2.4.2 Ionothermal synthesis .....	21
2.4.3 Microwave assisted-MOFs synthesis.....	22
2.4.4 Mechanochemical synthesis.....	23
2.5 Post-Synthetic Modification.....	24
2.6 Characterization and properties study of MOFs.....	26
2.6.1 Single-crystal X-ray diffraction (sc-XRD).....	27
2.6.2 Powder X-ray diffraction (PXRD).....	27
2.6.3 Scanning electron microscopy (SEM).....	28
2.6.4 Fourier Transform Infrared Spectroscopy (FT-IR).....	29
2.6.5 Nitrogen adsorption-desorption.....	29
2.6.6 Elemental analysis (EA).....	31
2.6.7 Thermogravimetric Analysis (TGA).....	31
2.7 Applications of metal-organic frameworks.....	32
2.8 Calix[4]arene-Based Organic linkers.....	33
<b>CHAPTER III EXPERIMENTAL</b> .....	<b>36</b>
3.1 Analytical Instruments.....	36
3.2 Experimental Procedure.....	38
3.2.1 Synthesis of Organic linkers.....	38
3.2.1.1 Synthesis of 1,3-alternate calix[4]arene tetra- <i>p</i> - benzoic acid ( <b>3A</b> ).....	38
3.2.1.1.1 Synthesis of 1,3-dimethyl- <i>p</i> -benzoate calix[4]arene ( <b>1A</b> ).....	39
3.2.1.1.2 Synthesis of 1,3-alternate calix[4]arene tetra methyl- <i>p</i> -benzoate ( <b>2A</b> ).....	40



	<b>Page</b>
3.2.1.1.3 Synthesis of 1,3-alternate calix[4]arene tetra- <i>p</i> -benzoic acid ( <b>3A</b> ).....	41
3.2.1.2 Synthesis of 1,3-alternate calix[4]arene tetra- <i>m</i> -benzoic acid ( <b>3B</b> ).....	42
3.2.2.2.1 Synthesis of 1,3-dimethyl- <i>m</i> -benzoate calix[4]-arene ( <b>1B</b> ).....	43
3.2.2.2.2 Synthesis of 1,3-alternate calix[4]arene tetramethyl- <i>m</i> -benzoate ( <b>2B</b> ).....	44
3.2.2.2.3 Synthesis of 1,3-alternate calix[4]arene tetra- <i>m</i> -benzoic acid ( <b>3B</b> ).....	45
3.2.2 Synthesis of Metal Organic Frameworks.....	46
3.2.3 Catalytic study.....	56
<b>CHAPTER IV RESULTS AND DISCUSSION</b> .....	58
4.1 Synthesis of Organic linkers.....	58
4.1.1 Synthesis of 1,3-alternate calix[4]arene tetra- <i>p</i> -benzoic acid ( <b>3A</b> ).....	58
4.1.2 Synthesis of 1,3-alternate calix[4]arene tetra- <i>m</i> -benzoic acid ( <b>3B</b> ).....	59
4.2 Synthesis of 1,3-alternate calyx[4]arene-based MOFs using 1,3-alternate calix[4]arene tetrabenzoic acid derivatives as organic linkers.....	61
4.2.1 Preparation using conventional heating method .....	61
4.2.1.1 IR spectroscopic study.....	61
4.2.1.2 XRD study.....	62
4.2.1.3 SEM study.....	66
4.2.1.4 Thermal stability.....	69
4.2.1.5 Nitrogen Adsorption-Desorption study.....	70
4.2.2 Preparation of MOFs via solvothermal in seal vials and auto-clave.....	74
4.2.2.1 Crystal structure of <b>CU-SCRUI</b> .....	75

	<b>Page</b>
4.2.2.2 Crystal structure of <b>CU-SCRU2</b> .....	78
4.2.2.3 Crystal structure of <b>CU-SCRU3</b> and <b>CU-SCRU4</b> .....	81
4.3 Study of catalytic activities .....	91
<b>CHAPTER V CONCLUSION</b> .....	93
<b>REFERENCES</b> .....	95
<b>APPENDICES</b> .....	105
Appendix A.....	106
Appendix B.....	122
<b>VITA</b> .....	129

## LIST OF TABLES

Table		Page
2.1	IUPAC classification of pores.....	30
3.1	Code of 1,3-alternate calix[4]arene-based MOFs via conventional heating.....	46
3.2	Effects of metal salts and the solvents in synthesis <b>3A-Zn MOF</b> .....	53
3.3	Syntheses of metal-organic frameworks by using <b>3A</b> with various metal ions.....	54
3.4	Syntheses of metal-organic frameworks by using <b>3B</b> with various metal ions.....	55
3.5	Effects of the ratio between <b>3B</b> and Cd <sup>2+</sup> .....	56
3.6	Optimize condition of the Friedel-Crafts alkylation.....	57
4.1	SEM images of synthesized MOFs and particle size.....	67
4.2	Textural properties of synthesized MOFs with pretreatment temperature at 250 °C.....	71
4.3	Crystallographic Data for <b>CU-SCRU1</b> and <b>CU-SCRU2</b> .....	76
4.4	Crystallographic Data for <b>CU-SCRU3</b> and <b>CU-SCRU4</b> .....	82
4.5	Optimize condition of the Friedel-craft alkylation reaction.....	91
B-1	Crystal data and structure refinement for compound <b>2B</b> .....	123
B-2	Crystal data and structure refinement for compound <b>3A</b> .....	124
B-3	Selected Bond Lengths (Å) and Bond Angles (deg) for <b>CU-SCRU1</b> and <b>CU-SCRU2</b> .....	125
B-4	Selected Bond Lengths (Å) and Bond Angles (deg) for <b>CU-SCRU3</b> ..	126
B-5	Selected Bond Lengths (Å) and Bond Angles (deg) for <b>CU-SCRU4</b> ..	127

## LIST OF FIGURES

Figure	Page
1.1	1,3-alternate tetrabenzoic acid calix[4]arene derivatives..... 3
2.1	The approach for design of networks base upon the geometry of metal node..... 5
2.2	The example of SBUs ..... 7
2.3	(a) $[\text{Zn}_4\text{O}]^{6+}$ SBUs, the carboxylic acid used in the synthesis of (b) MOF-5 and (c) MOF-177, the structures of (d) MOF-5 and (e) MOF-177..... 7
2.4	Crystal structure of HKUST-1. Green, gray, and red spheres represent Cu, C, and O atoms, respectively; H atoms are omitted for clarity..... 8
2.5	Coordination modes of carboxylate organic linkers. (a) monodentate, (b) chelating bidentate, (c) bidentate, (d) bridging bidentate..... 10
2.6	Some of carboxylate ligands used in the synthesis MOFs..... 10
2.7	Isorecticular metal-organic frameworks are composed of $[\text{Zn}_4\text{O}]^{6+}$ SBUs and linear dicarboxylate organic linkers..... 11
2.8	Some of pyridyl ligands used in the synthesis MOFs..... 12
2.9	Comparison of pKa values with the metal-ligand bond strength..... 13
2.10	(a) Coordination environment of Cd(II) ion which is in an octahedral coordination geometry; (b) Overall 2D structure of $\text{Cd}(\text{L}^2)_2(\text{NO}_3)_2(\text{H}_2\text{O})_2$ ..... 15
2.11	(a) Coordination environment of Cd(II) ion which is in the octahedral coordination geometry; (b) Overall 2D structure of $\{[\text{Cd}(\text{L}^2)_2(\text{H}_2\text{O})_2].(\text{ClO}_4)_2\}_\infty$ ..... 16
2.12	Doubly interpenetrated network of IRMOF-15 $[\text{Zn}_4\text{O}(\text{tpdc})_3]$ (tpdc = pterphenyl-4,4'-dicarboxylate)..... 17
2.13	(a) A Teflon-lined stainless steel autoclave. (b) Setting of autoclave..... 21

<b>Figure</b>	<b>Page</b>
2.14 (a) Coordination spheres of zinc atoms, (b) 3-D framework of the [Zn <sub>4</sub> (BTC) <sub>2</sub> (μ <sub>4</sub> -O)(H <sub>2</sub> O) <sub>2</sub> ] compound.....	22
2.15 Ball mill: stainless steel vessel with a ball bearing.....	23
2.16 (a) single-crystal X-ray diffractometer (b) An example single-crystal of MOFs (c) The single-crystal structure of MOFs.....	27
2.17 Powder XRD pattern of the fresh (a) and reused (b) MOF-199.....	28
2.18 SEM image of MOF-5 was prepared from microwave-assisted method.....	28
2.19 Example of compared IR spectra of carboxylate organic linker (a) and MOFs-based carboxylate.....	29
2.20 Six types of adsorption isotherm.....	30
2.21 An example thermogram of MOF-5.....	31
2.22 Conformations of calix[4]arene.....	34
2.23 (a) A <i>p</i> -tert-butyl-calix[4]arene-1,3-diacid ( <b>H<sub>4</sub>L</b> ) (b) The proposed structure of complex between <b>H<sub>4</sub>L</b> and Cu <sup>2+</sup> ion.....	34
4.1 Crystal structure of 1,3-alternate calix[4]arene tetra- <i>p</i> -benzoic acid ( <b>3A</b> )...	60
4.2 Crystal structure of 1,3-alternate calix[4]arene tetramethyl- <i>m</i> -benzoate ( <b>2B</b> ).....	60
4.3 The distance of H-bond in the organic linker ( <b>3A</b> ).....	61
4.4 Compared IR spectra of <b>3A</b> , MOFs <b>M1</b> ( <b>3A</b> + Zn(NO <sub>3</sub> ) <sub>2</sub> ), <b>M2</b> ( <b>3A</b> + Zn(OAc)) and <b>M3</b> ( <b>3A</b> + Cu(NO <sub>3</sub> ) <sub>2</sub> ).....	62
4.5 Powder X-ray diffraction patterns of MOFs <b>M1</b> , <b>M3</b> , <b>M5</b> , <b>M6</b> .....	63
4.6 Powder X-ray diffraction patterns of MOFs <b>M1</b> , <b>M2</b> , <b>M3</b> , <b>M4</b> .....	64
4.7 Powder X-ray diffraction patterns of MOFs <b>M7</b> , <b>M8</b> , <b>M9</b> .....	64
4.8 Powder X-ray diffraction patterns of MOFs <b>M10</b> , <b>M11</b> , <b>M12</b> .....	65
4.9 Powder X-ray diffraction patterns of MOFs <b>M13</b> , <b>M14</b> , <b>M15</b> .....	66
4.10 Thermogram of MOF <b>M1</b> ( <b>3A</b> -Zn).....	70
4.11 Nitrogen adsorption-desorption isotherms of MOFs <b>M1</b> , <b>M3</b> , <b>M5</b> and <b>M6</b> .....	72

<b>Figure</b>	<b>Page</b>
4.12 Nitrogen adsorption-desorption isotherms of MOFs <b>M1</b> , <b>M2</b> , <b>M3</b> and <b>M4</b> .....	72
4.13 Nitrogen adsorption-desorption isotherms of MOFs <b>M7</b> , <b>M8</b> and <b>M9</b> .....	73
4.14 Nitrogen adsorption-desorption isotherms of MOFs <b>M10</b> , <b>M11</b> and <b>M12</b> .....	73
4.15 Nitrogen adsorption-desorption isotherms of MOFs <b>M13</b> , <b>M14</b> and <b>M15</b> .....	74
4.16 Coordination environment of <b>CU-SCRU1</b> .....	76
4.17 Overall 1D chain of <b>CU-SCRU1</b> generated with the Mercury.....	76
4.18 2D structure of <b>CU-SCRU1</b> generated by Mercury. (a) Side view, (b) Top view.....	77
4.19 Top view of the overall 3D structure of <b>CU-SCRU1</b> .....	77
4.20 Coordination modes of the tetracarboxylate ligand <b>3A</b> with Zn(II) ion in the complex <b>CU-SCRU1</b> .....	78
4.21 Coordination environment of <b>CU-SCRU2</b> .....	79
4.22 Overall 1D chain of <b>CU-SCRU2</b> generated with the Mercury.....	80
4.23 (a) 2D structure of <b>CU-SCRU2</b> (side view) (b) 3D structure of <b>CU-SCRU2</b> (top view), generated by Mercury.....	80
4.24 Coordination modes of the tetracarboxylate ligand <b>3B</b> with Zn(II) ion in the complex <b>CU-SCRU2</b> .....	81
4.25 Coordination environment of <b>CU-SCRU3</b> .....	83
4.26 Overall 3D frameworks of <b>CU-SCRU3</b> generated by Mercury.....	84
4.27 Coordination environment of <b>CU-SCRU4</b> .....	85
4.28 Overall 3D frameworks of <b>CU-SCRU4</b> generated by Mercury.....	86
4.29 Coordination modes of the tetracarboxylate ligand <b>3B</b> in the complex <b>CU-SCRU3</b> and <b>CU-SCRU4</b> .....	87
4.30 Powder X-ray diffraction patterns of the synthesized sample and the pattern simulated on the basis of the single crystal structure of <b>CU-SCRU3</b> and <b>CU-SCRU4</b> .....	88

<b>Figure</b>	<b>Page</b>
4.31 Powder X-ray diffraction patterns of the synthesized sample by the different method.....	89
4.32 Compared IR spectra of <b>3B</b> and MOF- <b>3BCd</b> ( <b>CU-SCRU3</b> and <b>CU-SCRU4</b> ).....	89
4.33 SEM images (top) and microscope images (down) of MOF <b>3B</b> -Cd.....	90
4.34 <sup>1</sup> H NMR spectrum of desired product.....	92
A-1 <sup>1</sup> H NMR spectrum of compound <b>1A</b> .....	107
A-2 <sup>13</sup> C NMR spectrum of compound <b>1A</b> .....	107
A-3 IR spectrum of compound <b>1A</b> .....	108
A-4 Mass spectrum of compound <b>1A</b> .....	108
A-5 <sup>1</sup> H NMR spectrum of compound <b>2A</b> .....	109
A-6 <sup>13</sup> C NMR spectrum of compound <b>2A</b> .....	109
A-7 IR spectrum of compound <b>2A</b> .....	110
A-8 MALDI-TOF mass spectrum (CCA) of <b>2A</b> .....	110
A-9 <sup>1</sup> H NMR spectrum of compound <b>3A</b> .....	111
A-10 <sup>13</sup> C NMR spectrum of compound <b>3A</b> .....	111
A-11 IR spectrum of compound <b>3A</b> .....	112
A-12 MALDI-TOF mass spectrum (CCA) of compound <b>3A</b> .....	112
A-13 <sup>1</sup> H NMR spectrum of compound <b>1B</b> .....	113
A-14 <sup>13</sup> C NMR spectrum of compound <b>1B</b> .....	113
A-15 IR spectrum of compound <b>1B</b> .....	114
A-16 MALDI-TOF mass spectrum (CCA) of compound <b>1B</b> .....	114
A-17 <sup>1</sup> H NMR spectrum of compound <b>2B</b> .....	115
A-18 <sup>13</sup> C NMR spectrum of compound <b>2B</b> .....	115
A-19 IR spectrum of compound <b>2B</b> .....	116
A-20 MALDI-TOF mass spectrum (CCA) of <b>2B</b> .....	116
A-21 <sup>1</sup> H NMR spectrum of compound <b>3B</b> .....	117
A-22 <sup>13</sup> C NMR spectrum of compound <b>3B</b> .....	117
A-23 IR spectrum of compound <b>3B</b> .....	118

<b>Figure</b>	<b>Page</b>
A-24 MALDI-TOF mass spectrum (CCA) of compound <b>3B</b> .....	118
A-25 Compared IR spectra of <b>3A</b> , MOFs <b>M4</b> ( <b>3A</b> + Cu(OAc)), <b>M5</b> ( <b>3A</b> + Ni(NO <sub>3</sub> ) <sub>2</sub> ) and <b>M6</b> ( <b>3A</b> + Cd(NO <sub>3</sub> ) <sub>2</sub> ).....	119
A-26 Compared IR spectra of <b>3A</b> , MOFs <b>M7</b> ( <b>3A</b> + Er(NO <sub>3</sub> ) <sub>3</sub> ), <b>M8</b> ( <b>3A</b> + EuCl <sub>3</sub> ) and <b>M9</b> ( <b>3A</b> + Tb(NO <sub>3</sub> ) <sub>3</sub> ).....	119
A-27 Compared IR spectra of <b>3B</b> , <b>M10</b> ( <b>3B</b> + Zn(NO <sub>3</sub> ) <sub>2</sub> ), <b>M11</b> ( <b>3B</b> + Cu(NO <sub>3</sub> ) <sub>2</sub> ) and <b>M12</b> ( <b>3B</b> + Ni(NO <sub>3</sub> ) <sub>2</sub> ).....	120
A-28 Compared IR spectra of <b>3B</b> , MOFs <b>M13</b> ( <b>3A</b> + Er(NO <sub>3</sub> ) <sub>3</sub> ), <b>M14</b> ( <b>3A</b> + EuCl <sub>3</sub> ) and <b>M15</b> ( <b>3A</b> + Tb(NO <sub>3</sub> ) <sub>3</sub> ).....	120
A-29 Nitrogen adsorption-desorption isotherms of bulk MOFs ( <b>CU-SCRU3</b> and <b>CU-SCRU4</b> ) .....	121
B-1 Non-classical H-bonding between 1D-polymeric chain of <b>CU-SCRU1</b> .....	128



## LIST OF SCHEMES

Scheme		Page
2.1	Coordination environment of Cu <sup>2+</sup> ion in [Cu <sub>2</sub> (4,4'-bipy) <sub>4</sub> ·(D-HCam)·(4,4'-bipy) <sub>2</sub> ·12H <sub>2</sub> O].....	6
2.2	Coordination environment of Cd <sup>2+</sup> ion in [Cd(4,4'-bpy) <sub>2</sub> (H <sub>2</sub> O) <sub>2</sub> (ClO <sub>4</sub> ) <sub>2</sub> ·1.5(4,4'-bpy)] .....	6
2.3	Construction of a 3D MOF from the 2D layer formed of paddle-wheel SBUs and the second pillaring ligand.....	9
2.4	Chemical synthesis of MOFs based-1,4 Benzeneditetraazole.....	13
2.5	Synthesis of Co-MOF based 1,4 benzenedipyrazole.....	14
2.6	Coordination environment of cadmium and 3D-net in compound <b>1</b> and <b>2</b> .....	17
2.7	Two different frameworks prepared from Zn(II) and NTB <sub>3</sub> in the different solvent systems. (a) Structure of [Zn <sub>4</sub> O(NTB) <sub>2</sub> ] <sub>n</sub> ·3nDEF <sub>3</sub> nEtOH prepared from DEF/EtOH/H <sub>2</sub> O (5:3:2, v/v) mixture. (b) The framework structure of [Zn <sub>3</sub> (NTB) <sub>2</sub> (EtOH) <sub>2</sub> ] <sub>n</sub> ·4nEtOH prepared from EtOH.....	18
2.8	The resulting MOFs from the same reaction except different temperature.....	19
2.9	Post-synthetic modification (PSM) of MOFs.....	24
2.10	Post-synthetic modification of MOFs with metal ion complexes.....	25
2.11	(a) The structural representation of ZIF-90 (b) Scheme of the post-synthetic modification reactions described for ZIF-90.....	26
2.12	The synthesis routes of 3D Network of four novel MOFs-based thiacalix[4]arene.....	35
3.1	Synthetic pathway of 1,3-alternate calix[4]arene tetra- <i>p</i> -benzoic acid ( <b>3A</b> ).....	38
3.2	Synthetic pathway of 1,3-alternate calix[4]arene tetra- <i>m</i> -benzoic acid ( <b>3B</b> ).....	42

<b>Scheme</b>		<b>Page</b>
3.3	Friedel-Crafts alkylation of benzyl bromide and 1,3,5-trimethoxybenzene catalyzed by synthesized MOFs.....	56
4.1	Synthetic pathway of 1,3-alternate calix[4]arene tetra- <i>p</i> -benzoic acid ( <b>3A</b> ).....	58
4.2	Synthetic pathway of 1,3-alternate calix[4]arene tetra- <i>m</i> -benzoic acid ( <b>3B</b> ).....	59
4.3	Friedel-craft alkylation reaction of benzyl bromide and 1,3,5-trimethoxy benzene.....	91

## LIST OF ABBREVIATIONS

Å	:	Angstrom
H <sub>3</sub> BTC	:	1,3,5-Benzebetricarboxylic acid
H <sub>2</sub> BDP	:	1,4-Benzenedipyrazole
H <sub>2</sub> BDT	:	1,4-Benzeneditetrazole
bpy	:	4,4'-Bipyridine
bipy	:	4,4'-Bipyridine
br	:	Broad (NMR)
BET	:	Brunauer-emmett-teller
Cd(NO <sub>3</sub> ) <sub>2</sub>	:	Cadmium(II) nitrate
calcd	:	Calculated
<sup>13</sup> C NMR	:	Carbon Nuclear Magnetic Resonance
δ	:	Chemical shift
CHCl <sub>3</sub>	:	Chloroform
Co(NO <sub>3</sub> ) <sub>2</sub>	:	Cobalt(II) nitrate
Cu(OAc) <sub>2</sub>	:	Copper acetate
Cu(NO <sub>3</sub> ) <sub>2</sub>	:	Copper nitrate
<i>J</i>	:	Coupling constant
cm <sup>3</sup> /g	:	Cubic centimeter per gram
°C	:	Degree Celsius
CDCl <sub>3</sub>	:	Deuterated chloroform
DEF	:	Diethylformamide
DTG	:	Differential Thermogravimetric Analysis
DMF	:	Dimethylformamide
bpta	:	3,6-Di(4-pyridyl)-1,2,4,5-tetrazine
H <sub>2</sub> NTD	:	2,6-Di(1 <i>H</i> -tetrazol-5-yl)naphthalene
d	:	Doublet (NMR)
Er(NO <sub>3</sub> ) <sub>3</sub>	:	Erbium(III) nitrate
EA	:	Elemental analysis
EtOH	:	Ethanol
EtOAc	:	Ethyl acetate

EuCl <sub>3</sub>	:	Europium(III) chloride
FT-IR	:	Fourier Transform Infrared Spectroscopy
g	:	Gram (s)
DMSO	:	Hexadeuterated dimethylsulfoxide
Hz	:	Hertz (s)
h	:	Hour (s)
HCl	:	Hydrochloric acid
IRMOF	:	Isorecticular Metal-Organic Framework
K	:	Kelvin
MS	:	Mass Spectrometry
m/z	:	Mass to Charge
MALDI-TOF-MS	:	Matrix Assisted Laser Desorption/Ionization- Time of Flight Mass Spectrometry
MOF	:	Metal-Organic Framework
m <sup>2</sup> /g	:	Meter square per gram
MeOH	:	Methanol
CH <sub>2</sub> Cl <sub>2</sub>	:	Methylene chloride
μm	:	Micrometer
mL	:	Milliliter (s)
mg	:	Milligram (s)
mmol	:	Millimole (s)
min	:	Minute
M	:	Molar
m	:	Multiplet (NMR)
Ni(NO <sub>3</sub> ) <sub>2</sub>	:	Nickel(II) nitrate
H <sub>3</sub> NTB	:	4,4',4''-Nitrilotrisbenzoic acid
N <sub>2</sub>	:	Nitrogen gas
nm	:	Nanometer
obsd	:	Observed
ppm	:	Parts per million
KBr	:	Potassium bromide
K <sub>2</sub> CO <sub>3</sub>	:	Potassium carbonate

KOH	:	Potassium hydroxide
P	:	Pressure
$^1\text{H}$ NMR	:	Proton Nuclear Magnetic Resonance
q	:	Quartet (NMR)
rt	:	Room temperature
SBU	:	Secondary Building Unit
s	:	Singlet (NMR)
$\text{NaHCO}_3$	:	Sodium hydrogencarbonate
NaOH	:	Sodium hydroxide
$\text{Na}_2\text{SO}_4$	:	Sodium sulfate
T	:	Temperature
$\text{Tb}(\text{NO}_3)_3$	:	Terbium(III) nitrate
$\theta$	:	Theta
TLC	:	Thin Layer Chromatography
TGA	:	Thermo Gravimetric Analysis
t	:	Triplet
v/v	:	Volume by volume
SEM	:	Scanning Electron Microscopy
XRD	:	X-ray diffraction
ZIF	:	Zeolitic Imidazolate Framework
$\text{Zn}(\text{OAc})_2$	:	Zinc acetate
$\text{Zn}(\text{NO}_3)_2$	:	Zinc nitrate

# CHAPTER I

## INTRODUCTION

During the past ten years, most energy sources derived from petroleum and natural gas have been used extensively causing a shortage of oil and natural gas. The current oil price is even more expensive and is likely to increase further. Therefore, both government agencies and the private sector promote the use of renewable energy and encourage research and development in renewable energy. Solar energy, wind energy, water energy and hydrogen energy can be a long term sustainable solution. It should be noted that, the use of petroleum and natural gas results in global warming causing by carbon dioxide from the combustion of fuels in the industry, household and vehicles on streets. Therefore, using of carbon-free energy that does not produce carbon dioxide gas should be a procedure of choice. Hydrogen gas can be used as raw material in fuel cells. This is a device that can convert chemical energy to electrical power lines. In this device, the reaction between hydrogen gas ( $H_2$ ) and oxygen gas ( $O_2$ ) form water ( $H_2O$ ), overall this process is used to produce electricity in fuel cells. Fuel cell does not produce greenhouse gases, dust and black soots like petroleum that pollute the environment. It also has a higher performance than hydrocarbon fuels. Furthermore, It can also be recycled (renewable). However, the limitation of using of hydrogen energy is the storage of hydrogen. The gravitational force between the molecules of hydrogen gas are very weak and have low density. Storage method used nowadays such as compressed hydrogen gas tank requires a very high pressure to compress the low density hydrogen gas. To withstand high pressure, a hydrogen container must be thick and made from heavy metals. This method is still in the issue of safety. Afterward, liquid hydrogen tank which store hydrogen in liquid form at atmospheric pressure and low temperatures can be used. This method does not required high pressure as the compressed hydrogen gas tank but requires a lot of energy to cool hydrogen gas into a liquid in insulated tanks. Both methods are not suitable for commercial use. Hence, using hydrogen energy in daily life is still a challenge. Many researcher try to develop the hydrogen storage materials lead to the

invention of solid materials for adsorption of hydrogen gas. Porous materials are an attractive candidate. Many types of porous materials can be used as hydrogen storage materials such as zeolites<sup>(1)</sup>, carbon nanotubes (CNT)<sup>(2)</sup>, covalent organic frameworks (COFs)<sup>(3)</sup> and metal-organic frameworks (MOFs)<sup>(4)</sup> etc.

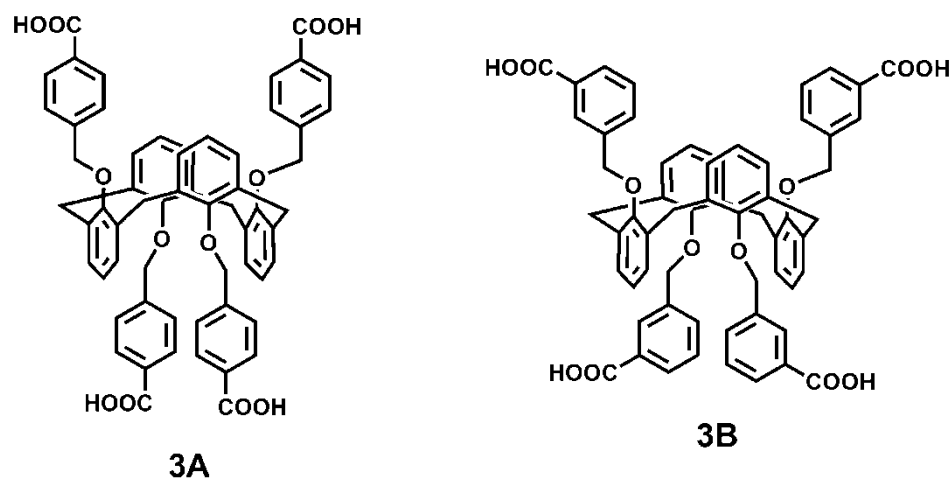
Metal-organic frameworks (MOFs) are a class of the crystalline porous materials which are constructed from metal ions with multifunctional organic linkers through the coordination bond. Topologies and structures of MOFs can be designed by varying metal centers or organic linkers. These reasons make MOF a subject of interests. Moreover, Due to the high pore volume and surface area of MOFs, many researchers have reported application of MOFs in the absorption of light gases such as hydrogen, nitrogen and methane. Moreover, MOFs have many other potential applications, for example, gas separation, catalysis, drug delivery and luminescence.

Calix[4]arene is one of the most popular building blocks in supramolecular chemistry due to its conformations that can be controlled by chemical reagents and also its easy functionalization. Furthermore, calix[4]arene is a cavity-shaped cyclic molecule and has a lot of  $\pi$ -electrons which may provide specific properties of new MOFs. In this research, calix[4]arene compound is being synthesized and functionalized to use as organic linker for construction of new MOFs, calix[4]arene - based MOFs.

## 1.1 Objectives

1.1.1 To synthesize 1,3-alternate tetrabenzoic acid calix[4]arene derivatives (Figure 1.1) for using as organic linkers.

1.1.2 To synthesize 1,3-alternate tetrabenzoic acid calix[4]arene-based MOFs and to study their gas adsorption properties.



**Figure 1.1** 1,3-alternate tetrabenzoic acid calix[4]arene derivatives.

## 1.2 Scope of Research

1.2.1 Synthesis and characterization of organic linkers, **3A** and **3B**.

1.2.2 Synthesis of 1,3-alternate tetrabenzoic acid calix[4]arene-based MOFs by using the conventional heating method. Study their gas adsorption properties and their characteristic by using Nitrogen adsorption-desorption isotherm, Powder X-ray diffraction (PXRD), Scanning electron microscopy (SEM), Fourier Transform Infrared Spectroscopy (FT-IR) and Thermogravimetric Analysis (TGA).

1.2.3 Crystallize 1,3-alternate tetrabenzoic acid calix[4]arene-based MOFs and characterize them by single-crystal X-ray diffraction (sc-XRD) technique for solving the resulting structure.



## CHAPTER II

### BACKGROUND AND LITERATURE REVIEWS

#### 2.1 An overview of metal-organic frameworks

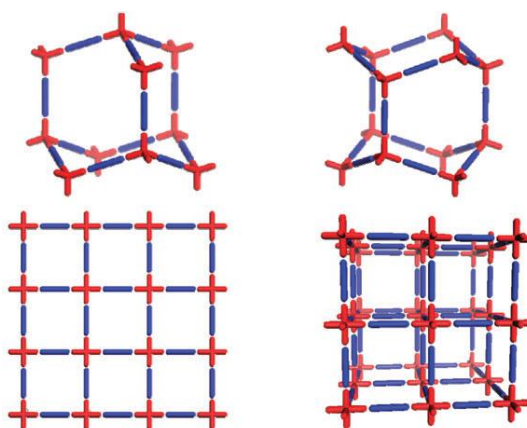
Metal–organic frameworks (MOFs) are a new class of porous materials which composed of metal ions and organic linkers connecting via coordination bond which also known as coordination polymers. Due to their high pore volume and surface area make MOFs in the field of materials science. Many MOFs have been employed in various applications such as absorption of light gases such as hydrogen<sup>(5)</sup>, carbondioxide<sup>(6)</sup> and methane<sup>(7)</sup> etc. Furthermore, MOFs have been used in other applications, for example, gas separation<sup>(8)</sup>, catalysis<sup>(9)</sup>, drug delivery<sup>(10)</sup> and luminescence<sup>(11)</sup> etc. There are many factors that should be concerned in the synthetic process of MOFs. Key factors are metal ions and organic linkers, but other factors such as temperature, pH values, solvent, synthetic methods which play an important role in directing the topologies and properties of frameworks leading to their efficient applications<sup>(12)</sup> are also considered. Novel MOFs have been prepared by using commercially available or synthesized organic linkers in the laboratory with the appropriate metal ions under optimum conditions to yield fascinating frameworks and also useful applications<sup>(13)</sup>.

#### 2.2 Factors influencing on topologies and properties of metal-organic frameworks

The coordination geometry of metal ion/cluster and the chemical structure of organic linkers play an important role in constructing frameworks and yielding their chemical, physical properties. A variety of different architectures can be formed during MOFs formation. Most of reported MOFs structures preparing from carboxylate derivatives as organic linkers have a coordination bonds with d-block metal ions. Different structures and functional groups of organic linkers as well as many metal cluster building blocks gave the opportunity to obtain infinite frameworks.

### 2.2.1 Metal centers

The *d*-block transition metal ions are the most popular centers in synthesis of MOFs because of their different coordination geometry. For example  $\text{Zn}^{2+}$  ion and  $\text{Cu}^{2+}$  ion can be found in tetrahedral geometry and octahedral geometry<sup>(14, 15)</sup>. However,  $\text{Cd}^{2+}$  is frequently observed in octahedral geometry<sup>(16)</sup>. Figure 2.1 illustrates the approach for design of networks based of tetrahedral (above left cubic diamondoid, above right hexagonal diamondoid) and octahedral metal nodes (below left square grid, below right octahedral network).

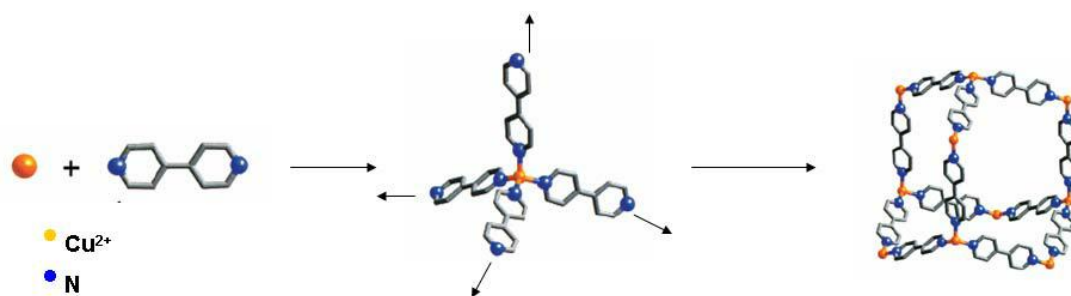


**Figure 2.1** The approach for design of networks base upon the geometry of metal node<sup>(17)</sup>. Metal ion node (red) and linear organic linkers (blue).

The characteristics of metal ions can be used in the design of metal-organic frameworks.

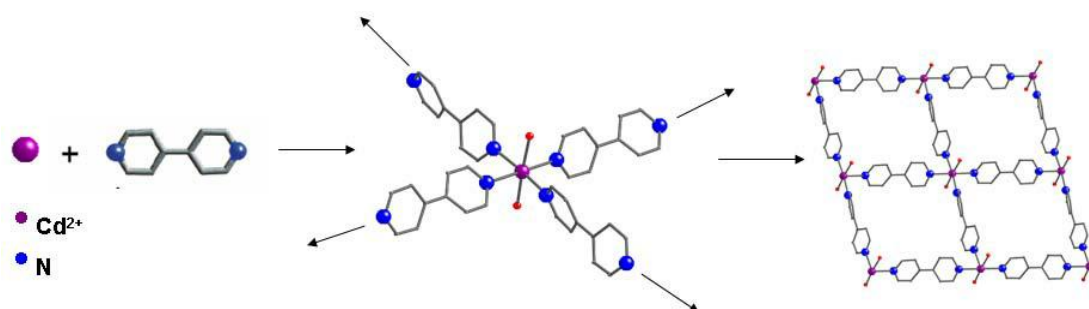
#### 2.2.1.1 Single metal ions

A single metal ion as a node effects the framework structure because of the tendency for a coordination environment with the specific geometry of the metal ions used. For example, the compound  $[\text{Cu}_2(4,4'\text{-bipy})_4] \cdot (\text{D-HCam}) \cdot (4,4'\text{-bipy})_2 \cdot 12\text{H}_2\text{O}$  and  $[\text{Cd}(4,4'\text{-bpy})_2(\text{H}_2\text{O})_2](\text{ClO}_4)_2 \cdot 1.5(4,4'\text{-bpy})$  were synthesized by Zhang group<sup>(18)</sup>. and Liu group<sup>(19)</sup>, respectively. These two compounds were prepared from the same organic linker (4,4'-bipyridine) but used different metal ions were used. For the first compound, the  $\text{Cu}^{2+}$  ion adopted a tetrahedral geometry and enlarged into a diamondoid network via 4,4'-bipyridine linkages as displayed in Scheme 2.1.



**Scheme 2.1** Coordination environment of  $\text{Cu}^{2+}$  ion in  $[\text{Cu}_2(4,4'\text{-bipy})_4]\cdot(\text{D-HCam})\cdot(4,4'\text{-bipy})_2\cdot 12\text{H}_2\text{O}$  locate in a tetrahedral geometry and acts as the node for the enlargement of a diamondoid network linked via 4,4'-bipyridine<sup>(20)</sup>.

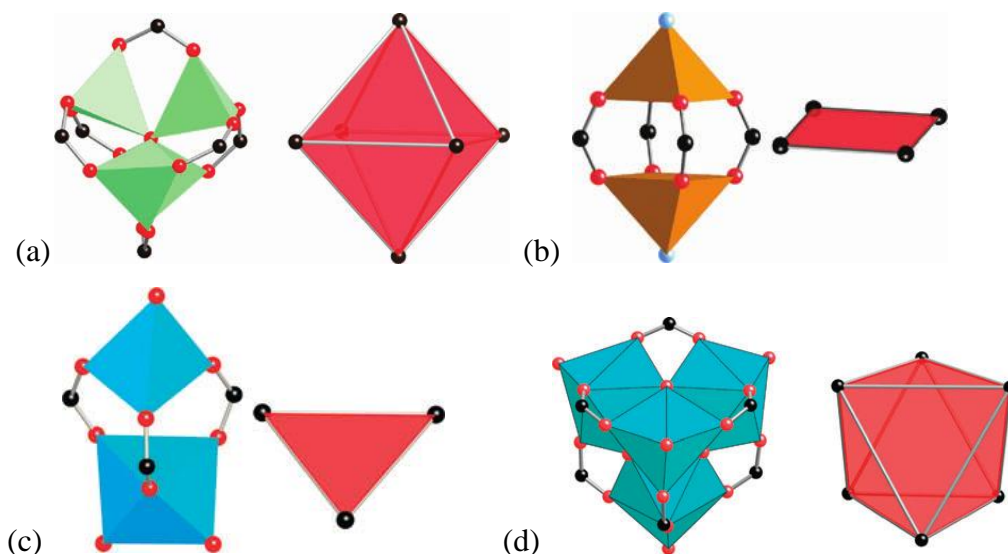
Comparing with the second compound,  $\text{Cd}^{2+}$  possessing in an octahedral geometry. The equatorial position were connected by four 4,4'-bipyridine molecules. The axial positions of the octahedral were completed by water molecules (solvent). In this case, due to the coordination geometry around the  $\text{Cd}^{2+}$  ion, a square net was formed in the expansive network as shown in Scheme 2.2.



**Scheme 2.2** Coordination environment of  $\text{Cd}^{2+}$  ion in  $[\text{Cd}(4,4'\text{-bpy})_2(\text{H}_2\text{O})_2](\text{ClO}_4)_2\cdot 1.5(4,4'\text{-bpy})$  locate in an octahedral geometry with two solvated water molecules (red = oxygen atoms) and four 4,4'-bipyridine molecules<sup>(20)</sup>.

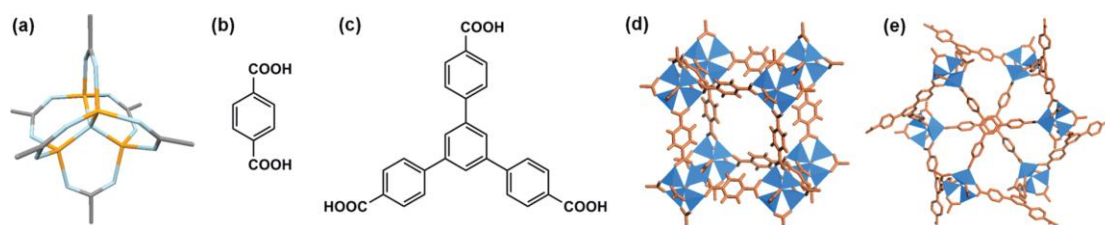
### 2.2.1.2 Secondary building units

The design of MOFs by the use of secondary building units (SBUs) approach has been introduced by Yaghi<sup>(21)</sup>. SBUs construct from one or more metal ions and the donor atoms of multidentate ligands creating rigid molecular cluster which are repeated throughout the whole framework. In short, bridging ligands are replaced with divergent ones, while the core structure of the network is remained. The common SBUs are shown in the Figure. 2.2.



**Figure 2.2** The example of SBUs, (a) Octahedral : metals (Zn, Co, Be), green; C, black; O, red. (b) Square paddle-wheel : metals (Cu, Ru, Rh, Mo, Fe, Ni, Co, Re, Cr, Zn, Mn, Cd, Bi), gold; C, black; O, red; N, blue. (c) Triangle : Zn, blue; C, black; O, red. (d) Octahedral : metals (Er, Yb, Nd), blue; C, black; O, red.<sup>(21)</sup>

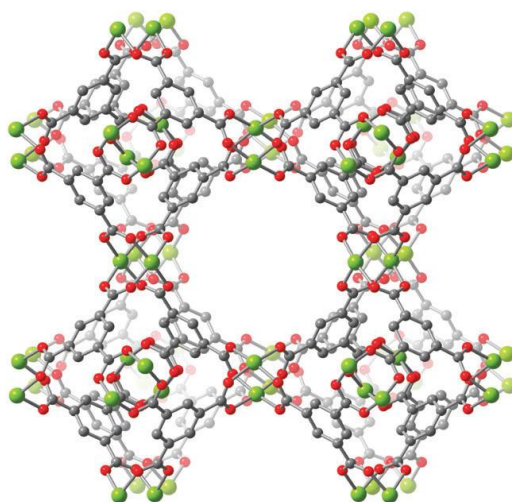
A molecular  $[\text{Zn}_4\text{O}]^{6+}$  cluster and six acetate anions SBUs was first reported by Yaghi in the MOF-5 where the acetate anions in this oxo-centered cluster replaced by divergent organic linkers. This SBU served as an octahedral geometry for the formation of a primitive cubic framework. This SBUs was also obtained in MOF-177<sup>(22)</sup> which the SBUs connected with tridentate ligand instead of bidentate ligand in MOF-5 to provide different 3D network as illustrated in figure 2.3.



**Figure 2.3** (a)  $[\text{Zn}_4\text{O}]^{6+}$  SBUs, the carboxylic acid used in the synthesis of (b) MOF-5 and (c) MOF-177, the structures of (d) MOF-5 and (e) MOF-177<sup>(23)</sup>.

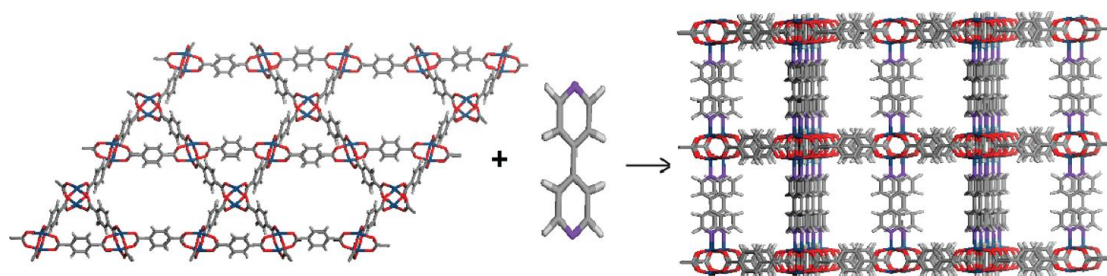
MOFs prepared by using the  $\text{Cu}^{2+}$  ion and carboxylic acids ligands are an enormous interesting class of MOFs comparing of a paddlewheel type  $[\text{Cu}_2(\text{OOC})_4]$  SBUs (Figure 2.4). MOF, HKUST-1<sup>(24)</sup> constructed from the Cu(II) paddle-wheel SBUs and BTC (1,3,5-benzenetricarboxylic acid) which shows a Langmuir surface area of  $1958 \text{ m}^2 \cdot \text{g}^{-1}$ <sup>(6)</sup>.

In paddlewheel type SBUs, the axial positions of metal ion are generally coordinated by solvent molecules, which can be easily removed by heating and/or evacuating without destroying the framework structure leading to the formation of open metal sites. MOFs with open metal sites can be use as heterogeneous catalyst and also provide high surface areas due to the stronger interactions between metal sites and gas molecules.



**Figure 2.4** Crystal structure of HKUST-1. Green, gray, and red spheres represent Cu, C, and O atoms, respectively; H atoms are omitted for clarity<sup>(5)</sup>.

As described above, the axial positions of the metal center in the paddlewheel type SBU are usually occupied by coordinated solvent molecules. However, the axial position can combine with neutral, divergent Lewis basic ligands to provide further points of extension for frameworks growth as shown in the scheme 2.3. Two-dimensional (2D) networks can form from dicarboxylate ligand and square  $[\text{Zn}_2(\text{OOC})_4]$  paddle-wheel units connecting with a second Lewis basic ligand, such as 4,4-bipyridine (4,4-bpy) or 3,6-di(4-pyridyl)-1,2,4,5-tetrazine (bpta), to provide the 3D framework. The divergent basic ligand acted as the pillar<sup>(23)</sup>.



**Scheme 2.3** Construction of a 3D MOF from the 2D layer formed of paddle-wheel SBUs and the second pillaring ligand. Color scheme: Zn, blue; O, red; N, violet; C, gray; H, light gray.<sup>(23)</sup>

In addition, not only transition metal ions were employed to construct MOFs but lanthanide metal ions were also used. Generally, lanthanide metal ions<sup>(25)</sup> have more coordination numbers than transition metal ions leading to a varieties of frameworks, and their also have luminescence properties<sup>(26)</sup> that attracted interest from many researchers. Moreover, alkaline-earth metal ion are also employed in constructing MOFs<sup>(27)</sup>.

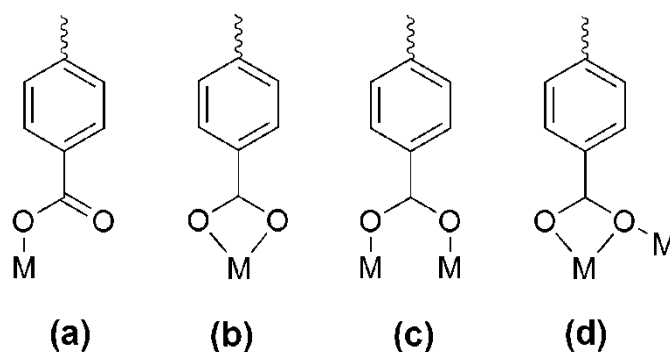
## 2.2.2 Organic linkers

In the part of organic linkers, Due to many ligands are available commercial and can also be synthesized in the laboratory. Leading to, there are plenty of MOFs reported with different kinds of organic linkers with specific properties depending on the chemical structure of their ligands used. The organic linkers play an important role in the resulting architecture as well as the chemical and physical properties of MOFs. There are many types of functional groups, such as carboxylate<sup>(28)</sup>, N-donor<sup>(29)</sup>, phosphonate<sup>(30)</sup>, sulfonate<sup>(31)</sup> and mixed functional group ligands<sup>(32)</sup>.

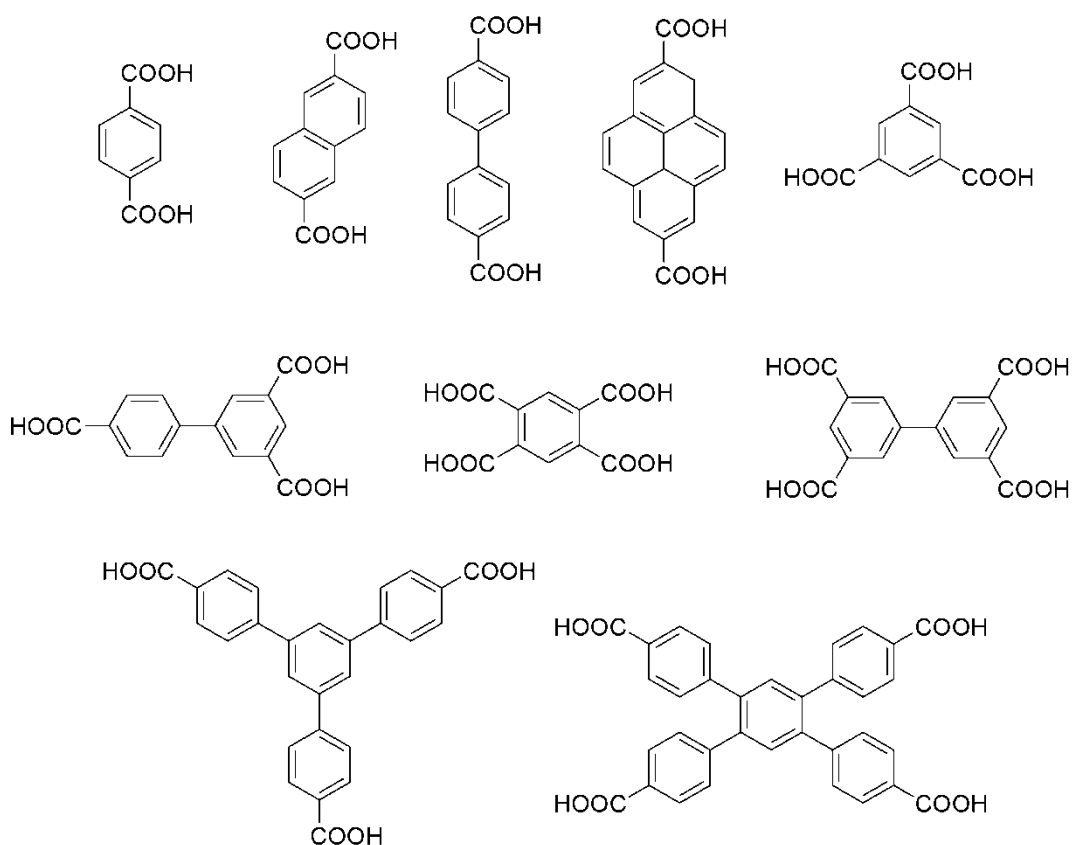
### 2.2.2.1 Carboxylate organic linkers

Carboxylate donor group<sup>(33)</sup> is one of the most common organic linkers which have several advantages such as many modes to coordinate with metal ions as shown in Figure 2.5<sup>(34)</sup>, strong electrostatic attractions between negative charges of carboxylates and positive charges of metal ions. As a result, the total charge of resultant frameworks is zero to provide the stable MOFs. A lot of

carboxylate organic linkers have been reported. Figure 2.6 illustrates the example of carboxylate organic linkers.

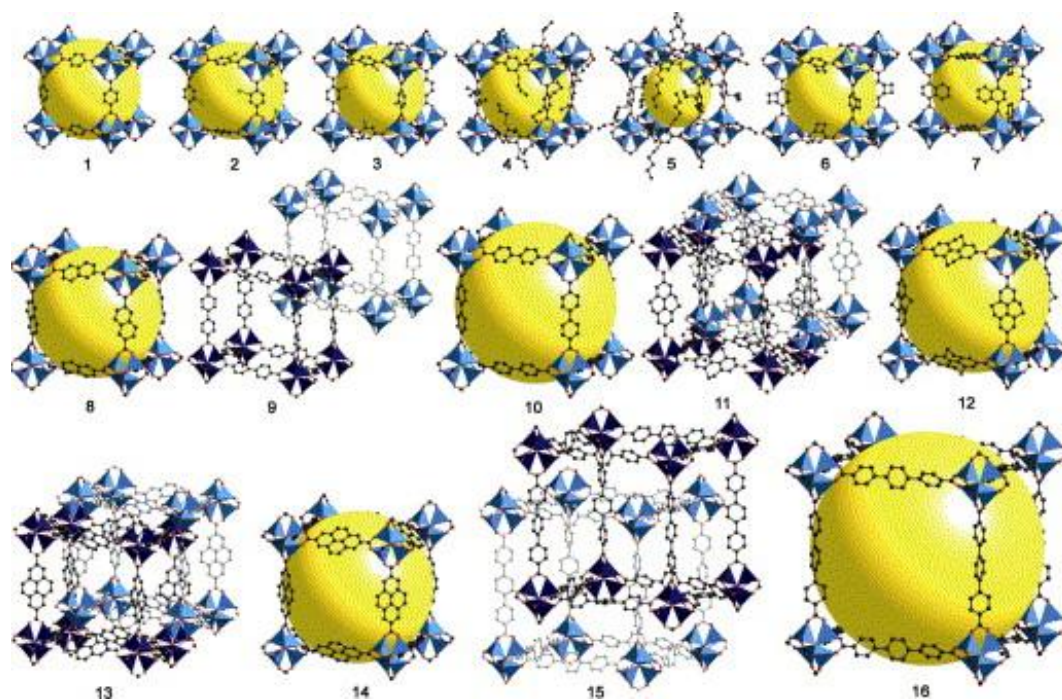


**Figure 2.5** Coordination modes of carboxylate organic linkers. (a) monodentate, (b) chelating bidentate, (c) bidentate, (d) bridging bidentate.



**Figure 2.6** Some carboxylate ligands used in the synthesis MOFs

Well-known MOFs were constructed from carboxylate organic linkers with transition metal ions with the high surface area for storage applications. For example, MOF-5 synthesized by Yaghi composed of 1,4-benzenedicarboxylic acid and  $[\text{Zn}_4\text{O}]^{6+}$  SBU. Its BET surface area was very high, around  $2,296 \text{ m}^2/\text{g}$ <sup>(5)</sup>. Yaghi mimicked the structure of MOF-5 by using longer spacer ligands or functionalized 1,4-benzenedicarboxylic acid in some positions of the benzene ring using the same metal cluster  $[\text{Zn}_4\text{O}]^{6+}$  to provide to same cubic frameworks as MOF-5 but different in pore size as illustrated in Figure 2.7. This approach is known as isorecticular synthesis<sup>(33)</sup>.



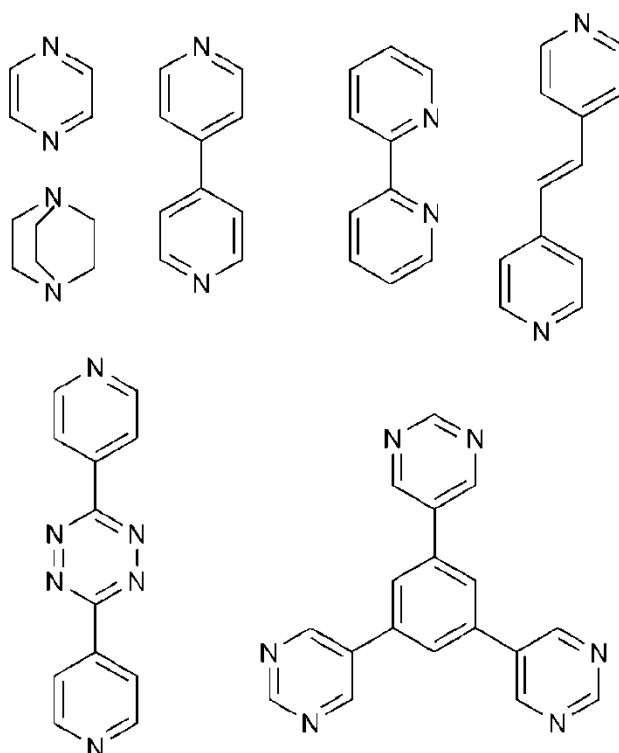
**Figure 2.7** Isorecticular metal-organic frameworks composed of  $[\text{Zn}_4\text{O}]^{6+}$  SBUs and linear dicarboxylate organic linkers<sup>(33)</sup>.

#### 2.2.2.2 N-donor organic linkers

N-donor ligands<sup>(35)</sup> are mostly neutral, such as pyridyl ligands<sup>(37)</sup>. However, they reacted with a cationic metal center leading to the resulting cationic MOFs. Positive charges of frameworks have to be balanced by counter anions incorporated into the framework. These anions are often located within pores of the framework, decreasing the cavity size. However, the cationic frameworks have

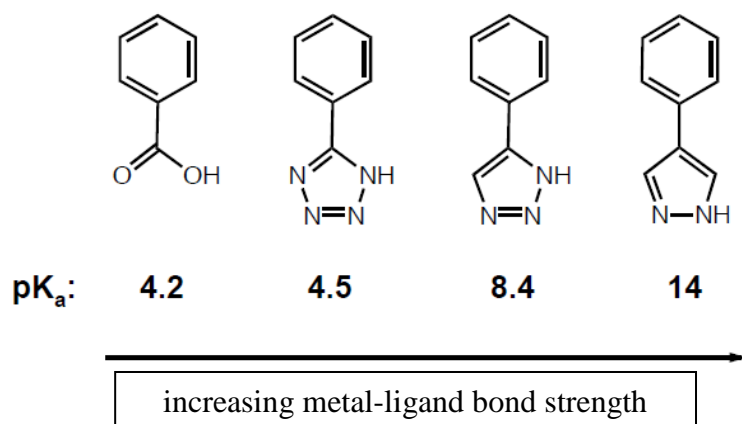


some advantages, such as reducing or stopping the formation of interpenetration form because the presence of the anions reduced excessive pore space of the framework<sup>(36)</sup>. Moreover, it can be used as anion exchanger<sup>(37)</sup>. Pyridyl derivatives have been reported both as the main ligand and co-ligand for MOFs construction<sup>(38)</sup> as shown in Figure 2.8.



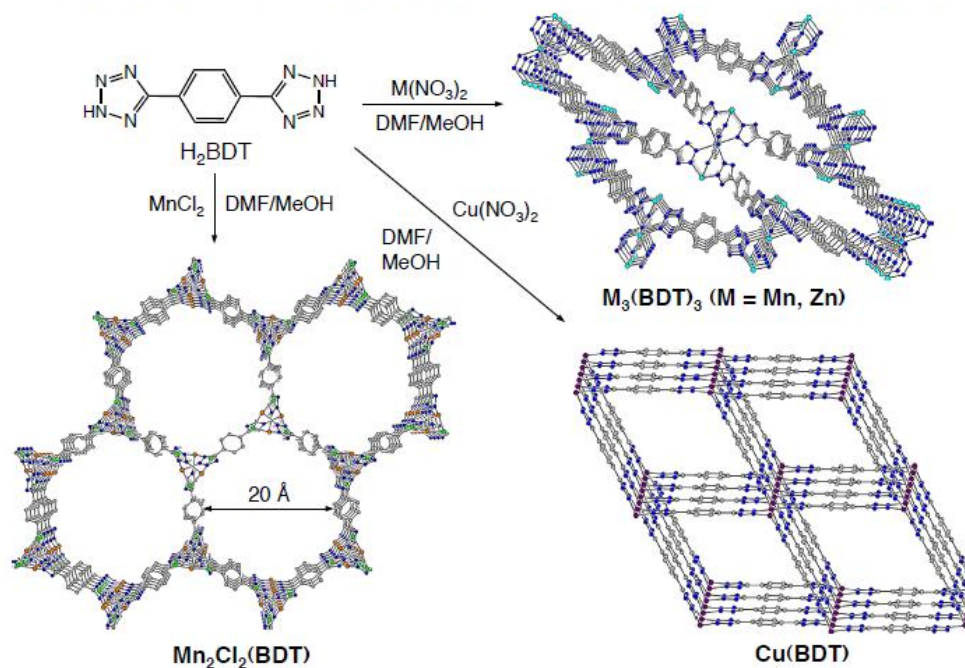
**Figure 2.8** Some of pyridyl ligands used in the synthesis MOFs

Pyrazole, triazole and tetraazole derivatives are also used as N-donor ligands in the construction of MOFs. The metal-ligand bond strength depends on  $pK_a$  values as shown in figure 2.9. As a result, many MOFs using pyrazole, triazole and tetraazole derivatives with various metal clusters were found to provide special properties<sup>(39, 40)</sup>.



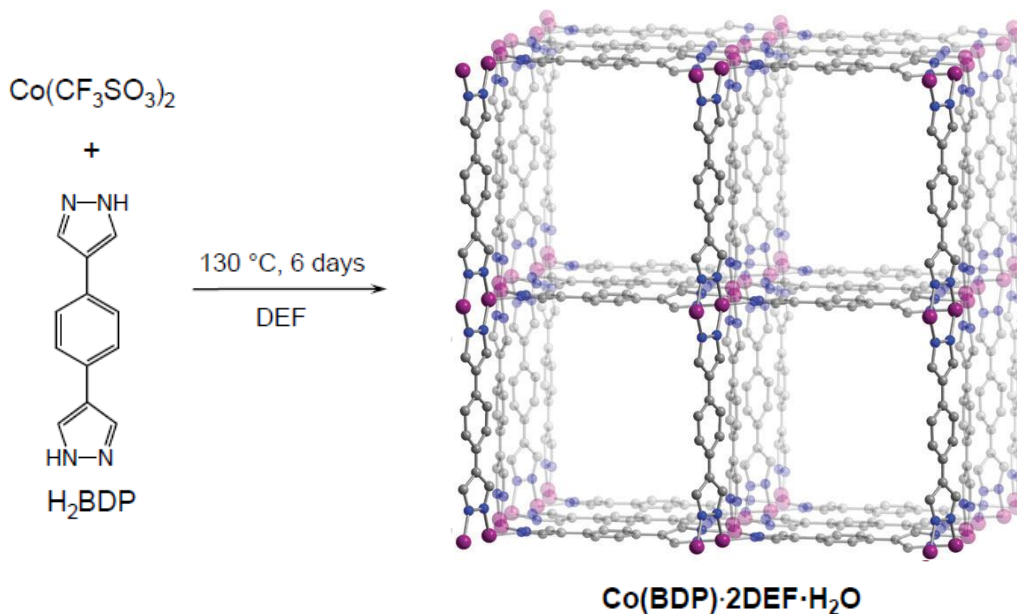
**Figure 2.9** Comparison of  $\text{pK}_a$  values with the metal-ligand bond strength<sup>(42)</sup>

In 2006, Dinca and co-workers<sup>(41)</sup> used tetraazole derivatives ( $\text{H}_2\text{BDT}$ ) to synthesize MOFs with various metal center in appropriate reaction conditions and obtained different resulting frameworks as displayed in scheme 2.4. This finding supported the important role of metal ions on the final network and the reaction condition should be considered carefully.



**Scheme 2.4** Chemical synthesis of MOFs based-1,4-benzeneditetraazole<sup>(41)</sup>

Furthermore, in 2008, this research group<sup>(42)</sup> also successfully prepared metal-organic framework by using pyrazole derivative ( $H_2BDP$ ) with  $Co^{2+}$  ion. Extreme conditions were required to obtain a pure crystalline product as shown in scheme 2.5.



**Scheme 2.5** Synthesis of Co-MOF based 1,4-benzenedipyrazole<sup>(42)</sup>

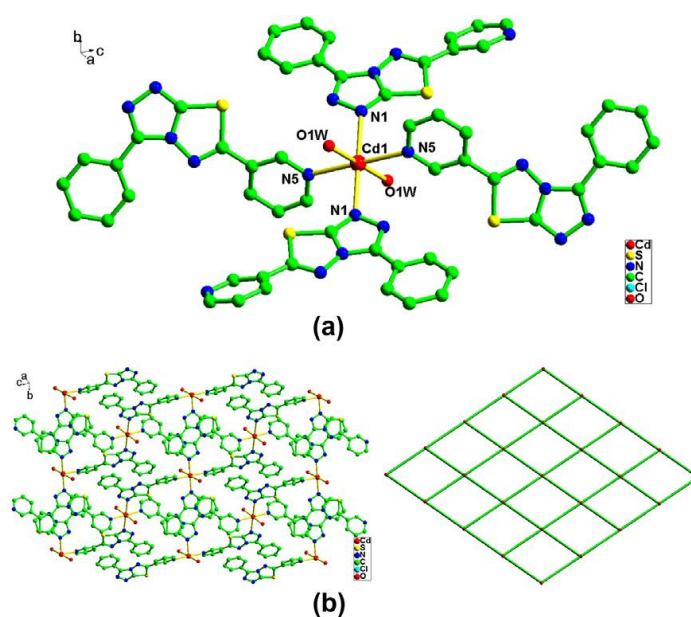
Most MOFs were prepared by using carboxylate or nitrogen-donor organic linkers. However, other functional group ligands were also used in the syntheses of MOFs such as,  $\beta$ -diketonate<sup>(43)</sup>, phosphonate<sup>(44)</sup> and sulfonate ligand<sup>(45)</sup>.

### 2.3 The effect of reaction condition on the topologies and properties of metal-organic frameworks.

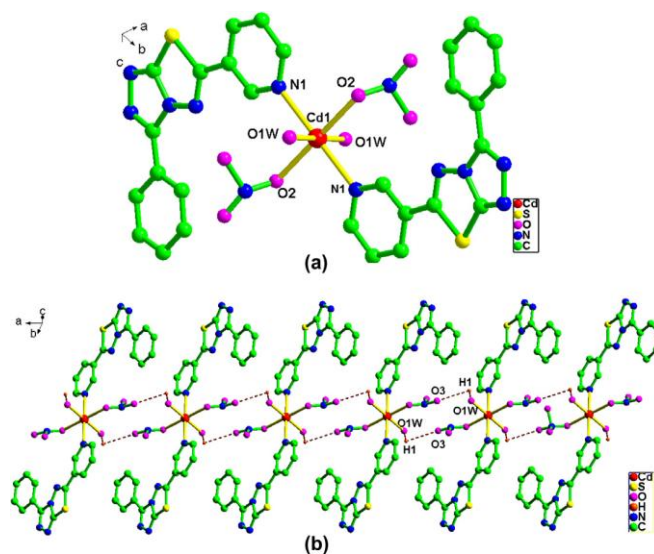
There are many factors that should be considered in the formation of MOFs, not only metal ions and organic linkers but also the reaction condition such as temperature, pH values, solvent, synthetic methods etc. which play an important role in directing the topologies and properties of frameworks leading to their applications.

### 2.3.1 Counter anions of metal salt

Counter anions of metal salts are important factors on the resulting frameworks. Wang *et al.*<sup>(46)</sup> synthesized MOFs,  $\{[\text{Cd}(\text{L}^2)_2(\text{H}_2\text{O})_2] \cdot (\text{ClO}_4)_2\}_\infty$  and  $\text{Cd}(\text{L}^2)_2(\text{NO}_3)_2(\text{H}_2\text{O})_2$  by using ligand  $\text{L}^2$  with different metal salts,  $\text{Cd}(\text{ClO}_4)_2 \cdot 6\text{H}_2\text{O}$  and  $\text{Cd}(\text{NO}_3)_2 \cdot 6\text{H}_2\text{O}$ , respectively under the same reaction conditions. For  $\{[\text{Cd}(\text{L}^2)_2(\text{H}_2\text{O})_2] \cdot (\text{ClO}_4)_2\}_\infty$ , the coordination geometry of  $\text{Cd}^{2+}$  ion is an octahedral which completed by four nitrogen atom of  $\text{L}^2$  and two oxygen atoms of water molecules (Figure 2.10). The  $\text{ClO}_4^{2-}$  ion do not coordinate to  $\text{Cd}^{2+}$  ion. In the case of  $\text{Cd}(\text{L}^2)_2(\text{NO}_3)_2(\text{H}_2\text{O})_2$ , the coordination geometry of  $\text{Cd}^{2+}$  ion is also octahedral geometry with two oxygen atoms from two water molecules and two nitrogen atoms of pyridine from two distinct ligands  $\text{L}^2$  and two oxygen atoms from two different  $\text{NO}_3^-$  anions (Figure 2.11). The presence of anions in coordination sites of the framework lead to the different the structures and properties of MOFs.



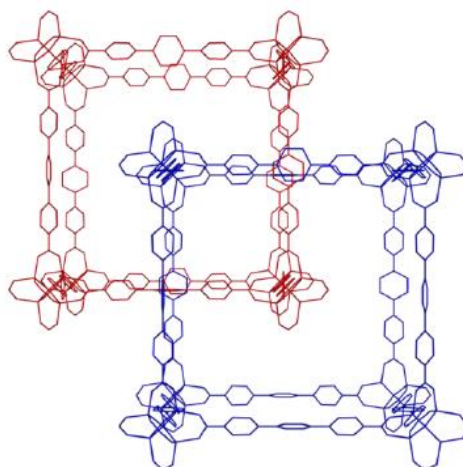
**Figure. 2.10** (a) Coordination environment of Cd(II) ion; (b) Overall 2D structure of  $\text{Cd}(\text{L}^2)_2(\text{NO}_3)_2(\text{H}_2\text{O})_2$ <sup>(46)</sup>.



**Figure 2.11** (a) Coordination environment of Cd(II) ion; (b) Overall 2D structure of  $\{[\text{Cd}(\text{L}^2)_2(\text{H}_2\text{O})_2] \cdot (\text{ClO}_4)_2\}_\infty$ <sup>(46)</sup>.

### 2.3.2 Concentration

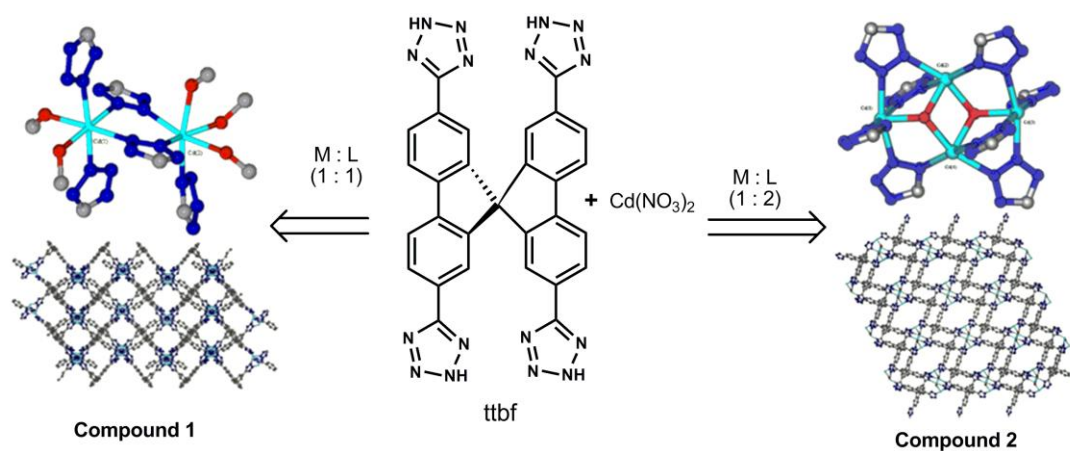
The rate of crystal growth depends on the reaction mixture concentration as well. In high concentration condition, small particles may form because the reaction between metal ions and ligands is faster when comparing with the lower concentration reaction. Furthermore, concentration also effects to the formation of interpenetrated frameworks. The interpenetration in metal-organic frameworks normally occurs when increasing the size of the bridging ligands in MOF structures which can produce larger cavities. At, high concentration reaction mixture, it is possible to form a sub-lattice in the voids of the structure that provides the interpenetrated frameworks. For example, IRMOF-15<sup>(47)</sup>  $[\text{Zn}_4\text{O}(\text{tpdc})_3]$  (tpdc = p-terphenyl-4,4-dicarboxylate) which is isorecticular with MOF-5 structure previously seen in figure 2.10. The structure composed of the same  $\text{Zn}_4\text{O}(\text{O}_2\text{CR})_6$  SBUs in MOF-5 but linked together by longer tpdc linkers. In this case, the structure is a doubly interpenetrated network (Figure 2.12). The comparative non-interpenetrated framework can be synthesized using more dilute solutions during the synthesis (Figure 2.7).



**Figure. 2.12** Doubly interpenetrated network of IRMOF-15 [ $\text{Zn}_4\text{O}(\text{tpdc})_3$ ] (tpdc = pterphenyl-4,4'-dicarboxylate)<sup>(47)</sup>.

### 2.3.3 Metal-ligand ratio

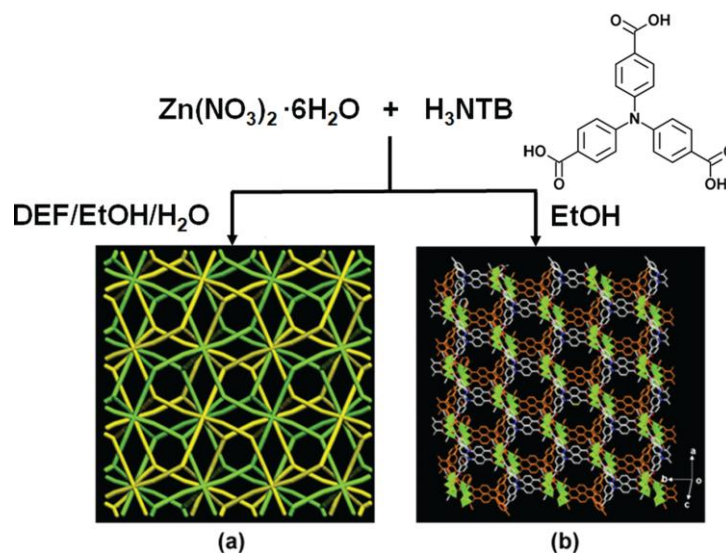
Tuning ratio of metal and organic linkers could result in different forms of coordination environment or SBUs. In 2008, Collins et al.<sup>(48)</sup> reported new metal-organic frameworks were prepared from the same organic linker, tetrakis(tetrazolate) and metal salt,  $\text{Cd}(\text{NO}_3)_2$  under the same synthetic method but differing metal to ligand ratio which were 1:1 and 1:2 to provide compound 1 and compound 2, respectively. The coordination environment of these compounds are different as shown in Scheme 2.6.



**Scheme 2.6** Coordination environment of cadmium and 3D-net in compound 1 and 2<sup>(48)</sup>

### 2.3.4 Solvents

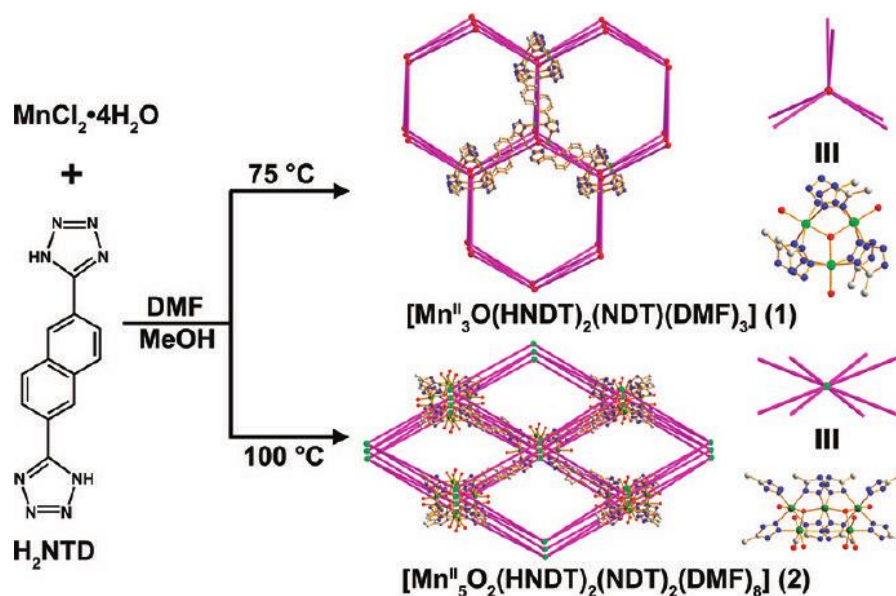
The solvent system often greatly affects the formation of MOFs which consequently affects their properties. In general, highly polar organic solvents such as, DMF, DEF, DMA and EtOH as well as water are used in the synthesis of MOFs in order to dissolve the high polar organic linker and metal salts. The solvent not only acts as a solvate but also as a directing agent. For example, Suh and co-worker<sup>(49)</sup> prepared new MOFs,  $[\text{Zn}_4\text{O}(\text{NTB})_2]_n \cdot 3n\text{DEF} \cdot n\text{EtOH}$ , from  $\text{Zn}(\text{NO}_3)_2 \cdot 6\text{H}_2\text{O}$  and  $\text{H}_3\text{NTB}$  (4,4',4''-nitrilotrisbenzoic acid) in a mixed solvent of DEF, EtOH and  $\text{H}_2\text{O}$ . For this structure,  $\text{Zn}_4\text{O}(\text{CO}_2)_6$  octahedral SBUs were linked by the  $\text{NTB}_3$  units to form PdF<sub>2</sub> type (3,6) connected nets. The removal of guest solvent molecules did not destroy its single crystal nature and the activated framework  $[\text{Zn}_4\text{O}(\text{NTB})_2]_n$  exhibited permanent porosity. In the case of the one solvent system consisted only EtOH under the similar solvothermal synthesis, a 3D network  $[\text{Zn}_3(\text{NTB})_2(\text{EtOH})_2]_n \cdot 4n\text{EtOH}$  was obtained. The frameworks released the coordinated EtOH as well as guest EtOH molecules to give the de-solvated sample,  $[\text{Zn}_3(\text{NTB})_2]_n$  which retained the single crystallinity as shown in Scheme 2.7.



**Scheme 2.7** Two different frameworks prepared from Zn(II) and  $\text{NTB}_3$  in the different solvent systems. (a) Structure of  $[\text{Zn}_4\text{O}(\text{NTB})_2]_n \cdot 3n\text{DEF} \cdot n\text{EtOH}$  prepared from DEF/EtOH/ $\text{H}_2\text{O}$  (5:3:2, v/v) mixture. (b) The framework structure of  $[\text{Zn}_3(\text{NTB})_2(\text{EtOH})_2]_n \cdot 4n\text{EtOH}$  prepared from EtOH.<sup>(23)</sup>

### 2.3.5 Temperature

The reaction temperature also play a vital role on the construction of MOFs. This factor affect the crystalline growth. In the reaction both organic linkers and metal ions are solvated. Temperature would effect the reaction rate that provide crystalline frameworks. Furthermore, SBUs generated in the different reaction temperatures will result in different coordination modes between metal node and linkers. Therefore, using the different reaction temperature may provide different resulting framework as shown in scheme 2.8. The synthesis of metal-organic framework using tetrazole derivative (H<sub>2</sub>NTD) and MnCl<sub>2</sub>·4H<sub>2</sub>O in a mixture of DMF and MeOH at two slightly different reaction temperature, 75 and 100 °C<sup>(50)</sup> provided two different crystal structures, [Mn<sup>II</sup><sub>3</sub>O(HNDT)<sub>2</sub>(NDT)(DMF)<sub>3</sub>](1) and [Mn<sup>II</sup><sub>5</sub>O<sub>2</sub>(HNDT)<sub>2</sub>(NDT)<sub>2</sub>(DMF)<sub>8</sub>](2). Their crystal structures demonstrated that they had different coordination environment of the metal centers.



**Scheme 2.8** The resulting MOFs from the same reaction with different temperatures<sup>(50)</sup>



### 2.3.6 pHs

The reaction pH is one of the important factors in the formation of the coordination polymer. Normally, the organic linkers contained carboxylic acid group which deprotonate and react with the metal center. Therefore, if the rate of deprotonation is too fast, it might effect to the coordination of organic linker anions with metal ions without the formation of crystalline solids.

In 2008, Liu at el.<sup>(51)</sup> have reported the five new metal-organic frameworks based on multi-carboxylate ligands and a chelate ligand by hydrothermal reactions via a different reaction pH. The resulting frameworks have been investigated by X-ray single crystal diffraction technique. The differences of the five metal-organic frameworks reveal that the reaction pH play an important effect on the structure of these complexes. Additionally, the lower reaction pH tends to form complicated framework than the higher one.

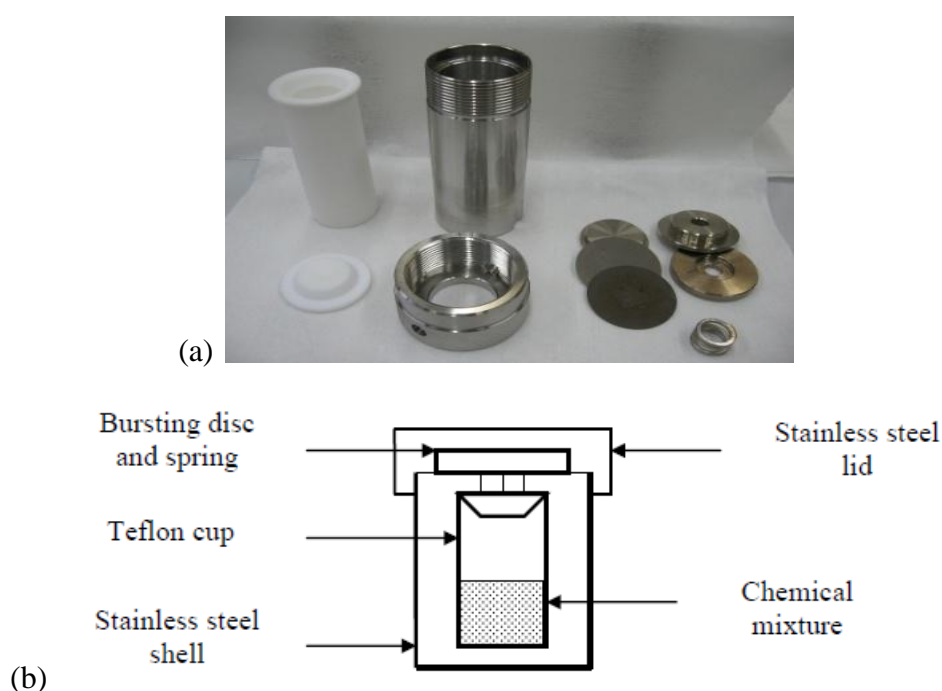
## 2.4 Synthetic methods of metal-organic frameworks

In general, MOFs were synthesized from solvothermal reactions with metal and organic building blocks in organic solvents that have high boiling points such as DMF and DEF. Furthermore, there are other methods reported for preparation of MOFs which can provide the new MOFs with fascinating structures and useful properties as well as it can be used as alternative method for cases that cannot prepare from conventional techniques, for example, ionothermal synthesis, microwave assisted-MOFs synthesis, and mechanochemical synthesis.

### 2.4.1 Hydrothermal/solvothermal synthesis

Hydrothermal/solvothermal synthesis technique are the popular method to prepare MOFs material due to the simple instrument and the easy operation. This method consists of the various techniques for crystallizing substances at high-reaction temperature and high vapour pressures. Most reported MOFs were synthesized via solvothermal and hydrothermal synthetic methods<sup>(52)</sup>, often by using sealed vessel such as a Teflon-lined stainless steel autoclave (Figure 2.13). Hydrothermal synthesis which uses water as the solvent and solvothermal synthesis that uses other solvents except water as solvents. Not only the pure solvent but mixtures of water and other

solvents also have been employed to synthesize various MOFs<sup>(53)</sup>. Hydrothermal techniques play a significant role in preparing robust and stable MOF materials. The solubility of the reactants increases under high temperature hydrothermal methods causing the reaction to occur at lower temperatures than is expected. This techniques enables the formation of polymeric units through molecular building blocks. However, the reaction variables, such as the solvent type, temperature, time, and pH can influence the product.

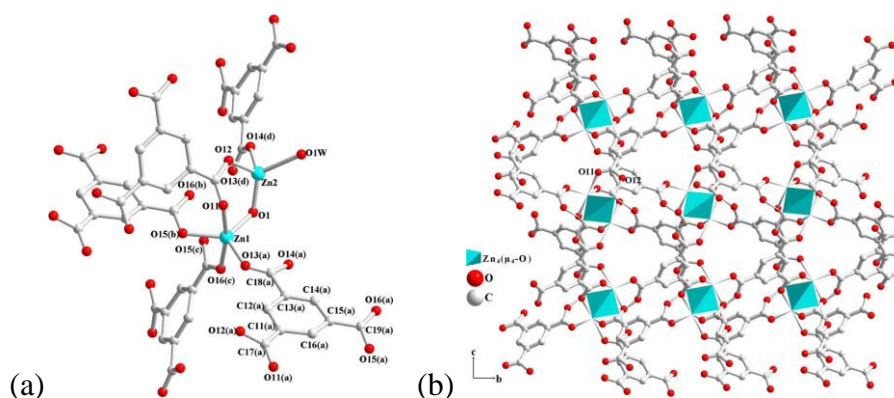


**Figure 2.13** (a) A Teflon-lined stainless steel autoclave<sup>(54)</sup> (b) Setting of autoclave<sup>(55)</sup>.

#### 2.4.2 Ionothermal synthesis

Ionothermal synthesis<sup>(56)</sup> is a subclass of the solvothermal syntheses in which ionic liquids are used as solvents, structure directing agents, templates, and charge-compensating agents. Ionic liquids (ILs) are a class of the organic solvent consisting of cations and anions. There are a lot of examples in which ILs have been successfully applied to the construction of new metal-organic frameworks (MOFs). Physical properties of ILs such as variation of the length of the alkyl group on the imidazolium cation can be tailored. With the increase of the alkyl chain length, the viscosity of the IL also increases but the melting point decreases. However, this trend

is reverted when there are more than seven carbons in the alkyl chain. In addition, these ionic liquids can be recycled for further use. In many cases, ionothermal synthesis frequently give novel materials, which can not (or not easily) be prepared by conventional method. For example,  $[\text{Zn}_4(\text{BTC})_2(\mu_4\text{-O})(\text{H}_2\text{O})_2]$  compound<sup>(57)</sup> was synthesized by using  $\text{Zn}(\text{NO}_3)_2 \cdot 6\text{H}_2\text{O}$  and 1,3,5-benzenetricarboxylic acid ( $\text{H}_3\text{BTC}$ ) via ionothermal approach in 1-ethyl-3-methylimidazolium bromide ionic liquid as reaction media. This compound features in 3D framework constructed by linking  $[\text{Zn}_4(\mu_4\text{-O})]$  subunits with  $\text{BTC}^{3-}$  ligands. They consist of two five-coordinated and two four-coordinated  $\text{Zn}^{2+}$  ions, different from the  $[\text{Zn}_4(\mu_4\text{-O})]$  units of other MOFs as shown in Figure 2.14.



**Figure 2.14** (a) Coordination spheres of zinc atoms, (b) 3-D framework of the  $[\text{Zn}_4(\text{BTC})_2(\mu_4\text{-O})(\text{H}_2\text{O})_2]$  compound<sup>(57)</sup>.

### 2.4.3 Microwave assisted-MOFs synthesis

Most metal–organic frameworks (MOFs) are synthesized in molecular solvents under hydrothermal/solvothermal conditions or by slow solution diffusion methods which take a long time (nearly 1/2 day to several days) for a reaction cycle. Microwave-assisted<sup>(58)</sup> solvothermal method has been used as a means of accelerating the chemical reaction rate approach to perform high speed synthesis in under seconds to minutes. This method has been successfully applied to synthesis coordination polymers with known structures. The properties of the crystals prepared by the microwave-assisted process are of the same quality as those produced by the standard solvothermal process. Although, most cases, the microwave method cannot give

crystals with a size suitable for single X-ray analysis, its homogeneous effects could generate a uniform seeding condition so that the size and shape of the crystals can be well controlled and the synthesis cycle can be largely shortened for many practical applications. Recently, there has been a report<sup>(59)</sup> of the formation of unknown MOFs under controlled heat and pressure via microwave heating process which yields crystals with a size big enough for single X-ray analysis

#### 2.4.4 Mechanochemical synthesis

Mechanochemical<sup>(60)</sup> synthesis is also known as grinding conditions. In this method, the solvents are not required. The organic linker and hydrated metal salts are placed in a stainless steel vessel with a ball mill, mixed and grinded in a ball mill mixer (Figure 2.15) to provide the desired MOFs. In some cases, the acetate anion of metal salts produced acetic acid as a side-product in the reactions which might promote reaction by the solvent effect. The presence of acetic acid in the pores of MOFs usually found but it can be easily removed by heating under vacuum.

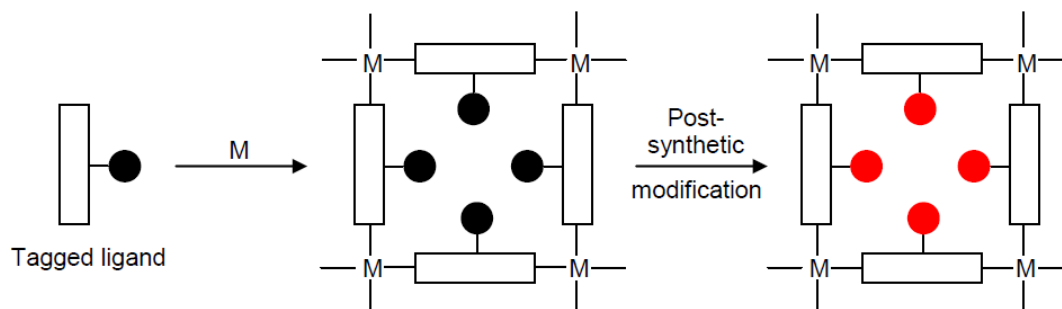


**Figure 2.15** Ball mill: stainless steel vessel with a ball bearing.<sup>(61)</sup>

In addition, The grinding conditions with the presence of a small amount of solvents can be done. This approach known as liquid assisted grinding or LGA. In 2010, Yuan *et al.*<sup>(62)</sup> reported the preparation of MOFs by using this method. Their finding revealed that the structure of MOFs changed to other structures under grinding conditions with a small amount of solvents.

## 2.5 Post-Synthetic Modification

Most metal-organic frameworks are generally obtained in one-pot reaction which use the commercially available ligands due to ease to synthesis. In recent years there are many synthetic organic linkers reported in the literature. The functionality can be introduced to these organic linkers which may provide the useful for specific applications. However, some functional group cannot survive under MOF synthesis conditions (e.g., temperature, pH). In some cases, the present of functional group do not provide the desire framework because it often competes with the donor group of organic linkers. For these reason post-synthetic modification (PSM) approach has been developed<sup>(63)</sup>. This strategy uses the bridging ligands with the presence of an additional functional group or a tag. The definition of tag is a group or functionality that is stable enough to retain during the MOF synthesis and do not involve in coordinate to the metal center, but can be transformed by the post-synthetic modification. This approach is demonstrated in Scheme 2.9.

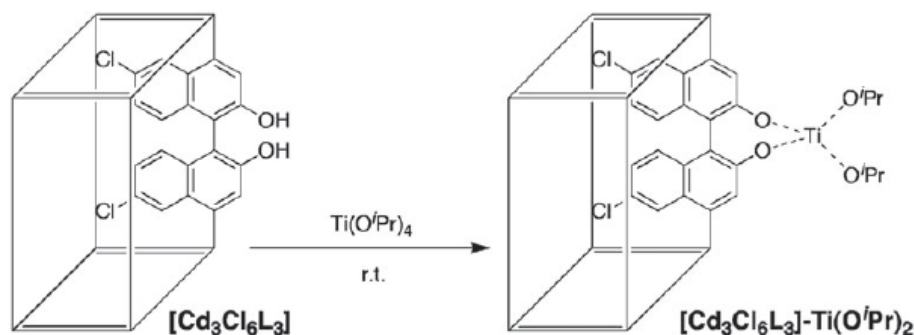


**Scheme 2.9** Post-synthetic modification (PSM) of MOFs<sup>(64)</sup>

This synthetic method allows the pore within a preformed MOF to be tailored for the specific applications in order to “tune” the material for selective adsorption<sup>(65)</sup>, catalysis<sup>(66)</sup> as well as can be provided the MOF materials which could not be prepared from the direct synthesis. Post-synthetic modification can be done by non-covalent interactions, coordinative interactions and covalent bonds<sup>(67)</sup>.

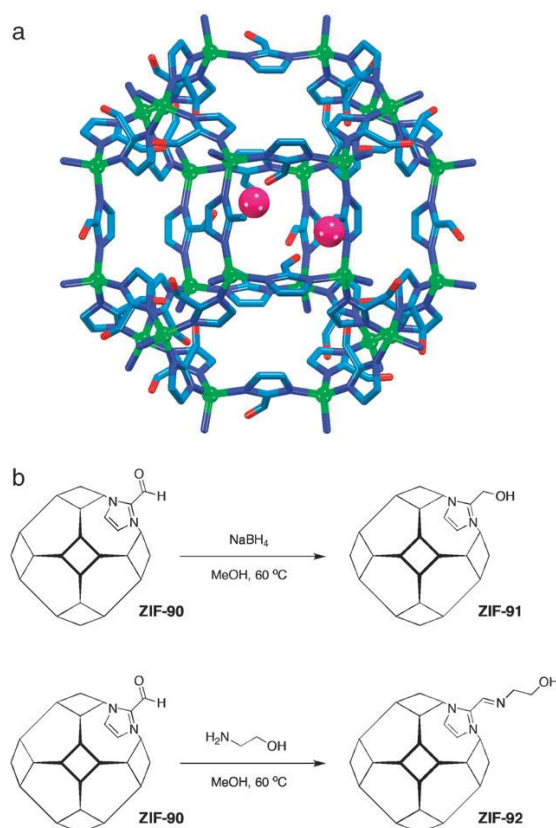
The use of post-synthetic modification approach by coordinative interactions have been reported, Lin *et al.*<sup>(68)</sup> prepared  $[\text{Cd}_3\text{Cl}_6\text{L}_3]$  compound from Cd(II) ion and 1,1'-bi-2-naphthol as bridging ligand in which the hydroxy groups do not incorporate in the coordination of metal ions. Then  $[\text{Cd}_3\text{Cl}_6\text{L}_3]$  compound was placed in the

solution of  $\text{Ti}(\text{O}^i\text{Pr})_4$  at room temperature to give the complex  $[\text{Cd}_3\text{Cl}_6\text{L}_3]-\text{Ti}(\text{O}^i\text{Pr})_2$  which was used as Lewis-acid catalyst as shown in Scheme 2.10.



**Scheme 2.10** Post-synthetic modification of MOFs with metal ion complexes<sup>(68)</sup>

The covalent transformations of preformed MOFs are reported by using various reactions that they are suitable for MOFs modification, such as condensation of amine and aldehyde<sup>(69)</sup>, click reaction<sup>(70)</sup>, amide coupling<sup>(71)</sup>, urea formation<sup>(72)</sup>, tandem reaction<sup>(73)</sup> etc. Yaghi *et al.*<sup>(74)</sup> synthesized a sodalite-like zeolitic imidazolate framework (ZIF), ZIF-90 by using Zn(II) ion and imidazolate-2-carboxyaldehyde. The introduction of the free aldehyde functional group within the pores of framework permits the covalent modification. ZIF-90 was reacted with ethanolamine to give imine group in the framework, ZIF-92. The reaction completed within 3 hours as confirmed by  $^{13}\text{C}$  CP-MAS NMR and FTIR spectroscopy. The PXRD pattern showed the retained crystallinity of the imine-functionalized ZIF-92. However,  $\text{N}_2$  adsorption measurements showed an extremely low uptake due to the presence of functional group possessing severe constriction of the pore aperture. Furthermore, ZIF-90 is very high thermal and chemical stability which allowed the framework to be modified under relatively harsh reaction conditions. The reduction of free aldehyde group by using  $\text{NaBH}_4$  in methanol at  $60\text{ }^\circ\text{C}$  for 24 h to yield an alcohol, ZIF-91 which crystallinity and porosity was well maintained with only a slightly decrease in surface area. The modification of ZIF-90 illustrated in Scheme 2.11.



**Scheme 2.11** (a) The structural representation of ZIF-90 (b) Scheme of the post-synthetic modification reactions described for ZIF-90.

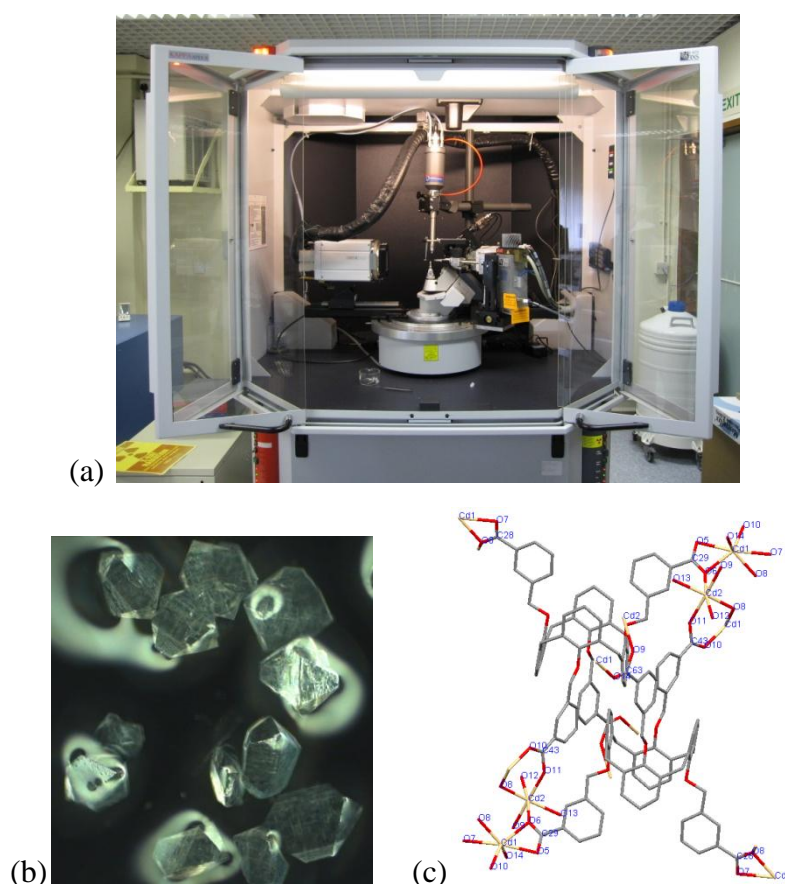
## 2.6 Characterization and properties study of MOFs

Metal-organic frameworks (MOFs) are porous solid materials. The structural characterization of the obtained MOFs required many techniques and their properties which normally use the following techniques:

- (a) Single-crystal X-ray diffraction (sc-XRD)
- (b) Powder X-ray diffraction (XRD)
- (c) Scanning electron microscopy (SEM)
- (d) Fourier Transform Infrared Spectroscopy (FT-IR)
- (e) Nitrogen adsorption-desorption
- (f) CHNS/O Elemental analysis (EA)
- (g) Thermogravimetric Analysis (TGA)

### 2.6.1 Single-crystal X-ray diffraction (sc-XRD)

The atomic structure of the resulting MOFs are investigated by single-crystal X-ray diffraction techniques. The sample MOF have to be a single-crystal which can be used with this instrument. Therefore, the crystallization of MOFs are required which not be easy to get single-crystal MOFs. Figure 2.16 demonstrates the instrument of single-crystal X-ray diffractometer, a sample of MOFs and an example of the structure examined by this techniques.



**Figure 2.16** (a) single-crystal X-ray diffractometer <sup>(75)</sup>

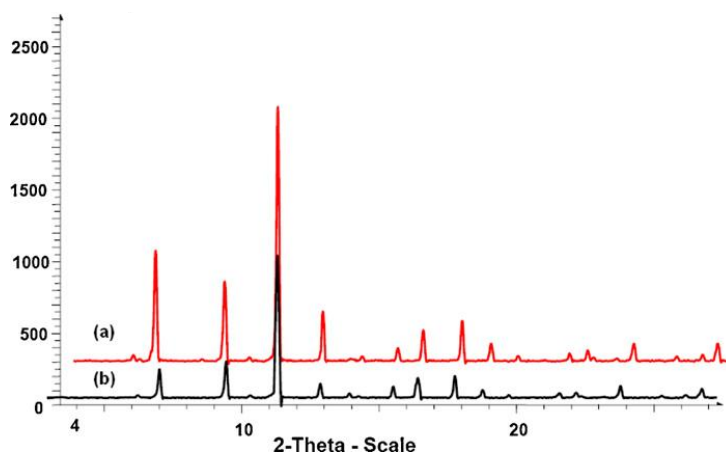
(b) example single-crystal of MOFs (c) single-crystal structure of MOFs.

### 2.6.2 Powder X-ray diffraction (PXRD)

MOFs generally exhibited the property of crystalline materials. Their purity phases were examined by powder X-ray diffraction (XRD) techniques. The powder X-ray diffraction patterns of crystalline materials showed sharp peak with high intensity, while that of amorphous materials is broad. Furthermore, this



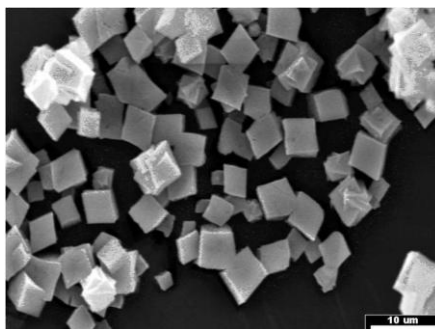
technique is used to characterize and confirm the identity of the obtained MOFs. XRD patterns act as fingerprints of the synthesized MOFs. Figure 2.17 shows an example of powder X-ray diffraction patterns of MOFs. Comparing the XRD pattern of MOF-199 (a) and after used in catalytic application (b).



**Figure 2.17** Powder XRD pattern of the fresh (a) and reused (b) MOF-199<sup>(76)</sup>.

### 2.6.3 Scanning electron microscopy (SEM)

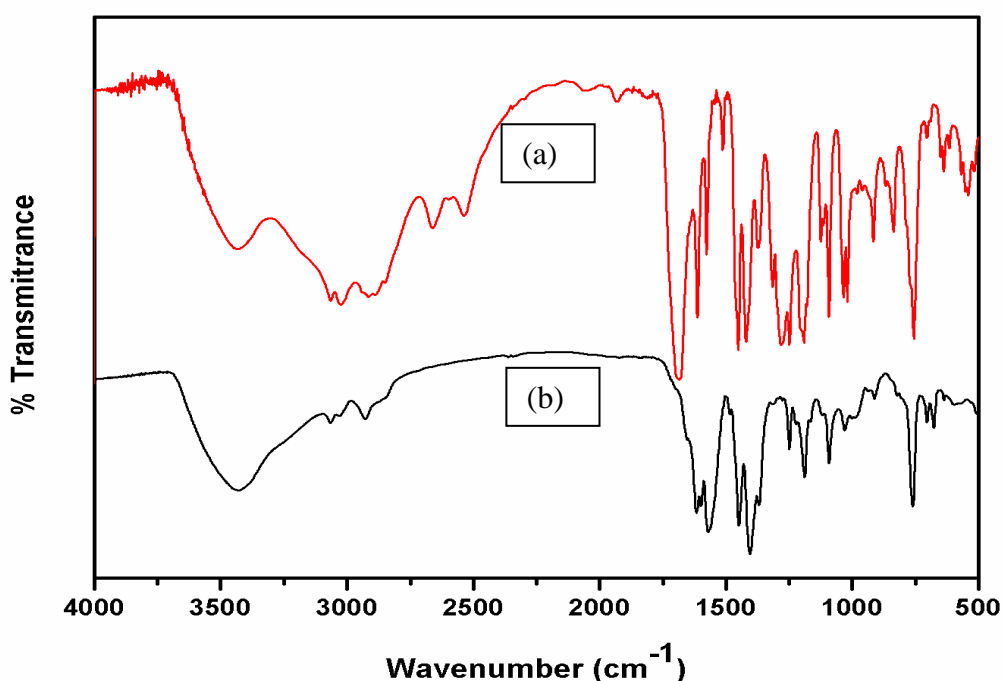
The morphology and particle size of metal-organic frameworks are analyzed by scanning electron microscopy (SEM). The samples suitable for this technique should have the conductivity in order to obtain the clearly images. In the case of samples having low conductivity, they should be coated with sputtering gold before the SEM measurement to generate an electrically conductive surface, Figure 2.18.



**Figure 2.18** SEM image of MOF-5 was prepared from microwave-assisted method<sup>(77)</sup>

#### 2.6.4 Fourier Transform Infrared Spectroscopy (FT-IR)

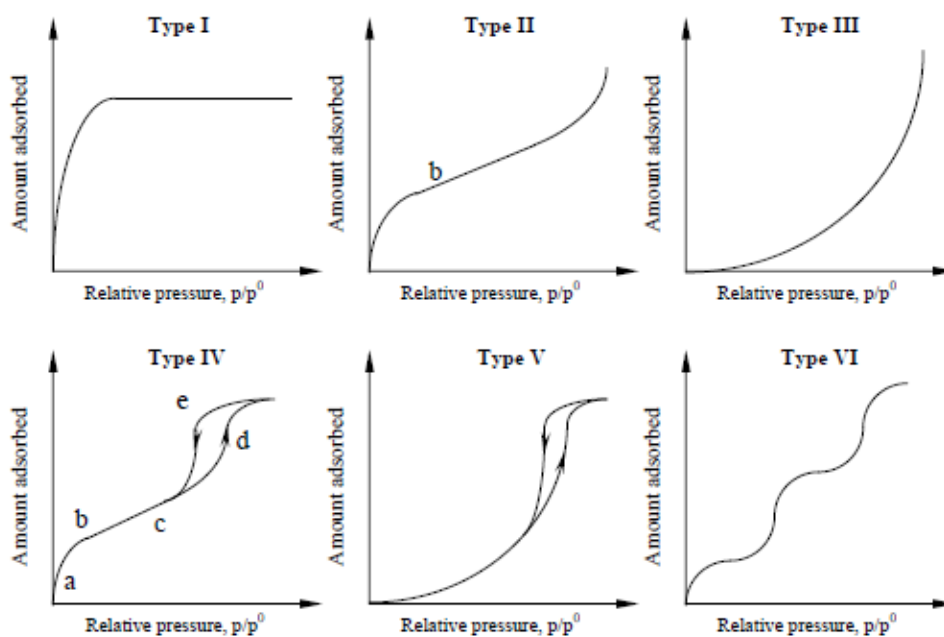
The formation of coordination bonds between functional groups of ligands and metal ions is characterized by fourier transform infrared spectroscopy (FT-IR). The original vibrational wave number of functional groups of organic linkers are shift to new wave number when complexes were formed<sup>(78)</sup>. Figure 2.19 showed an example of compared IR spectra of carboxylate organic linker (a) and MOFs-based carboxylate (b).



**Figure 2.19** Example of compared IR spectra of carboxylate organic linker (a) and MOFs-based carboxylate (b).

#### 2.6.5 Nitrogen adsorption-desorption

The Nitrogen adsorption-desorption technique is used to investigate the physical properties of porous materials, such as surface area, pore volume, pore diameter and pore size distribution. One of important data from this technique is adsorption-desorption isotherm which use to classify the type of materials. There are six types of adsorption-desorption isotherm as shown in Figure 2.20<sup>(79)</sup>. Table 2.1 illustrates pore sizes and gas sorption isotherms that reflected the relationship between porosity and sorption properties which have been proposed by IUPAC conventions<sup>(80)</sup>.



**Figure 2.20** Six types of adsorption isotherm<sup>(79)</sup>.

**Table 2.1** IUPAC classification of pores.

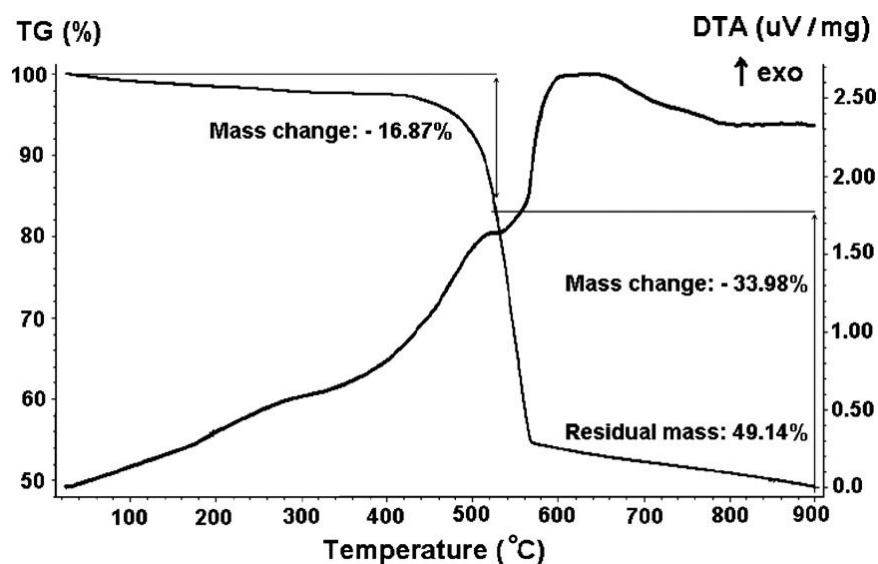
Type	Features	
	Interaction between sample surface and gas adsorbate	Porosity
I	Relatively strong	Microporous
II	Relatively strong	Nonporous
III	weak	Nonporous
IV	Relatively strong	Mesoporous
V	weak	Microporous or Mesoporous
VI	Relatively strong sample surface has an even distribution of energy	Nonporous

### 2.6.6 Elemental analysis (EA)

The amount of atomic content as well as the purity of organic compound and metal-organic framework are confirmed by elemental analysis (EA). This technique reveals the amount of (%) of carbon, hydrogen, nitrogen, sulphur and oxygen of the sample comparing with the calculated percentage of their chemical formula.

### 2.6.7 Thermogravimetric Analysis (TGA)

Thermal stability of MOFs are tested by thermogravimetric analysis (TGA) which measures the change in amount of sample under increasing temperature. Generally, temperatures are in range room temperature to 1000 °C which reveal the decomposition of the sample. For metal-organic frameworks possessing a number of pore which solvent are captured in their pore as result in the decomposition of solvent molecules. The data of thermogravimetric analysis is important can help to chose the appropriately pretreated temperature of MOFs before nitrogen adsorption-desorption study. Figure 2.21 shows an example thermogram of MOFs.



**Figure 2.21** An example thermogram of MOF-5<sup>(81)</sup>.

## 2.7 Applications of metal-organic frameworks

MOFs have received a great deal of considerable attention due to their high surface area and large pore volume. Their structure can be tunable or modified to the desired structures which provide the specific purposed applications and unique properties leading to MOFs have adopted in many areas as follows.

### 1. Gas storage

The challenging of the using energy from H<sub>2</sub> is the storage system that must be safe, efficient and economic. The ideas of using porous materials have been developed. Among the porous materials, MOFs have much attracting attention. There are a number MOF materials reported for using as hydrogen storage<sup>(82)</sup>.

### 2. Heterogenous catalyst

In recent years, there are a number of MOFs been successfully used as catalyst. Using MOFs as heterogeneous catalysts have several advantages such as recoverable, reusable, and environmentally friendly. MOFs have been employed as solid catalysts or catalyst supports for a variety of organic transformations such as Friedel–Crafts alkylation and acylation, cyanosilylation, aza-Michael condensation, hydrogenation, Suzuki cross-coupling, Sonogashira reaction, transesterification reaction, Knoevenagel condensation, aldol condensation, epoxide ring-opening reaction etc<sup>(83, 84)</sup>.

### 3. Gas separation,

A number of availability building blocks of both metal ions and organic linkers let it possible to construct novel MOFs with various structures, topologies, and porosity. These features can be applied in separation science. MOFs have been used as the stationary phase in the capillary column of the gas chromatography<sup>(85)</sup>.

### 4. Luminescence,

The luminescence properties of MOFs can be came from both metal center and bridging ligands<sup>(86, 87)</sup>. The organic linkers can exhibit their luminescence properties. Therefore, MOFs which prepared from luminescence organic linkers would also show these properties. Not only organic linkers but metal center can also incorporate into the luminescence phenomenon, mostly from lanthanide metal ions. Luminescence properties of MOFs and other characteristic features can be used in sensor applications<sup>(88)</sup>.

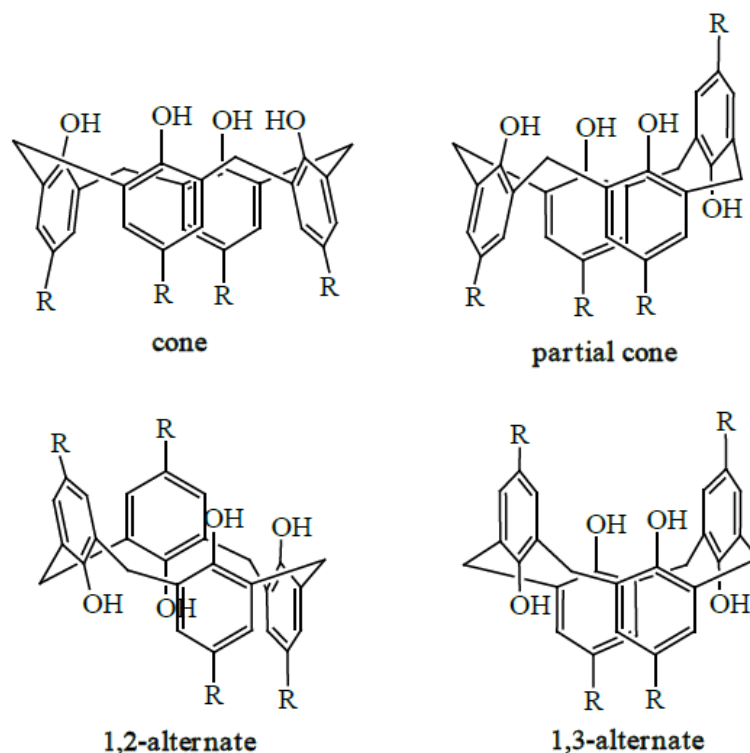
## 5. Biological and medical applications

The stability of MOFs is another issue often regarding for the potential applications. Normally, MOFs are relative poor stability in hydrolytic condition. MOFs can be used in biological systems as long as they retain intact long enough to finish their functions<sup>(89)</sup>.

### 2.8 Calix[4]arene-Based Organic linkers

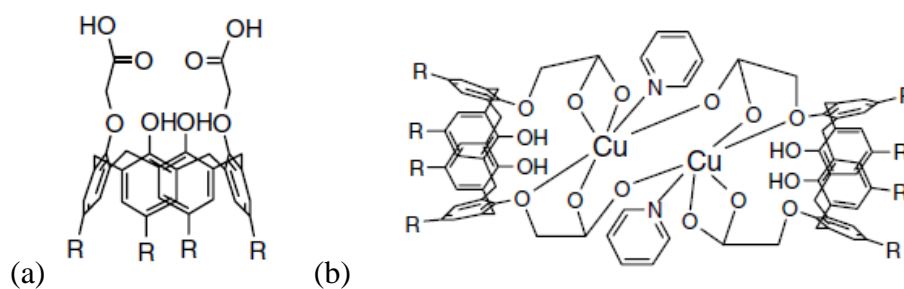
Calix[4]arene has been used as building blocks in supramolecular chemistry. It was synthesized from the condensation of formaldehyde and *p-tert*-butylphenol via base catalyzed. Its structure is a cavity-shaped cyclic molecule like a beaker shape and can be modified easily with many kind of functional groups which many researchers have functionalized calix[4]arene for using as chemical sensors<sup>(90)</sup>.

In the solution, there are four conformation isomer of calix[4]arene<sup>(91)</sup>: are cone, partial cone, 1,2-alternate and 1,3-alternate as displayed in figure 2.22. Each of them have a specific characteristic property which can chose for the appropriate applications. The functionalize of calix[4]arene at the phenol sites provide many calix[4]arene derivatives which the chemical used can control the desire conformation of them. For example, using KOH normally yields the 1,3-alternate calix[4]arene which in the case of NaOH mostly give cone conformation<sup>(92)</sup>.



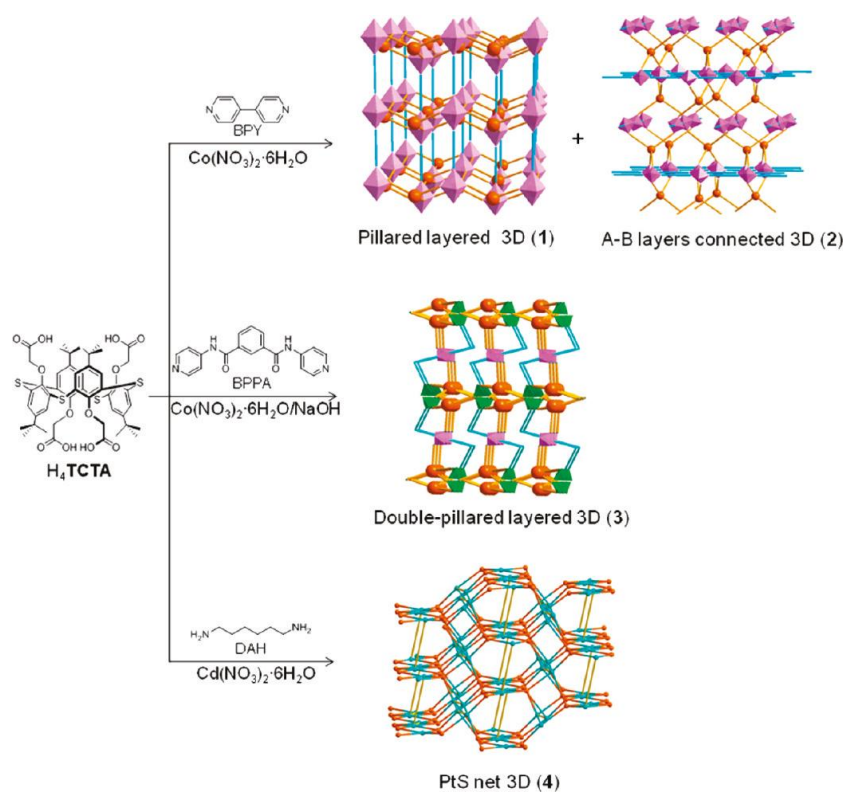
**Figure 2.22** Conformations of calix[4]arene.

There are a few reports which used calix[4]arene as organic linker for preparing of metal-organic frameworks. Among their conformation isomers, 1,3 alternate is interesting due to its can be functionalized to be a divergent ligands which might provide the new MOFs with a specific properties owing to its nature characteristic. In 2004, Ali *et al.*<sup>(93)</sup> synthesized calix[4]arene-1,3-dicarboxylic acid as cone conformational isomer. The complexation of calix[4]arene-1,3-dicarboxylic acid with  $\text{Cu}^{2+}$  ion yielded a dimer coordination as illustrated in Figure 2.23.



**Figure 2.23** (a) A *p*-tert-butyl-calix[4]arene-1,3-diacid ( $\text{H}_4\text{L}$ ) (b) The proposed structure of complex between  $\text{H}_4\text{L}$  and  $\text{Cu}^{2+}$  ion

In 2011, Kim *et al.*<sup>(94)</sup> have reported four novel MOFs which synthesized from tetracarboxylic acid 1,3-alternate thiacalix[4]arene and N-donor ligands as co-ligand with various metal ions under solvothermal synthesis method as shown in scheme 2.12.



**Scheme 2.12** The synthesis routes of 3D Network of four novel MOFs-based thiacalix[4]arene<sup>(94)</sup>.

Form these example data supported that 1,3 alternate calix[4]arene might be better building block than other conformers to use as organic linkers in the preparing MOFs.



## CHAPTER III

### EXPERIMENTAL

#### 3.1 Analytical Instruments

All reagents as analytical grade were used as received without further purification. Commercial grade solvents were purified by distillation. Anhydrous solvents were dried over  $\text{CaH}_2$  and freshly distilled under nitrogen atmosphere. Calix[4]arene was prepared following literature procedures.<sup>(95)</sup> Thin layer chromatography (TLC) was performed on silica gel plates (Kieselgel 60, F<sub>254</sub>, 1 mm).

$^1\text{H}$  NMR and  $^{13}\text{C}$  NMR spectra were obtained in deuterated chloroform ( $\text{CDCl}_3$ ), hexadeuterated dimethylsulfoxide ( $\text{DMSO-}d_6$ ) using Varian Mercury plus 400 MHz NMR (Varian Company, CA, USA) and Bruker Avance 400 MHz (Bruker company, Germany) NMR spectrometers operated at 400 MHz for  $^1\text{H}$  and 100 MHz for  $^{13}\text{C}$  nuclei. Chemical shifts ( $\delta$ ) are reported in parts per million (ppm) relative to the residual  $\text{CHCl}_3$  peak (7.26 ppm for  $^1\text{H}$  NMR and 77.16 ppm for  $^{13}\text{C}$  NMR), and  $\text{DMSO-}d_6$  peak (2.50 ppm for  $^1\text{H}$  NMR and 39.52 ppm for  $^{13}\text{C}$  NMR). Coupling constants (J) are reported in Hertz (Hz).

Mass spectra were obtained using a matrix-assisted laser desorption ionization mass spectrometry (MALDI-MS) (Bruker Microflex MALDI-TOF mass spectrometer, Bruker company, Germany) technique by using 2-cyano-4-hydroxycinnamic acid (CCA) and dithranol as a matrix.

Infrared (IR) spectra were performed on a Nicolet Impact 412 FT-IR spectrophotometer (Thermo Fisher Scientific Company, USA) using KBr disk method. The samples were scanned over a range of 500-4000  $\text{cm}^{-1}$  at a resolution of 4  $\text{cm}^{-1}$  and a number of scan was 32. The measurement was controlled by OMNIC software.

The X-ray powder diffractometer was used for investigation of the phase purity and structure of samples. The XRD patterns were collected on a Rigaku, D/max

2200/ultima plus X-ray powder diffractometer (Rigaku company, Japan) with a monochromator and Cu K $\alpha$  radiation (40kV, 30mA). The 2-theta angle was ranged from 3 to 30 degree with scan speed of 3 degree/min and sampling width of 0.02 degree. The scattering slit, divergent slit and receiving slit were fixed at 0.5 degree, 0.5 degree and 0.3 mm, respectively. The measured diffractograms were analyzed using MDI software (Jade 6.5)

JEOL JSM-6480LV scanning electron microscope (SEM) (JEOL Ltd. company, Japan) was used to identify the morphology and particle size of samples. The samples were dispersed on the carbon tape, depositing on the target, and coated with sputtering gold under vacuum prior to the SEM measurement to provide an electrically conductive surface.

Nitrogen adsorption-desorption isotherms of materials were performed in a BELSORP-II instrument (BELSORP-mini II, BEL Japan Inc. company, Japan). The materials were pretreated at 250°C for 3 hours before the surface area measurement. Surface area and micropore volume of the material were calculated by the BET equation. The external surface areas were obtained from the analysis of adsorption branch of the isotherm by the t-plot method.

Elemental analysis was obtained by CHNS/O Analyzer, Perkin Elmer PE2400 Series II (Perkin Elmer, Inc. company, USA).

Thermogravimetric analysis (TGA) was performed by using Netzsch STA 409 thermogravimetric analyzer (Netzsch company, Germany) that was heated from 25 °C to 1000°C at heating rate of 10°C/min under nitrogen gas. The result of thermal stability was reported in percentage weight residue of sample.

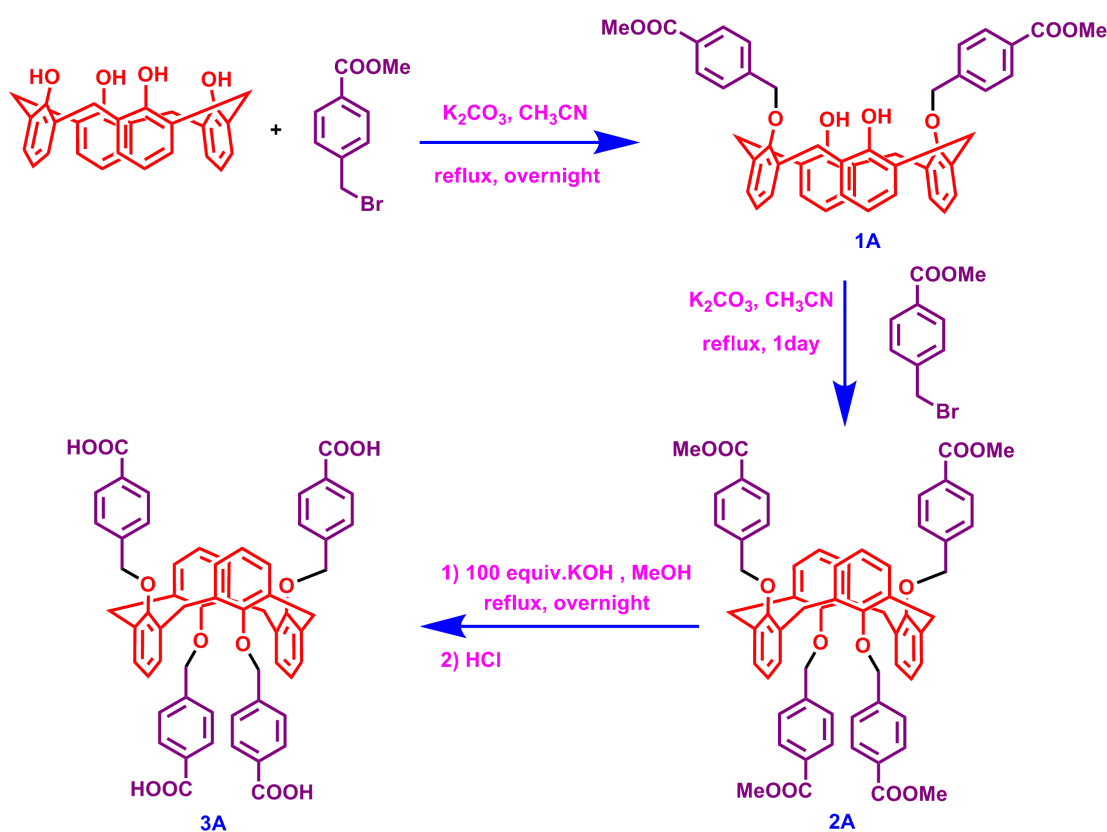
Crystal Data were obtained by Bruker Smart CCD diffractometer. (Bruker X8 APEX, Bruker company, Germany)

### 3.2 Experimental Procedure

The experimental section of thesis are divided in three parts. The first part concerns synthesis of the calix[4]arene derivatives for using as organic linkers. The second part focuses on the synthesis of 1,3-alternate calix[4]arene-based metal-organic frameworks and the final part describes a preliminary catalytic property study of the obtained metal-organic frameworks in selected reactions.

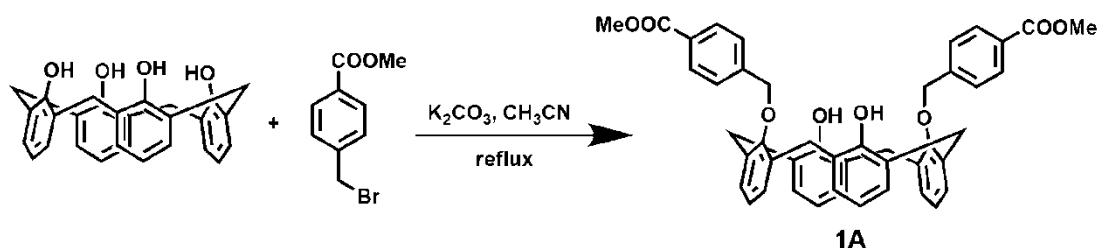
#### 3.2.1 Synthesis of Organic linkers

##### 3.2.1.1 Synthesis of 1,3-alternate calix[4]arene tetra-*p*-benzoic acid (3A)



**Scheme 3.1.** Synthetic pathway of 1,3-alternate calix[4]arene tetra-*p*-benzoic acid (3A)

### 3.2.1.1.1 Synthesis of 1,3-dimethyl-*p*-benzoate calix[4]arene (**1A**)



Into a 100 mL two-necked round-bottom flask, calix[4]arene (0.531 g, 1.25 mmol) and potassium carbonate ( $K_2CO_3$ ) (0.691 g, 6.25 mmol) in dried acetonitrile (30 mL) were charged and refluxed with stirring under nitrogen atmosphere for 1 hr. A solution of methyl-4-(bromomethyl)benzoate (0.573 g, 2.5 mmol) in dried acetonitrile (10 mL) was added. The reaction mixture was refluxed overnight. Potassium carbonate was filtered off. The mixture was diluted with dichloromethane (20 mL), washed with aqueous 3M HCl (10 mL) and washed with water ( $3 \times 10$  mL) and brine ( $3 \times 10$  mL). The organic layer was dried with anhydrous  $Na_2SO_4$ , and concentrated under reduced pressure. The product was precipitated by methanol. The white solid was filtered and washed with methanol to obtain the desired product (**1A**) (0.664 g, 73%).

#### Characterization data for compound **1A**:

**$^1H$  NMR spectrum (400 MHz,  $CDCl_3$ ):**  $\delta$  7.98 (d,  $J = 8.0$  Hz, 4H, Ar-*H*), 7.81 (d,  $J = 6.4$  Hz, 4H, Ar-*H*), 7.06 (d,  $J = 7.6$  Hz, 4H, Ar-*H*), 6.91 (d,  $J = 7.2$  Hz, 4H, Ar-*H*), 6.78 (t,  $J = 7.6$  Hz, 2H, Ar-*H*), 6.66 (t,  $J = 7.6$  Hz, 2H, Ar-*H*), 5.13 (s, 4H, Ar $CH_2O$ ), 4.28 (d,  $J = 13.2$  Hz, 4H, Ar $CH_2Ar$ ), 3.92 (s, 6H, Ar $COOCH_3$ ), 3.36 (d,  $J = 13.2$  Hz, 4H, Ar $CH_2Ar$ );

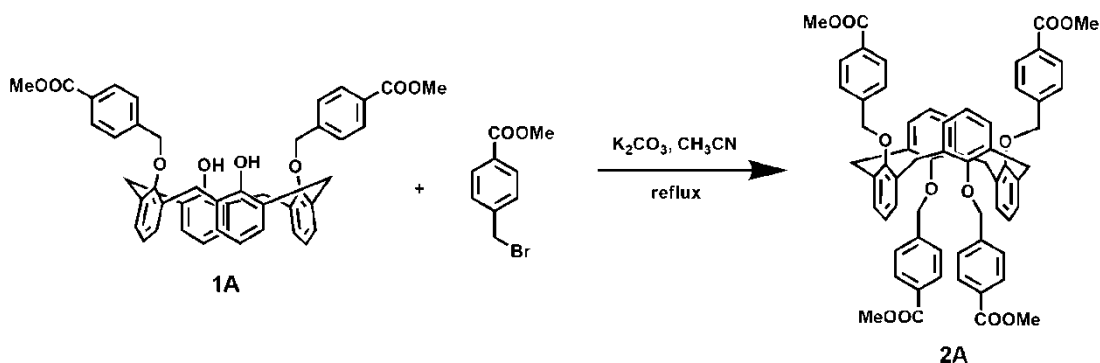
**$^{13}C$  NMR spectrum (100 MHz,  $CDCl_3$ ):**  $\delta$  166.8, 153.2, 151.7, 141.8, 133.0, 130.1, 129.8, 129.2, 128.6, 127.8, 126.9, 125.7, 119.2, 77.6, 52.1, 31.4;

**IR (Nujol):** ( $\nu_{max}$ ,  $cm^{-1}$ ) 3373 (br m, O-H stretching), 2924 (s, C-H stretching), 1722 (s, C=O, stretching), 1612 (m, C=C stretching), 1463 (s, C-H bending), 1279, 1197, 1108 (s, C-O stretching), 756 (s, C-H out of plane bending).

**Elemental analysis:** Anal. Calcd for  $C_{46}H_{40}O_8$  C, 76.65; H, 5.59; O, 17.76 Found C, 76.52; H, 5.43; O 18.05.

**High mass analysis:** Anal. Calcd for  $[C_{46}H_{40}O_8 + Na^+]$ : 743.2615 Found 743.2634.

### 3.2.1.1.2 Synthesis of 1,3-alternate calix[4]arene tetra methyl-*p*-benzoate (2A):



A mixture of 1,3-calix[4]arene-dibenzoate (**1A**) (0.433 g, 0.60 mmol) and potassium carbonate ( $K_2CO_3$ ) (1.382 g, 10.0 mmol) were placed into a 100 mL two-necked round-bottom flask in dried acetonitrile (30 mL) was added. The reaction mixtures were refluxed for 1 hr with stir under nitrogen atmosphere. A solution of methyl-4-(bromomethyl) benzoate (0.302 g, 1.32 mmol) in dried acetonitrile (10 mL) was added. The reaction mixture was refluxed for 1 day. Potassium carbonate was filtered. The mixture was diluted with dichloromethane, washed with aqueous 3M HCl (10 mL) and then washed with water ( $3 \times 10$  mL) and brine ( $3 \times 10$  mL). The organic layer was dried with anhydrous  $Na_2SO_4$ , and concentrated. The product was precipitated by methanol. The white solid was filtered and washed with methanol to obtain the desired product (**2A**) (0.352 g, 57%).

#### Characterization data for compound 2A:

$^1H$  NMR spectrum (400 MHz,  $CDCl_3$ ):  $\delta$  8.15 (d,  $J = 7.6$  Hz, 8H, Ar-*H*), 7.20 (d,  $J = 7.6$  Hz, 8H, Ar-*H*), 6.66 (d,  $J = 7.6$  Hz, 8H, Ar-*H*), 6.45 (t,  $J = 7.4$  Hz, 4H,

Ar-H), 4.92 (s, 8H, ArCH<sub>2</sub>O), 4.05 (s, 12H, ArCOOCH<sub>3</sub>), 3.63 (s, 8H, ArCH<sub>2</sub>Ar);

<sup>13</sup>C NMR spectrum (100 MHz, CDCl<sub>3</sub>): δ 167.2, 155.5, 143.0, 133.9, 131.1, 129.2, 129.1, 126.5, 122.7, 71.2, 52.2, 37.4;

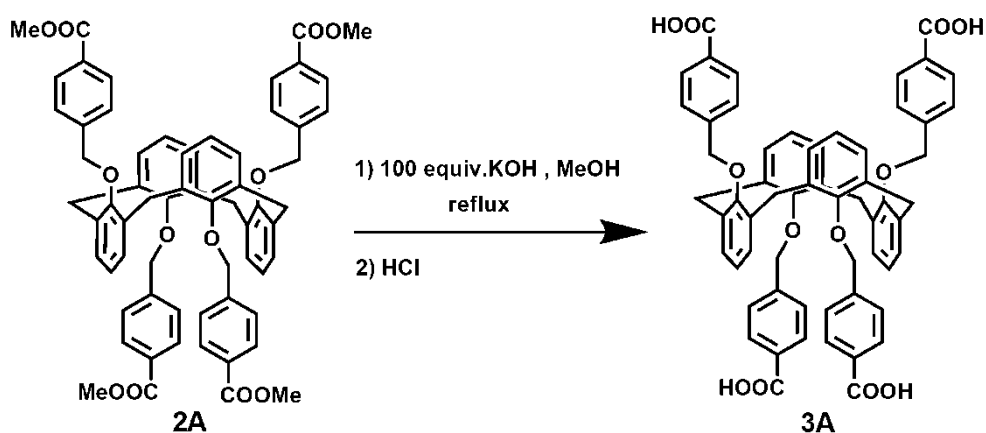
**IR (Nujol):** (ν<sub>max</sub>, cm<sup>-1</sup>) 2949 (s, C-H stretching), 1718 (s, C=O, stretching), 1613 (s, C=C stretching), 1452 (s, C-H bending), 1287, 1196, 1107, 1020 (s, C-O stretching), 754 (s, C-H out of plane bending).

**Elemental analysis:** Anal. calcd for C<sub>64</sub>H<sub>58</sub>O<sub>12</sub> C, 75.42; H, 5.74; O, 18.84  
Found C, 75.60; H, 5.78; O 18.62.

**MALDI-TOF mass(m/z):** Anal. calcd for [C<sub>64</sub>H<sub>58</sub>O<sub>12</sub> + Na<sup>+</sup>]: 1041.382  
Found 1039.513.

### 3.2.1.1.3 Synthesis of 1,3-alternate calix[4]arene tetra-*p*-benzoic acid

(**3A**):



1,3-Alternate tetra(methyl benzoate)calix[4]arene (**2A**) (1.018 g, 1 mmol) was dissolved in methanol (30 mL) in a 100 mL in two-necked round-bottom flask and gently heated until tetrabenzoate-calix[4]arene (**2A**) was completely soluble. Then, the solution of potassium hydroxide (5.600 g, 100 mmol) in water (10 mL) was added drop wise. The reaction mixture was refluxed until completion (TLC analysis). The reaction mixture was concentrated by rotary evaporator and quenched with 3M HCl (30 mL) with stir for 10 min. The precipitate was filtered and washed with water to obtained desired product (**3A**) (0.870 g, 90%).

### Characterization data for compound 3A.

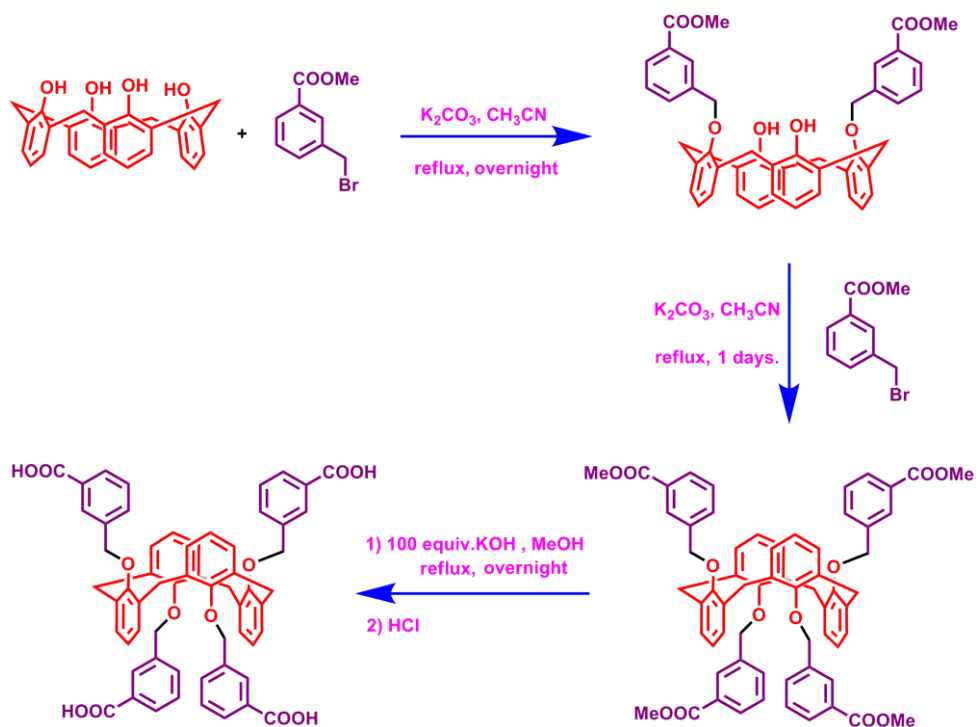
**<sup>1</sup>H NMR spectrum (400 MHz, d<sub>6</sub>-DMSO):** δ 12.93 (s, 4H, ArCOOH), 8.00 (d, *J* = 7.6 Hz, 8H, Ar-*H*), 7.23 (d, *J* = 7.6 Hz, 8H, Ar-*H*), 6.59 (d, *J* = 7.6 Hz, 8H, Ar-*H*), 6.28 (d, *J* = 7.0 Hz, 4H, Ar-*H*), 4.86 (s, 8H, ArCH<sub>2</sub>O); 3.59 (s, 8H, ArCH<sub>2</sub>Ar);

**<sup>13</sup>C NMR spectrum (100 MHz, DMSO-*d*<sub>6</sub>):** δ 167.3, 155.6, 143.1, 133.7, 130.4, 129.5, 128.6, 126.9, 121.7, 71.0, 36.5;

**FT-IR (KBr pellet, ν/cm<sup>-1</sup>):** 3466 (br m, O-H stretching), 2915 (s, C-H stretching), 1682 (s, C=O, stretching), 1453, 1418, (s, C-H bending), 1279, 1195, 1092, 1034 (s, C-O stretching), 757 (s, C-H out of plane bending).

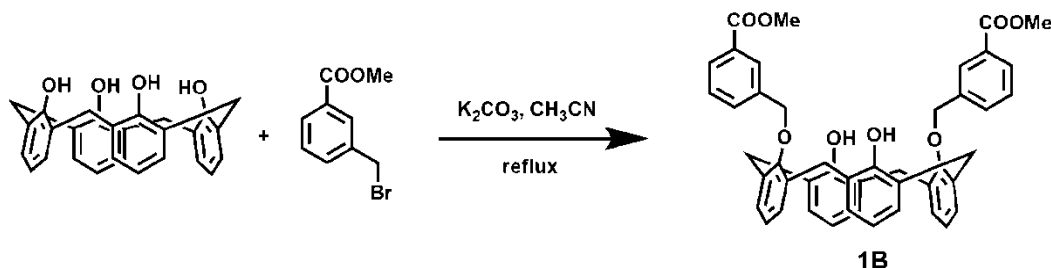
**MALDI-TOF mass (m/z):** Anal. calcd for [C<sub>60</sub>H<sub>50</sub>O<sub>12</sub> + Na<sup>+</sup>] : 985.320  
Found 983.657.

### 3.2.2.2 Synthesis of 1,3-alternate calix[4]arene tetra-*m*-benzoic acid (3B)



**Scheme 3.2.** Synthetic pathway of 1,3-alternate calix[4]arene tetra-*m*-benzoic acid (3B)

### 3.2.2.2.1 Synthesis of 1,3-dimethyl-*m*-benzoate calix[4]-arene (**1B**)



1,3-Dibenzoate calix[4]arene (**1B**) was obtained by a similar procedure to that used for preparation of **1A** except for using methyl-3-(bromomethyl) benzoate (0.573 g, 2.5 mmol) instead of methyl-4-(bromomethyl)benzoate as starting material. The white solid was filtered and washed with methanol to obtain the desired product (**1B**) (0.625 g, 69%).

#### Characterization data for compound **1B**:

**<sup>1</sup>H NMR spectrum (400 MHz, CDCl<sub>3</sub>):**  $\delta$  8.16 (s, 2H, Ar-*H*), 8.02 (t,  $J = 7.2$  Hz, 4H, Ar-*H*), 7.73 (s, 2H, Ar-*H*), 7.32 (t,  $J = 7.6$  Hz, 2H, Ar-*H*), 7.04 (d,  $J = 7.6$  Hz, 4H, Ar-*H*), 6.88 (d,  $J = 7.6$  Hz, 4H, Ar-*H*), 6.76 (t,  $J = 7.4$  Hz, 2H, Ar-*H*), 6.66 (t,  $J = 7.4$  Hz, 2H, Ar-*H*), 5.11 (s, 4H, ArCH<sub>2</sub>O), 4.50 (d,  $J = 12.8$  Hz, 4H, ArCH<sub>2</sub>Ar), 3.87 (s, 6H, ArCOOCH<sub>3</sub>), 3.33 (d,  $J = 13.2$  Hz, 4H, ArCH<sub>2</sub>Ar);

**<sup>13</sup>C NMR 100 MHz (100 MHz, CDCl<sub>3</sub>):**  $\delta$  166.8, 153.3, 151.7, 137.2, 133.1, 132.2, 130.4, 129.3, 129.2, 129.1, 128.6, 128.5, 127.9, 125.6, 119.1, 77.8, 52.2, 31.4;

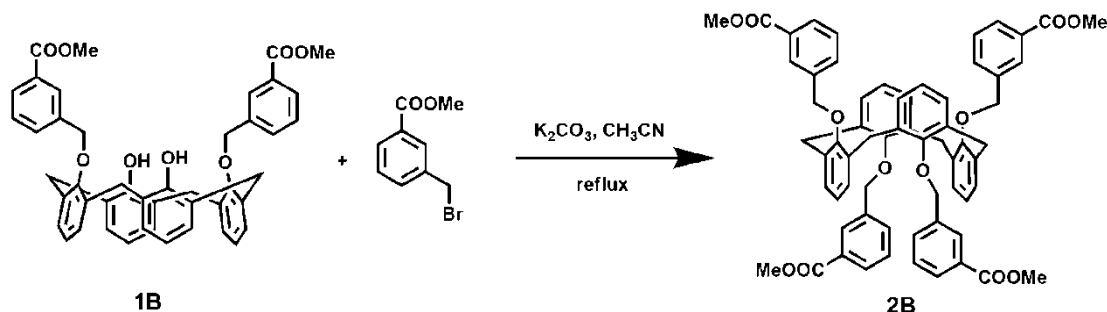
**FTIR (Nujol):** ( $\nu_{\max}$ , cm<sup>-1</sup>) 3394 (br m, O-H stretching), 2949 (s, C-H stretching), 1721 (s, C=O, stretching), 1590 (m, C=C stretching), 1465 (s, C-H bending), 1287, 1202, 1087 (s, C-O stretching), 747 (s, C-H out of plane bending).

**Elemental analysis:** Anal. Calcd for C<sub>46</sub>H<sub>40</sub>O<sub>8</sub>: C, 76.65; H, 5.59; O, 17.76 Found C, 76.67; H, 5.60; O, 17.73.

**MALDI-TOF mass (m/z):** Anal. calcd for [C<sub>46</sub>H<sub>40</sub>O<sub>8</sub> + Na<sup>+</sup>]: 743.264 Found 743.384.



### 3.2.2.2.2 Synthesis of 1,3-alternate calix[4]arenetetramethyl-*m*-benzoate (2B)



1,3-Alternate calix[4]arenetetramethyl-*m*-benzoate (**2B**) was obtained by a similar procedure to that used for preparation of **2A** except for using **1B** (0.702 g, 1.0 mmol) and methyl-3-(bromomethyl) benzoate (0.504 g, 2.2 mmol) instead of **1A** and methyl-4-(bromomethyl)benzoate as starting material. The white solid was filtered and washed with methanol to obtain the desired product (**2B**) (0.580 g, 56%).

#### Characterization data for compound **2B**:

**$^1H$  NMR spectrum (400 MHz,  $CDCl_3$ ):**  $\delta$  8.05 (d,  $J = 7.6$  Hz, 4H, Ar-*H*), 7.95 (s, 4H, Ar-*H*), 7.50 (d,  $J = 8.0$  Hz, 4H, Ar-*H*), 7.33 (d,  $J = 7.2$  Hz, 4H, Ar-*H*), 6.68 (8H, d,  $J = 7.2$  Hz, Ar-*H*), 6.46 (t,  $J = 7.6$  Hz, 4H, Ar-*H*), 4.86 (s, 8H, Ar- $CH_2O$ ), 3.97 (s, 12H, Ar- $COOCH_3$ ), 3.57 (s, 8H, Ar- $CH_2Ar$ );

**$^{13}C$  NMR spectrum (100 MHz,  $CDCl_3$ ):**  $\delta$  167.2, 155.7, 138.4, 133.8, 132.2, 131.1, 129.9, 128.4, 128.2, 127.7, 122.4, 71.9, 52.1, 37.1

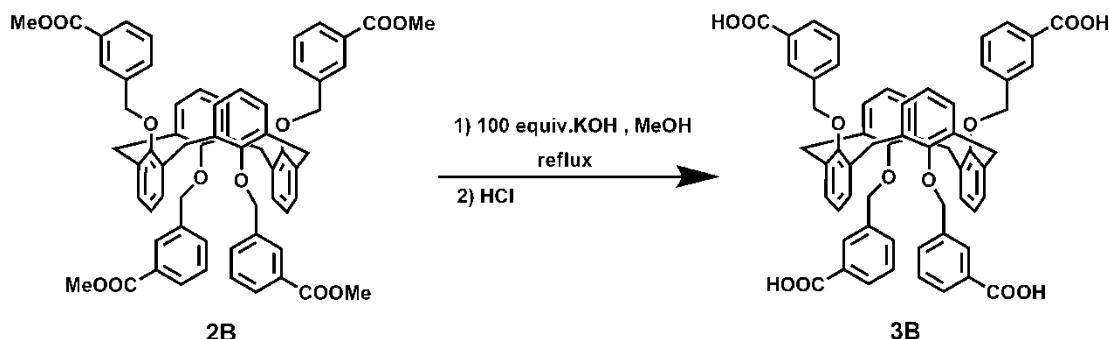
**FTIR (Nujol):** ( $\nu_{max}$ ,  $cm^{-1}$ ) 2949 (s, C-H stretching), 1721 (s, C=O stretching), 1588 (m, C=C stretching), 1454 (s, C-H bending), 1286, 1200, 1092 (s, C-O stretching), 747 (s, C-H out of plane bending).

**Elemental analysis:** Anal. calcd for  $C_{64}H_{58}O_{12}$ : C, 75.42; H, 5.74; O, 18.84  
Found C, 75.44; H, 5.74; O, 18.82.

**MALDI-TOF mass (m/z):** Anal. calcd for  $[C_{64}H_{58}O_{12} + Na^+]$ : 1041.382  
Found 1039.787

### 3.2.2.2.3 Synthesis of 1,3-alternate calix[4]arene tetra-*m*-benzoic acid

(**3B**):



1,3-Alternate calix[4]arene tetra-*m*-benzoic acid (**3B**) was obtained by a similar procedure to that used for preparation of **3A** except for using **2B** (0.309 g, 0.30 mmol) instead of **2A** as starting material. White precipitate of **3B** were manually isolated and washed with water several times (0.265 g, 90% yield).

#### Characterization data for compound **3B**:

**<sup>1</sup>H NMR spectrum (400 MHz, d<sub>6</sub>-DMSO):** δ 12.88 (s, 4H, ArCOOH), 7.89 (d, *J* = 9.2 Hz, 4H, Ar-*H*), 7.42 (d, *J* = 7.4 Hz, 4H, Ar-*H*), 7.22 (4H, d, *J* = 7.6 Hz, Ar-*H*), 6.60 (d, *J* = 7.6 Hz, 8H, Ar-*H*), 6.26 (t, *J* = 7.2 Hz, 4H, Ar-*H*), 4.74 (8H, s, ArCH<sub>2</sub>O), 3.52 (s, 8H, ArCH<sub>2</sub>Ar);

**<sup>13</sup>C NMR spectrum (100 MHz, d<sub>6</sub>-DMSO):** δ 167.4, 155.5, 138.4, 133.6, 132.2, 130.4, 130.2, 127.9, 127.8, 121.6, 71.4, 36.4

**FT-IR (KBr pellet, ν/cm<sup>-1</sup>):** 3428 (br m, O-H stretching), 2917 (s, C-H stretching), 1691 (s, C=O stretching), 1592 (s, C=C stretching), 1452 (s, C-H bending), 1306, 1203, 1094 (s, C-O stretching), 745 (s, C-H out of plane bending).

**MALDI-TOF mass (m/z):** Anal. calcd for [C<sub>60</sub>H<sub>50</sub>O<sub>12</sub> + Na<sup>+</sup>]: 985.320 Found 983.616.

### 3.2.2 Syntheses of Metal Organic Frameworks

The syntheses of metal organic frameworks were carried out by using solvothermal method. This method normally uses polar organic solvent to dissolve organic linker and metal salts which are heated up to desired temperature. There are many types of containers and heating sources such as conventional heating, autoclave with temperature program and isothermal vial in oven.

In this work, 1,3-alternate calix[4]arene-based MOFs using 1,3-alternate calix[4]arenetetrabenzoic acid derivatives as organic linkers were synthesized by solvothermal methods which are in different containers.

- By conventional solvothermal synthesis.

**Table 3.1** Code of 1,3-alternate calyx[4]arene-based MOFs via conventional heating.

Code of MOFs	Organic linkers + Metal salts
<b>M1</b>	<b>3A</b> + Zn(NO <sub>3</sub> ) <sub>2</sub>
<b>M2</b>	<b>3A</b> + Zn(OAc) <sub>2</sub>
<b>M3</b>	<b>3A</b> + Cu(NO <sub>3</sub> ) <sub>2</sub>
<b>M4</b>	<b>3A</b> + Cu(OAc) <sub>2</sub>
<b>M5</b>	<b>3A</b> + Ni(NO <sub>3</sub> ) <sub>2</sub>
<b>M6</b>	<b>3A</b> + Cd(NO <sub>3</sub> ) <sub>2</sub>
<b>M7</b>	<b>3A</b> + Er(NO <sub>3</sub> ) <sub>3</sub>
<b>M8</b>	<b>3A</b> + EuCl <sub>3</sub>
<b>M9</b>	<b>3A</b> + Tb(NO <sub>3</sub> ) <sub>3</sub>
<b>M10</b>	<b>3B</b> + Zn(NO <sub>3</sub> ) <sub>2</sub>
<b>M11</b>	<b>3B</b> + Cu(NO <sub>3</sub> ) <sub>2</sub>
<b>M12</b>	<b>3B</b> + Ni(NO <sub>3</sub> ) <sub>2</sub>
<b>M13</b>	<b>3B</b> + Er(NO <sub>3</sub> ) <sub>3</sub>
<b>M14</b>	<b>3B</b> + EuCl <sub>3</sub>
<b>M15</b>	<b>3B</b> + Tb(NO <sub>3</sub> ) <sub>3</sub>

- MOFs derived from 1,3-alternate calix[4]arene tetra-*p*-benzoic acid (**3A**) and 3*d*-transition metals.

#### Synthesis of **M1**.

A two-necked round-bottomed flask containing 1,3-alternate calix[4]arene tetra-*p*-benzoic acid **3A** (0.489 g, 0.5 mmol) and Zn(NO<sub>3</sub>)<sub>2</sub>·6H<sub>2</sub>O (0.301 g, 1.0 mmol) were charged with freshly distilled DMF (20 mL). The reaction mixture was stirred for 30 minutes and, then, heated to 110°C without stirring for 24 hr. The precipitate was filtered and washed with DMF to obtain the MOFs **M1** (0.458 g).

IR (KBr, v/cm<sup>-1</sup>): 3432 (br m, O-H stretching), 3060, 3026 (s, C-H (aromatic) stretching), 2923 (s, C-H stretching), 1655 (s, C=O stretching), 1608, 1552 (s, C=C stretching), 1409 (s, C-N stretching), 1190, 1094 (s, C-O stretching), 768 (s, C-H out of plane bending) (Figure 4.4);

XRD pattern: 2θ of 10.52, 19.12, 19.26 (Figure 4.5).

#### Synthesis of **M2**.

**M2** was synthesized by the same method as **M1** using 1,3-alternate calix[4]arene tetra-*p*-benzoic acid **3A** (0.244 g, 0.25 mmol) and Zn(OAc)<sub>2</sub> (0.122 g, 0.55 mmol) instead of Zn(NO<sub>3</sub>)<sub>2</sub>. The precipitate was filtered and washed with DMF to obtain the MOFs **M2** (0.223 g).

IR (KBr, v/cm<sup>-1</sup>): 3418 (br m, O-H stretching), 3056, 3033 (s, C-H (aromatic) stretching), 2927 (s, C-H stretching), 1655 (s, C=O stretching), 1608, 1549 (s, C=C stretching), 1416 (s, C-N stretching), 1190, 1094 (s, C-O stretching), 765 (s, C-H out of plane bending) (Figure 4.4);

XRD pattern: 2θ of 4.54, 4.95, 5.31, 8.26, 9.11, 9.54, 9.88, 10.45, 11.53, 18.16, 19.29, 20.30 (Figure 4.5)

#### Synthesis of **M3**.

In the case of **M3**, using the amount of 1,3-alternate calix[4]arene tetra-*p*-benzoic acid **3A** (0.244 g, 0.25 mmol) in the same method as upper condition but the reaction was charged with Cu(NO<sub>3</sub>)<sub>2</sub>·3H<sub>2</sub>O (0.1208 g, 0.50 mmol) instead of Zn(NO<sub>3</sub>)<sub>2</sub>. The blue precipitate was filtered and washed with DMF to obtain the MOFs **M3** (0.128 g).

IR (KBr,  $\text{v}/\text{cm}^{-1}$ ): 3488 (br m, O-H stretching), 3063 (s, C-H (aromatic) stretching), 2923 (s, C-H stretching), 1652 (s, C=O stretching), 1612, 1542 (s, C=C stretching), 1409 (s, C-N stretching), 1193, 1090 (s, C-O stretching), 765 (s, C-H out of plane bending) (Figure 4.4);

XRD pattern:  $2\theta$  of 4.82, 9.36, 10.72, 16.68, 17.36, 18.26, 18.66, 19.38, 19.64, 20.20, 20.78 (Figure 4.6)

#### Synthesis of **M4**.

**M4** was obtained by the similar procedure to that used for synthesis of **M1**. Using 1,3-alternate calix[4]arene tetra-*p*-benzoic acid **3A** (0.244 g, 0.25 mmol) and  $\text{Cu}(\text{OAc})_2$  (0.101 g, 0.50 mmol) instead of  $\text{Zn}(\text{NO}_3)_2$ . The precipitate was filtered and washed with DMF to obtain the MOFs **M4** (0.145 g).

IR (KBr,  $\text{cm}^{-1}$ ): 3428 (br m, O-H stretching), 3060, 3023 (s, C-H (aromatic) stretching), 2920 (s, C-H stretching), 1705, 1655 (s, C=O stretching), 1608, 1592 (s, C=C stretching), 1406 (s, C-N stretching), 1193, 1090 (s, C-O stretching), 765 (s, C-H out of plane bending) (Figure A-25);

XRD pattern:  $2\theta$  of 5.09, 8.92, 9.48, 10.07, 17.06, 18.01, 18.91, 20.86, 21.00 (Figure 4.6)

#### Synthesis of **M5**.

In the case of **M5**, 1,3-alternate calix[4]arene tetra-*p*-benzoic acid **3A** (0.244 g, 0.25 mmol) was used in the same method described previously but the reaction was charged with  $\text{Ni}(\text{NO}_3)_2 \cdot 6\text{H}_2\text{O}$  (0.145 g, 0.50 mmol) instead of  $\text{Zn}(\text{NO}_3)_2$ . The precipitate was filtered and washed with DMF to obtain the MOFs **M5** (0.258 g).

IR (KBr,  $\text{v}/\text{cm}^{-1}$ ): 3422 (br m, O-H stretching), 3060, 3026 (s, C-H (aromatic) stretching), 2927 (s, C-H stretching), 1655 (s, C=O stretching), 1612, 1539 (s, C=C stretching), 1396 (s, C-N stretching), 1193, 1090 (s, C-O stretching), 765 (s, C-H out of plane bending) (Figure A-25);

XRD pattern:  $2\theta$  of 4.67, 6.00, 8.48, 9.18, 10.48, 11.12, 11.81, 12.80, 13.90, 16.72, 18.48, 20.70, 21.2, 22.49, 25.43, 27.12 (Figure 4.5)

### Synthesis of **M6**.

**M6** was synthesized from 1,3-alternate calix[4]arene tetra-*p*-benzoic acid **3A** (0.244 g, 0.25 mmol) and used in the same method as described previously but the reaction was charged with Cd(NO<sub>3</sub>)<sub>2</sub>·4H<sub>2</sub>O (0.172 g, 0.50 mmol) instead of Zn(NO<sub>3</sub>)<sub>2</sub>. The precipitate was filtered and washed with DMF to obtain the MOFs **M6** (0.265 g).

IR (KBr, cm<sup>-1</sup>): 3432 (br m, O-H stretching), 3063, 3030 (s, C-H (aromatic) stretching), 2927 (s, C-H stretching), 1648 (s, C=O stretching), 1585, 1539 (s, C=C stretching), 1399 (s, C-N stretching), 1193, 1090 (s, C-O stretching), 771 (s, C-H out of plane bending) (Figure A-25);

XRD pattern: 2θ of 4.73, 9.58, 11.40, 13.97, 15.64, 16.19, 16.85, 17.40, 19.70, 20.76, 21.48, 26.06, 26.90, 28.02, 28.90 (Figure 4.5)

- MOFs derived from 1,3-alternate calix[4]arene tetra-*p*-benzoic acid (**3A**) and 4*f*-lanthanide metal ions.

### Synthesis of **M7**.

**M7** was synthesized by the same method as **M1**, using the amount of 1,3-alternate calix[4]arene tetra-*p*-benzoic acid **3A** (0.244 g, 0.25 mmol) in the same method as upper condition but the reaction was charged with Er(NO<sub>3</sub>)<sub>2</sub>·5H<sub>2</sub>O (0.222 g, 0.50 mmol) instead of Zn(NO<sub>3</sub>)<sub>2</sub>. The precipitate was filtered and washed with DMF to obtain the MOFs **M7** (0.343 g).

IR (KBr, v/cm<sup>-1</sup>): 3422 (br m, O-H stretching), 3066 (s, C-H (aromatic) stretching), 2927 (s, C-H stretching), 1658 (s, C=O stretching), 1588, 1542 (s, C=C stretching), 1422 (s, C-N stretching), 1193, 1090 (s, C-O stretching), 768 (s, C-H out of plane bending) (Figure A-26);

XRD pattern: 2θ of 4.56, 6.27, 9.15, 10.12, 13.74, 18.20, 20.40 (Figure 4.7)

### Synthesis of **M8**.

**M8** was prepared by using 1,3-alternate calix[4]arene tetra-*p*-benzoic acid **3A** (0.244 g, 0.25 mmol) in the similar procedure as **M1** but the reaction was charged with EuCl<sub>3</sub>·6H<sub>2</sub>O (0.183 g, 0.50 mmol) instead of Zn(NO<sub>3</sub>)<sub>2</sub>. The precipitate was filtered and washed with DMF to obtain the MOFs **M8** (0.281 g).

IR (KBr,  $\text{v}/\text{cm}^{-1}$ ): 3428 (br m, O-H stretching), 3060, 3033 (s, C-H (aromatic) stretching), 2927 (s, C-H stretching), 1652 (s, C=O stretching), 1588, 1535 (s, C=C stretching), 1412 (s, C-N stretching), 1193, 1094 (s, C-O stretching), 768 (s, C-H out of plane bending) (Figure A-26);

XRD pattern:  $2\theta$  of 5.07, 9.96, 11.46, 14.95, 17.90, 18.59, 20.64, 21.22 (Figure 4.7)

#### Synthesis of **M9**.

In the case of **M9**, the similar procedure for synthesis of **M1** was employed by using the amount of 1,3-alternate calix[4]arene tetra-*p*-benzoic acid **3A** (0.244 g, 0.25 mmol) but the reaction was charged with  $\text{Tb}(\text{NO}_3)_2 \cdot 5\text{H}_2\text{O}$  (0.217 g, 0.50 mmol) instead of  $\text{Zn}(\text{NO}_3)_2$ . The precipitate was filtered and washed with DMF to obtain the MOFs **M9** (0.164 g).

IR (KBr,  $\text{v}/\text{cm}^{-1}$ ): 3428 (br m, O-H stretching), 3066, 3020 (s, C-H (aromatic) stretching), 2920 (s, C-H stretching), 1655 (s, C=O stretching), 1612, 1532 (s, C=C stretching), 1416 (s, C-N stretching), 1190, 1094 (s, C-O stretching), 765 (s, C-H out of plane bending) (Figure A-27);

XRD pattern:  $2\theta$  of 4.91, 9.22, 9.84, 11.45, 17.42, 18.42, 19.75, 21.34 (Figure 4.7)

- MOFs derived from 1,3-alternate calix[4]arene tetra-*m*-benzoic acid (**3B**) and 3*d*-transition metals.

#### Synthesis of **M10**

1,3-alternate calix[4]arene tetra-*m*-benzoic acid (**3B**) (0.244 g, 0.25 mmol) and  $\text{Zn}(\text{NO}_3)_2 \cdot 6\text{H}_2\text{O}$  (0.155 g, 0.5 mmol) were placed into a two-necked round-bottom flask and charged with freshly distilled DMF (20 mL) and stirred for 30 minutes. The reaction mixture was heated to 110°C without stirring for 24 hr. The precipitate was filtered and washed with DMF to obtain the MOFs **M10** (0.172 g).

IR (KBr,  $\text{v}/\text{cm}^{-1}$ ): 3435 (br m, O-H stretching), 3060, 3026 (s, C-H (aromatic) stretching), 2927 (s, C-H stretching), 1615 (s, C=O stretching), 1595, 1569 (s, C=C

stretching), 1406 (s, C-N stretching), 1187, 1090 (s, C-O stretching), 758 (s, C-H out of plane bending) (Figure A-27);

XRD pattern:  $2\theta$  of 6.02, 8.58, 10.26 (Figure 4.8)

### Synthesis of **M11**

**M11** was prepared by the same method as **M10** using 1,3-alternate calix[4]arene tetra-*m*-benzoic acid **3B** (0.244 g, 0.25 mmol) but the reaction was charged with  $\text{Cu}(\text{NO}_3)_2 \cdot 6\text{H}_2\text{O}$  (0.145 g, 0.50 mmol) instead of  $\text{Zn}(\text{NO}_3)_2$ . The precipitate was filtered and washed with DMF to obtain the MOFs **M11** (0.141 g).

IR (KBr,  $\text{cm}^{-1}$ ): 3428 (br m, O-H stretching), 3063, 3023 (s, C-H (aromatic) stretching), 2923 (s, C-H stretching), 1658 (s, C=O stretching), 1622, 1578 (s, C=C stretching), 1402 (s, C-N stretching), 1187, 1094 (s, C-O stretching), 761 (s, C-H out of plane bending) (Figure A-27);

XRD pattern:  $2\theta$  of 5.77, 9.01, 9.50, 10.38, 11.58, 12.92, 15.65, 16.26, 17.62, 19.35, 20.33, 21.99, 23.08, 25.68, 25.68, 28.65 (Figure 4.8)

### Synthesis of **M12**

In the case of **M12**, 1,3-alternate calix[4]arene tetra-*m*-benzoic acid **3B** (0.244g, 0.25mmol) was used in the same method as **M10** but the reaction was charged with  $\text{Ni}(\text{NO}_3)_2 \cdot 6\text{H}_2\text{O}$  (0.145 g, 0.50 mmol) instead of  $\text{Zn}(\text{NO}_3)_2$ . The precipitate was filtered and washed with DMF to obtain the MOFs **M12** (0.216 g).

IR (KBr,  $\text{cm}^{-1}$ ): 3418 (br m, O-H stretching), 3063 (m, C-H (aromatic) stretching), 2927 (m, C-H stretching), 1652 (s, C=O stretching), 1592, 1569 (s, C=C stretching), 1396 (s, C-N stretching), 1187, 1090 (s, C-O stretching), 765 (s, C-H out of plane bending) (Figure A-27);

XRD pattern:  $2\theta$  of 5.26, 5.32, 5.58, 5.99, 7.64, 8.26, 8.99, 9.50, 10.33, 17.19, 17.40, 17.85, 18.10, 18.60, 19.27, 19.74, 20.17, 21.40 (Figure 4.8)



- MOFs derived from 1,3-alternate calix[4]arene tetra-*p*-benzoic acid (**3B**) and 4<sup>f</sup>-lanthanide metal ions

#### Synthesis of **M13**

**M13** was prepared by the same synthetic method as **M10**, used 1,3-alternate calix[4]arene tetra-*m*-benzoic acid **3B** (0.244 g, 0.25 mmol) but the reaction was charged with Er(NO<sub>3</sub>)<sub>2</sub>·6H<sub>2</sub>O (0.222 g, 0.50 mmol) instead of Zn(NO<sub>3</sub>)<sub>2</sub>. The precipitate was filtered and washed with DMF to obtain the MOFs **M13** (0.242 g).

IR (KBr, cm<sup>-1</sup>): 3422 (br m, O-H stretching), 3060, 3026 (s, C-H (aromatic) stretching), 2923 (s, C-H stretching), 1652 (s, C=O stretching), 1612, 1542 (s, C=C stretching), 1406 (s, C-N stretching), 1190, 1090 (s, C-O stretching), 759 (s, C-H out of plane bending) (Figure A-28);

XRD pattern: 2θ of 5.28, 6.16, 8.58, 9.22, 9.94, 10.01, 10.79, 16.82, 17.67, 18.47, 19.22 (Figure 4.9)

#### Synthesis of **M14**

**M14** was synthesized by the same method as **M10**, using 1,3-alternate calix[4]arene tetra-*m*-benzoic acid **3B** (0.244 g, 0.25 mmol) but the reaction was charged with EuCl<sub>3</sub>·6H<sub>2</sub>O (0.183 g, 0.50 mmol) instead of Zn(NO<sub>3</sub>)<sub>2</sub>. The precipitate was filtered and washed with DMF to obtain the MOFs **M14** (0.226 g).

IR (KBr, cm<sup>-1</sup>): 3408 (br m, O-H stretching), 3060, 3026 (s, C-H (aromatic) stretching), 2927 (s, C-H stretching), 1655 (s, C=O stretching), 1612, 1545 (s, C=C stretching), 1412 (s, C-N stretching), 1190, 1090 (s, C-O stretching), 758 (s, C-H out of plane bending) (Figure A-28);

XRD pattern: 2θ of 5.85, 6.23, 10.22, 19.78, 28.33 (Figure 4.9)

#### Synthesis of **M15**

In the case of **M15**, 1,3-alternate calix[4]arene tetra-*m*-benzoic acid **3B** (0.244 g, 0.25 mmol) was used in the same method as the preparing of **M10** but the reaction was charged with Tb(NO<sub>3</sub>)<sub>2</sub>·5H<sub>2</sub>O (0.217 g, 0.366 mmol) instead of Zn(NO<sub>3</sub>)<sub>2</sub>. The precipitate was filtered and washed with DMF to obtain the MOFs **M15** (0.215 g).

IR (KBr,  $\text{cm}^{-1}$ ): 3418 (br m, O-H stretching), 3060, 3030 (s, C-H (aromatic) stretching), 2930 (s, C-H stretching), 1655 (s, C=O stretching), 1612, 1542 (s, C=C stretching), 1409 (s, C-N stretching), 1187, 1090 (s, C-O stretching), 761 (s, C-H out of plane bending) (Figure A-28);

XRD pattern:  $2\theta$  of 4.96, 5.49, 6.00, 6.27, 8.22, 8.79, 9.80, 19.48 (Figure 4.9)

The synthesis of MOFs by using the solvothermal method gave desire, however, it did not provide single-crystals of those MOFs for characterization of their structures by sc-X ray technique. So, we tried to find suitable conditions for preparation of single crystals of MOFs. Normally, a small scale technique using small containers such as vial or glass tube is employed.

- By solvothermal in glass tube/vial.

**Table 3.2** Effects of metal salts and solvents in the synthesis of **3A-Zn MOF**.

Entry	Organic linker	Metal ion	Solvent
1 <sup>a</sup>	<b>3A</b>	Zn(NO <sub>3</sub> ) <sub>2</sub>	DMF
2 <sup>a</sup>	<b>3A</b>	Zn(OAc) <sub>2</sub>	DMF
3 <sup>a</sup>	<b>3A</b>	ZnCl <sub>2</sub>	DMF
4 <sup>b</sup>	<b>3A</b>	Zn(NO <sub>3</sub> ) <sub>2</sub>	DMF:DEF
5 <sup>b</sup>	<b>3A</b>	Zn(OAc) <sub>2</sub>	DMF:DEF
6 <sup>b</sup>	<b>3A</b>	ZnCl <sub>2</sub>	DMF:DEF

<sup>a</sup>**Reaction conditions:** **3A** (0.125g, 0.13 mmol) and Zn(NO<sub>3</sub>)<sub>2</sub> ( 0.077 g, 0.26 mmol, Entry 1), Zn(OAc)<sub>2</sub> ( 0.057 g, 0.26 mmol, Entry 2.) or ZnCl<sub>2</sub> ( 0.035 g, 0.26 mmol, Entry 3.) dissolved in DMF (10 mL) in a 20 mL Pyrex glass tube, 90 °C in oven for 48 h and room temperature over 24 h.

<sup>b</sup>**Reaction conditions:** Using same amounts of both **3A** and metal salts in the same method as upper condition dissolved in DMF:DEF (1:1, 10mL).

**Table 3.3** Syntheses of metal-organic frameworks by using **3A** with various metal ions.

Entry	Organic linker	Metal salt	Solvent
1 <sup>a</sup>	<b>3A</b>	Cu <sup>2+</sup>	DMF
2 <sup>b</sup>	<b>3A</b>	Cu <sup>2+</sup>	DMF:DEF
3 <sup>a</sup>	<b>3A</b>	Co <sup>2+</sup>	DMF
4 <sup>b</sup>	<b>3A</b>	Co <sup>2+</sup>	DMF:DEF
5 <sup>a</sup>	<b>3A</b>	Ni <sup>2+</sup>	DMF
6 <sup>b</sup>	<b>3A</b>	Ni <sup>2+</sup>	DMF:DEF
7 <sup>a</sup>	<b>3A</b>	Cd <sup>2+</sup>	DMF
8 <sup>b</sup>	<b>3A</b>	Cd <sup>2+</sup>	DMF:DEF
9 <sup>a</sup>	<b>3A</b>	Er <sup>3+</sup>	DMF
10 <sup>b</sup>	<b>3A</b>	Er <sup>3+</sup>	DMF:DEF
11 <sup>a</sup>	<b>3A</b>	Eu <sup>3+</sup>	DMF
12 <sup>b</sup>	<b>3A</b>	Eu <sup>3+</sup>	DMF:DEF
13 <sup>a</sup>	<b>3A</b>	Tb <sup>3+</sup>	DMF
14 <sup>b</sup>	<b>3A</b>	Tb <sup>3+</sup>	DMF:DEF

<sup>a</sup>**Reaction conditions:** **3A** (20 mg, 0.02 mmol) and Cu(NO<sub>3</sub>)<sub>2</sub> (11.6 mg, 0.04 mmol, Entry 1), Co(NO<sub>3</sub>)<sub>2</sub> (13.9 mg, 0.04 mmol, Entry 3), Ni(NO<sub>3</sub>)<sub>2</sub> (13.9 mg, 0.04 mmol, Entry 5), Cd(NO<sub>3</sub>)<sub>2</sub> (14.8 mg, 0.04 mmol, Entry 7), Er(NO<sub>3</sub>)<sub>3</sub> (21.3 mg, 0.04 mmol, Entry 9), EuCl<sub>3</sub> (17.6 mg, 0.04 mmol, Entry 11) or Tb(NO<sub>3</sub>)<sub>3</sub> (20.8 mg, 0.04 mmol, Entry 13), dissolved in DMF (2.5 mL) in a 10 mL vial, 90 °C in oven for 48 h and room temperature over 12 h.

<sup>b</sup>**Reaction conditions:** Using same amounts of both **3A** and metal salts and same condition as upper condition in DMF:DEF (1:1, 2.5 mL).

**Table 3.4** Syntheses of metal-organic frameworks by using **3B** with various metal ions.

Entry	Organic linker	Metal salt	Solvent
1 <sup>a</sup>	<b>3B</b>	Zn <sup>2+</sup>	DMF
2 <sup>b</sup>	<b>3B</b>	Zn <sup>2+</sup>	DMF:DEF
3 <sup>a</sup>	<b>3B</b>	Cu <sup>2+</sup>	DMF
4 <sup>b</sup>	<b>3B</b>	Cu <sup>2+</sup>	DMF:DEF
5 <sup>a</sup>	<b>3B</b>	Co <sup>2+</sup>	DMF
6 <sup>b</sup>	<b>3B</b>	Co <sup>2+</sup>	DMF:DEF
7 <sup>a</sup>	<b>3B</b>	Ni <sup>2+</sup>	DMF
8 <sup>b</sup>	<b>3B</b>	Ni <sup>2+</sup>	DMF:DEF
9 <sup>a</sup>	<b>3B</b>	Cd <sup>2+</sup>	DMF
10 <sup>b</sup>	<b>3B</b>	Cd <sup>2+</sup>	DMF:DEF
11 <sup>a</sup>	<b>3B</b>	Er <sup>3+</sup>	DMF
12 <sup>b</sup>	<b>3B</b>	Er <sup>3+</sup>	DMF:DEF
13 <sup>a</sup>	<b>3B</b>	Eu <sup>3+</sup>	DMF
14 <sup>b</sup>	<b>3B</b>	Eu <sup>3+</sup>	DMF:DEF
15 <sup>a</sup>	<b>3B</b>	Tb <sup>3+</sup>	DMF
16 <sup>b</sup>	<b>3B</b>	Tb <sup>3+</sup>	DMF:DEF

<sup>a</sup> **Reaction conditions** : **3B** (20 mg, 0.02 mmol) and Zn(NO<sub>3</sub>)<sub>2</sub> (14.3 mg, 0.04 mmol, Entry 1), Cu(NO<sub>3</sub>)<sub>2</sub> (11.6 mg, 0.04 mmol, Entry 3), Co(NO<sub>3</sub>)<sub>2</sub> ( 13.9 mg, 0.04 mmol, Entry 5), Ni(NO<sub>3</sub>)<sub>2</sub> ( 13.9 mg, 0.04 mmol, Entry 7), Cd(NO<sub>3</sub>)<sub>2</sub> (13.0mg, 0.04 mmol, Entry 9), Er(NO<sub>3</sub>)<sub>3</sub> (21.3 mg, 0.04 mmol, Entry 11), EuCl<sub>3</sub> (17.6 mg, 0.04 mmol, Entry 12) or Tb(NO<sub>3</sub>)<sub>3</sub> ( 20.8 mg, 0.04 mmol, Entry 15), dissolved in DMF (2.5 mL) was placed in a 10 mL vial and sealed. The vial was kept at 90 °C for 48 h, followed by cooling to room temperature over 12 h.

<sup>b</sup> **Reaction conditions** : Using the same amount of both **3B** and metal salts in the same method as upper condition but the reaction dissolved in DMF:DEF (1:1, 2.5 mL) instead of DMF (2.5 mL)

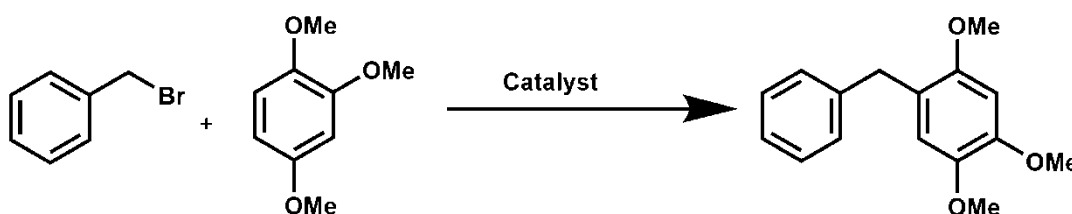
**Table 3.5** Effects of the ratio between **3B** and  $\text{Cd}^{2+}$ .

Entry <sup>a</sup>	<b>3B</b> : $\text{Cd}^{2+}$
1	1:1
2	1:2
3	1:3
4	1:4

<sup>a</sup> **Reaction conditions** : **3B** (20 mg, 0.02 mmol) and  $\text{Cd}(\text{NO}_3)_2$  (6.5 mg, 0.02 mmol, Entry 1),  $\text{Cd}(\text{NO}_3)_2$  (13.0 mg, 0.04 mmol, Entry 2),  $\text{Cd}(\text{NO}_3)_2$  (20.5 mg, 0.06 mmol, Entry 3),  $\text{Cd}(\text{NO}_3)_2$  (26.0 mg, 0.08 mmol, Entry 4), in a mixture of DMF:DEF (1:1, 2.5 mL) in a 10 mL vial, 90 °C in oven for 48 h, room temperature over 12 h.

### 3.2.3 Catalytic study

To investigate the catalytic activities of the obtained metal-organic frameworks (MOFs), Friedel-Crafts alkylation was used as a model reaction by employing benzyl bromide and 1,3,5-trimethoxy benzene as substrates.



**Scheme 3.3** Friedel-Crafts alkylation of benzyl bromide and 1,3,5-trimethoxybenzene catalyzed by synthesized MOFs.

**Table 3.6** Optimize condition of the Friedel-Crafts alkylation.

Entry	Catalyst
1	No catalyst
2	<b>M1</b> (MOF <b>3A</b> -Zn)
3	<b>M5</b> (MOF <b>3A</b> -Ni)

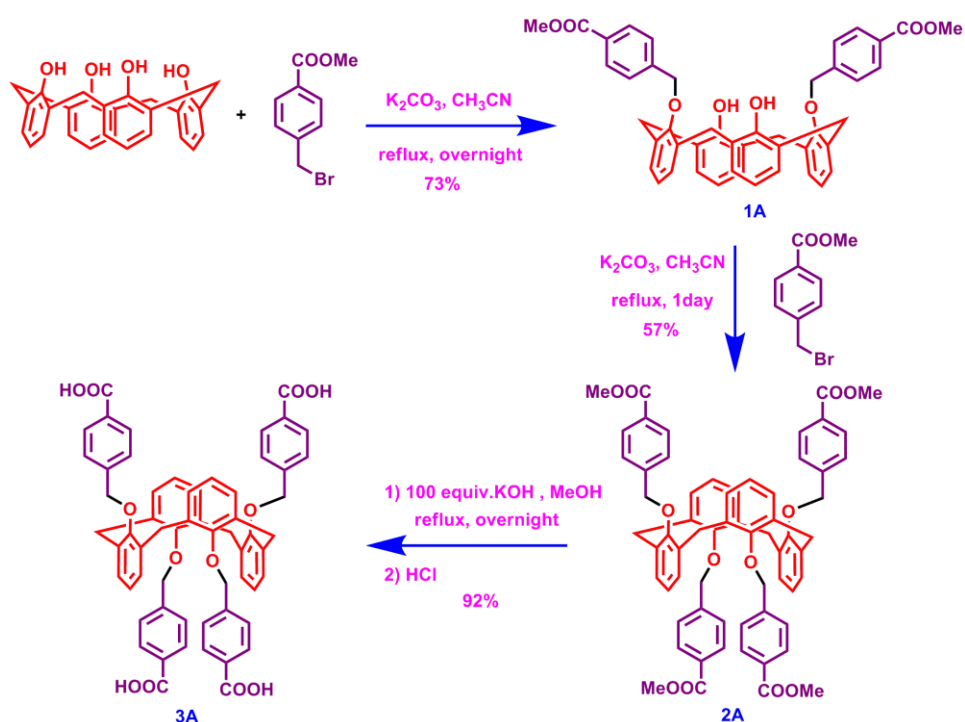
**General Procedure:** Benzyl bromide (0.74 mL, 6.22 mmol) and 1,3,5-trimethoxy benzene (1.5 mL, 10.0 mmol) were placed into a 25 mL 2 necked round bottom flask. No catalyst was used in entry 1 but 0.050 g of **M1** (MOF **3A**-Zn) and 0.050 g of **M5** (MOF **3A**-Ni) were employed in entries 2 and 3, respectively. The reaction mixture was heated at 80 °C. The completion of reaction was monitored by TLC analysis and, then, it was worked up and purified by column chromatography.

## CHAPTER IV

### RESULTS AND DISCUSSION

#### 4.1 Synthesis of Organic linkers

##### 4.1.1 Synthesis of 1,3-alternate calix[4]arene tetra-*p*-benzoic acid (3A)

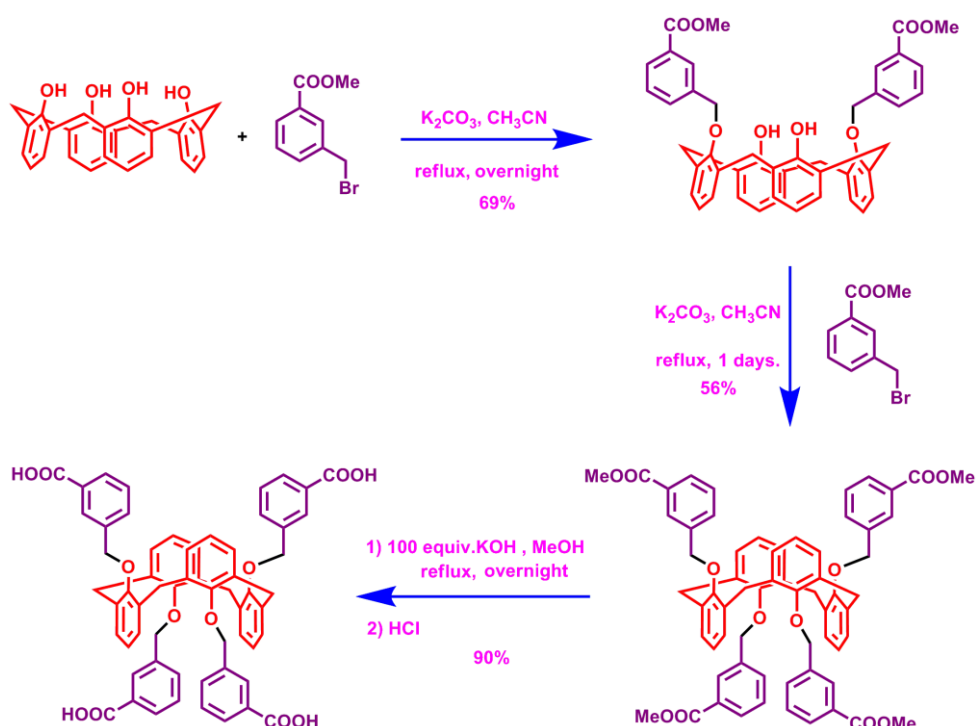


**Scheme 4.1** Synthetic pathway of 1,3-alternate calix[4]arene tetra-*p*-benzoic acid (3A).

The synthetic procedure of 1,3-alternate calix[4]arene tetra-*p*-benzoic acid **3A** is shown in the Scheme 4.1. The first step, calix[4]arene reacted with methyl-4-(bromomethyl) benzoate in dry  $CH_3CN$  and in the presence of  $K_2CO_3$  as base to provide 1,3-calix[4]arene-dimethyl-*p*-benzoate (**1A**) in 73% yield. The reaction of 1,3-calix[4]arene dimethyl-*p*-benzoate (**1A**) with methyl-4-(bromomethyl) benzoate gave the 1,3-alternate calix[4]arene tetramethyl-*p*-benzoate (**2A**) in 57% yield. The products in each step were easily precipitated in  $CH_2Cl_2/MeOH$  system to obtain

white precipitates. In the final step, 1,3-alternate calix[4]arene tetramethyl-*p*-benzoate (**2A**) was hydrolyzed by using KOH 100 equiv. and then acidified by 3M HCl to yield 1,3-alternate calix[4]arene tetra-*p*-benzoic acid (**3A**) in high yield. The obtained products were characterized by spectroscopic techniques which were in accordance with their structures. Fortunately, the single crystal of **3A** was obtained as shown in figure 4.1.

#### 4.1.2 Synthesis of 1,3-alternate calix[4]arene tetra-*m*-benzoic acid (**3B**)

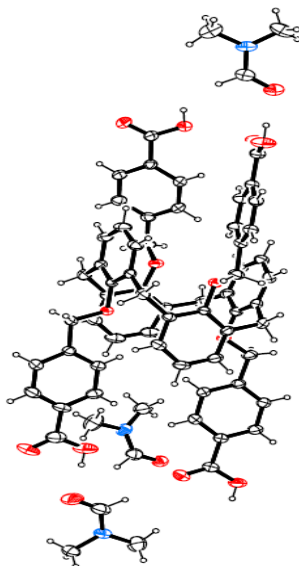


**Scheme 4.2** Synthetic pathway of 1,3-alternate calix[4]arene tetra-*m*-benzoic acid (**3B**).

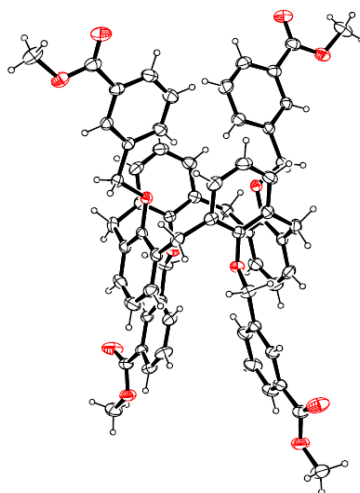
The synthesis of 1,3-alternate calix[4]arene tetra-*m*-benzoic acid (**3B**) was carried out using the same method as the preparation of 1,3-alternate calix[4]arene tetra-*p*-benzoic acid (**3A**) but using methyl-3-(bromomethyl) instead of benzoate methyl-4-(bromomethyl) benzoate as shown in Scheme 4.2. The obtained products in each step were in good agreement with their spectroscopy data. In addition, the crystal structure of **2B** was also obtained. The crystal structure is shown



in Figure 4.2. Crystal structures of **2B** and **3A** showed that the carboxylate groups pointed out in different directions and affected the morphologies of prepared MOFs.

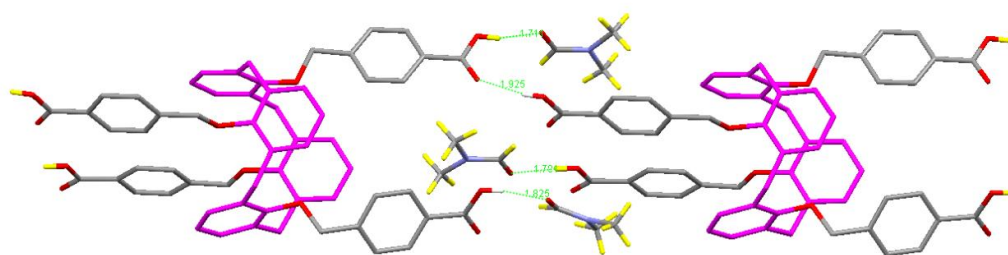


**Figure 4.1** Crystal structure of 1,3-alternate calix[4]arene tetra-*p*-benzoic acid (**3A**), with DMF solvate. (ORTEP draws of **3A** displacement ellipsoids are scaled to the 25% probability level.).



**Figure 4.2** Crystal structure of 1,3-alternate calix[4]arene tetramethyl-*m*-benzoate (**2B**), (ORTEP draws of **2B** displacement ellipsoids are scaled to the 25% probability level.).

The single-crystal of **2B** was obtained in the NMR tube in the  $\text{CDCl}_3$  solvent after several days. In the case of **3A**, its single-crystal was prepared by using the saturated solution of **3A** in DMF solvent which was placed in 10 mL vial and kept in the oven at 90 °C, 24 hrs. The crystal structure revealed the formation of H-bond between carboxylic acid group and DMF solvent. The distance of H-bond are 1.711-1.925 Å, which implied that they were strong H-bond interactions as shown in Figure 4.3.



**Figure 4.3** The distance of H-bond in the organic linker (**3A**).

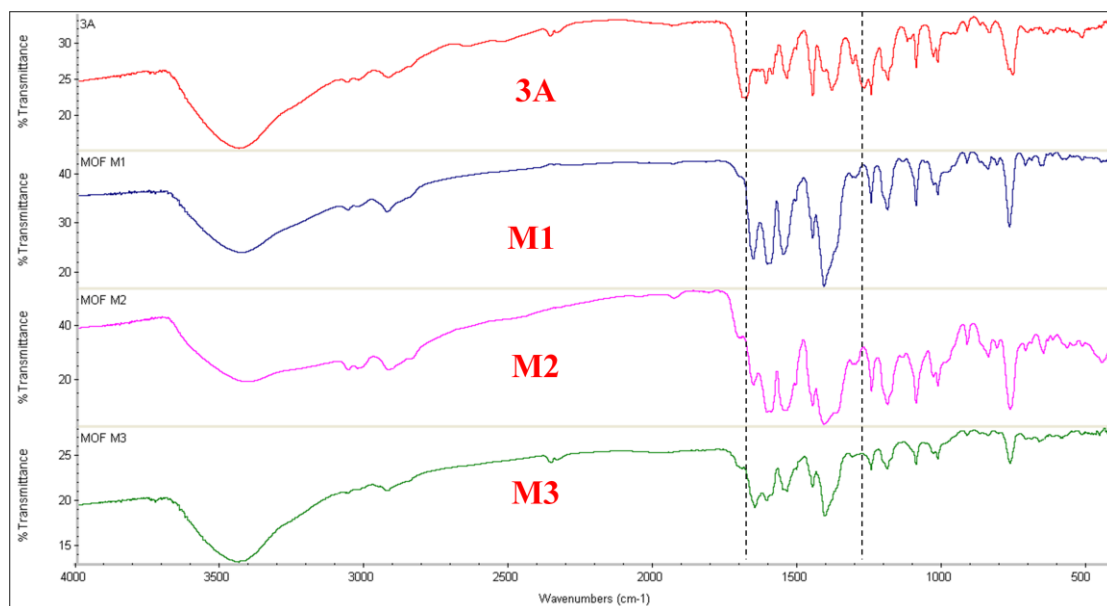
## 4.2 Synthesis of 1,3-alternate calix[4]arene-based MOFs using 1,3-alternate calix[4]arene tetrabenzoic acid derivatives as organic linkers

### 4.2.1 Preparation using conventional heating method

There were 15 MOFs (**M1-M15**) prepared by solvothermal synthesis under conventional heating method. The characterization of **M1-M15** are shown below.

#### 4.2.1.1 IR spectroscopic study

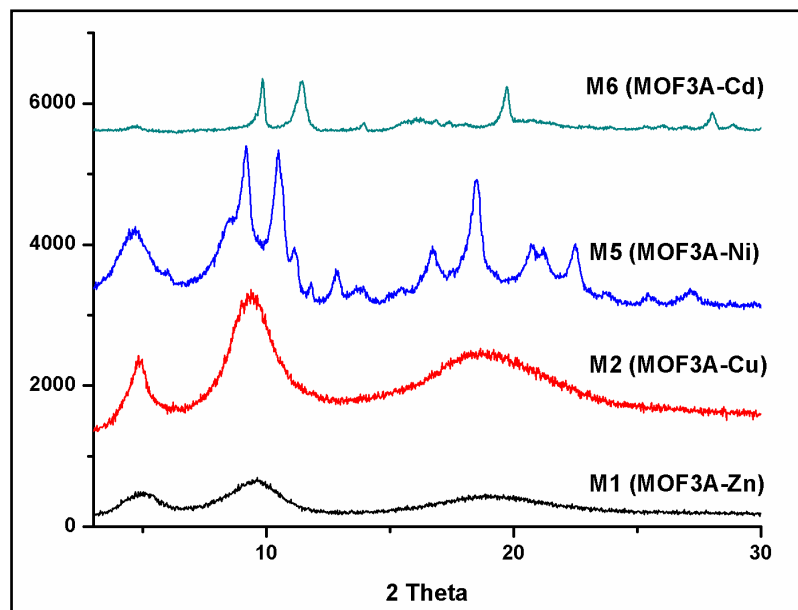
The obtained MOFs were characterized by IR spectroscopy. The compared infrared spectra of organic linkers, 1,3-alternate calix[4]arene tetrabenzoic acid (**3A** and **3B**) and the obtained MOFs (**M1-M3**) were shown in Figure 4.4 and **M4-M15** were displayed in the appendix A (Figure A-25-A-28). The carbonyl (C=O) and C-O stretchings of all 1,3-alternate tetrabenzoic acid calix[4]arene-based MOFs shifted to lower wavenumber comparing with **3A** or **3B** due to the complexation of carboxylate group with metal ions.



**Figure 4.4** Compared IR spectra of **3A**, MOFs **M1** (**3A** +  $\text{Zn}(\text{NO}_3)_2$ ), **M2** (**3A** +  $\text{Zn}(\text{OAc})$ ) and **M3** (**3A** +  $\text{Cu}(\text{NO}_3)_2$ ).

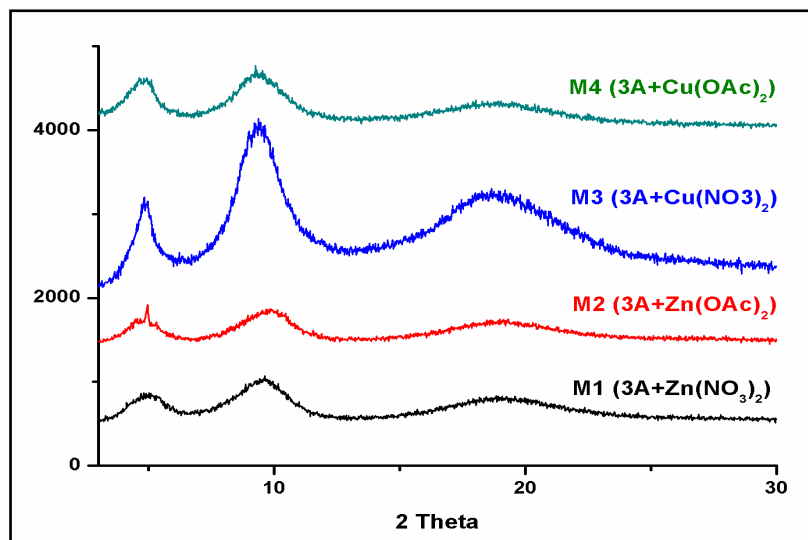
#### 4.2.1.2 XRD study

1,3-Alternate tetrabenzoic acid calix[4]arene-based MOFs were synthesized *via* conventional heating using **3A** as organic linker and different transition metal ions (zinc, copper, nickel, cadmium) Crystal structures showed different XRD patterns (see Figure 4.5) because of different coordination modes of metals. X-ray peak of MOF **M1** and **M3** indicated the amorphous phase as broad peak with low peak intensities. MOFs **M5** and **M6** showed higher purity phases than MOFs **M1** and **M3**.



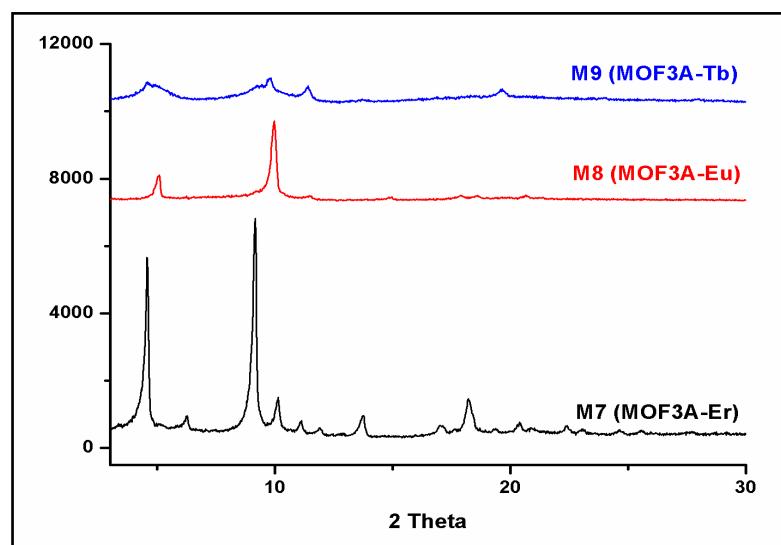
**Figure 4.5** Powder X-ray diffraction patterns of MOFs **M1**, **M3**, **M5**, **M6**.

To study the effect of the anion of metal salts on the formation of MOFs. **M1** and **M2** were prepared from different metal salts. **M1** was prepared from **3A** and  $\text{Zn}(\text{NO}_3)_2$ . **M2** was prepared from **3A** and  $\text{Zn}(\text{OAc})_2$ . MOFs **M3** and **M4** were prepared from **3A** with  $\text{Cu}(\text{NO}_3)_2$  and  $\text{Cu}(\text{OAc})_2$  respectively. They showed no significant change in the XRD pattern (Figure 4.6). Both  $\text{NO}_3^-$  and  $\text{OAc}^-$  gave the same result. However the data from SEM reveal that MOF that prepared from metal ion with  $\text{NO}_3^-$  as anions gave well-shape and homogenous particle sizes.



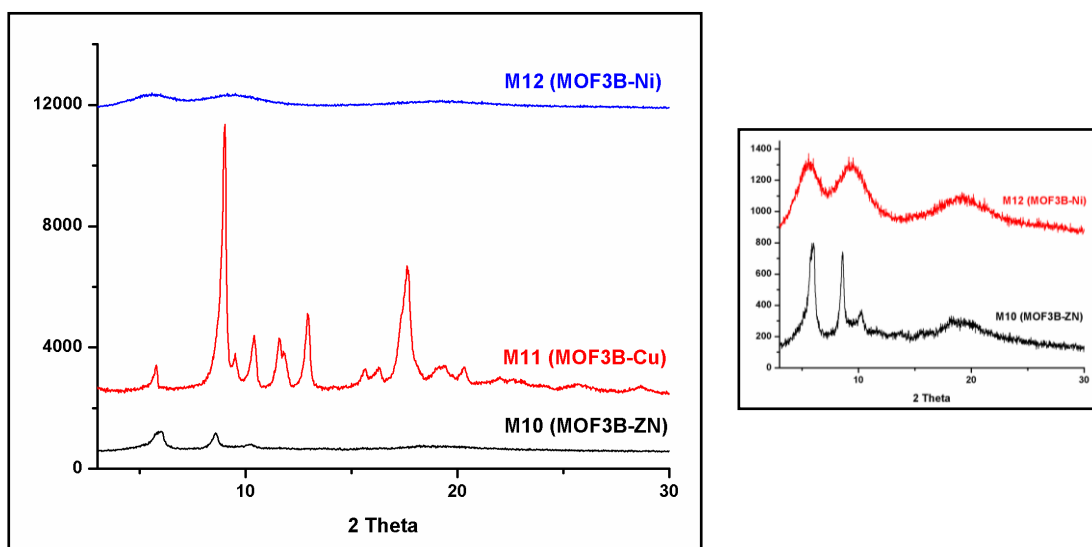
**Figure 4.6** Powder X-ray diffraction patterns of MOFs **M1**, **M2**, **M3**, **M4**.

In addition, lanthanide metal ions ( $\text{Er}^{3+}$ ,  $\text{Eu}^{3+}$ ,  $\text{Tb}^{3+}$ ) were also used with organic linker **3A**. They displayed different XRD patterns as shown in Figure 4.7. In the case of MOFs **M7** and **M8** showed sharp peaks which indicated the high crystallinity, but MOF **M9** exhibited broad peak and low intensity suggesting the amorphous structure.



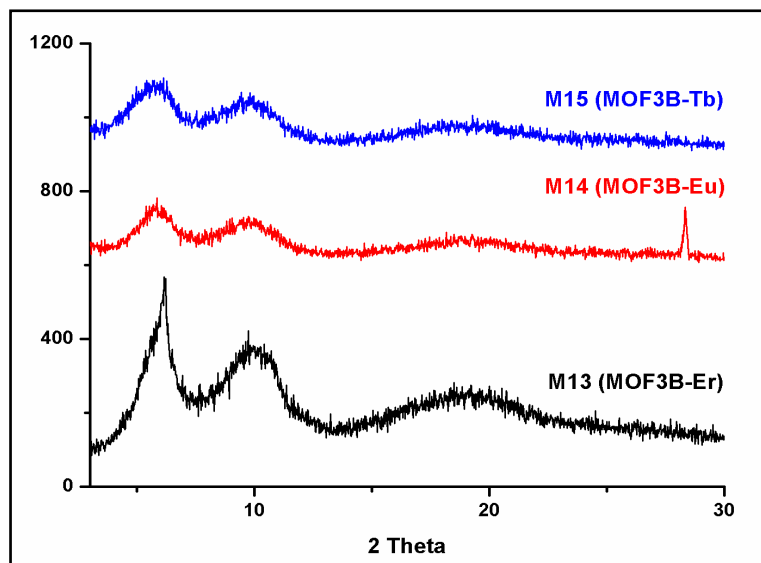
**Figure 4.7** Powder X-ray diffraction patterns of MOFs **M7**, **M8**, **M9**.

MOFs obtained from the organic linker **3B** with transition metal ions ( $\text{Zn}^{2+}$ ,  $\text{Cu}^{2+}$ ,  $\text{Ni}^{2+}$ ) showed different XRD pattern as display in Figure 4.8. MOF **M11** (**3B**- $\text{Cu}^{2+}$ ) exhibited high intensity and sharp peak owing to the high ordered structure and the high crystallinity of materials. However, XRD pattern of **M12** exhibited the amorphous phase as broad peaks with lower peak intensities. In the case of **M10**, the XRD pattern showed quite high pure phase.



**Figure 4.8** Powder X-ray diffraction patterns of MOFs **M10**, **M11**, **M12**.

For the lanthanide metal ion series with **3B** as organic linkers, the XRD patterns were illustrated in Figure 4.9. They have similar XRD pattern with broad peaks. These data implied that the obtained MOFs were amorphous materials. Comparing with the XRD pattern of **3A** with lanthanide metal ions, **M7**, **M8** showed high purity phase. These results implied that the different structures of organic linkers **3A** and **3B** have an important role in the resulting MOFs.




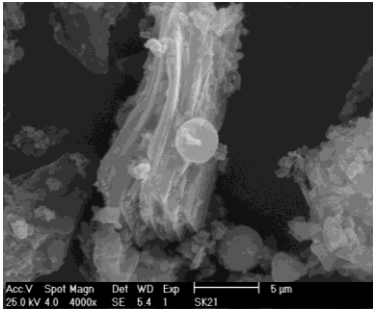
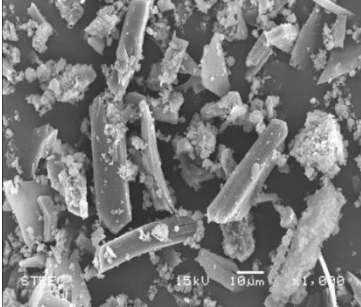
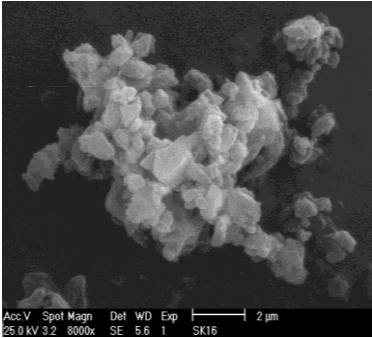
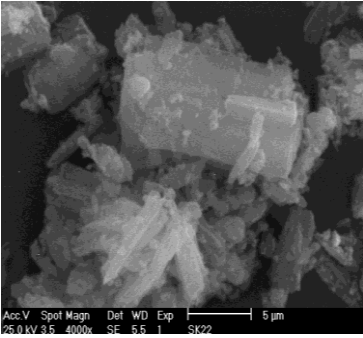
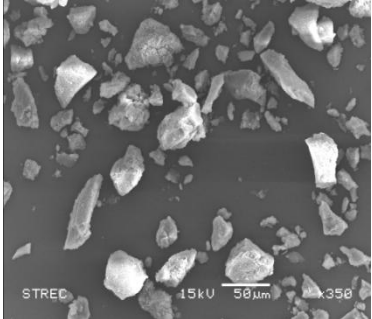
**Figure 4.9** Powder X-ray diffraction patterns of MOFs **M13**, **M14**, **M15**.

#### 4.2.1.3 SEM study

The morphology of all MOFs were studied by scanning electron microscopy (SEM) after gold deposition which exhibited as micro-particle of MOFs in various uniform of needle-like, cubic, rod and platelet shapes as demonstrated in Table 4. However, some of them formed aggregated particles or chunky particles.

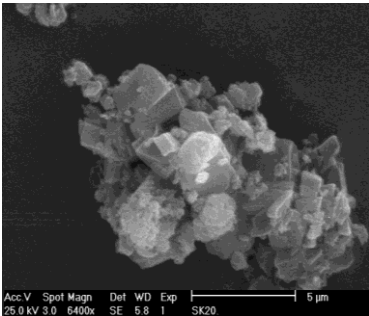
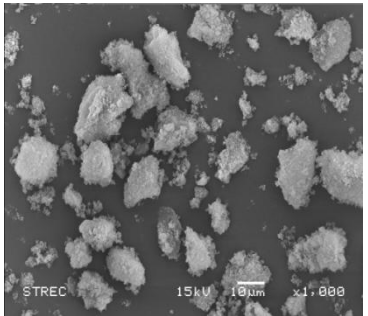
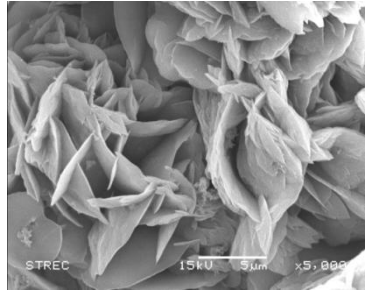
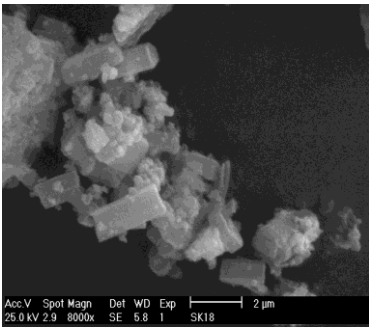
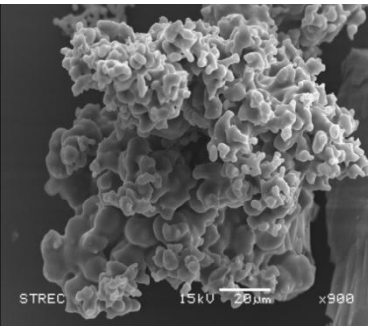
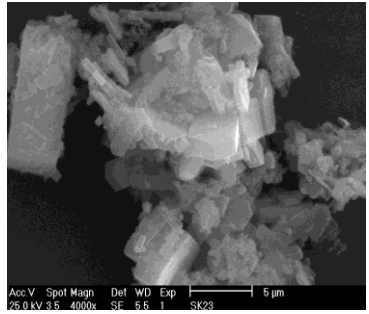
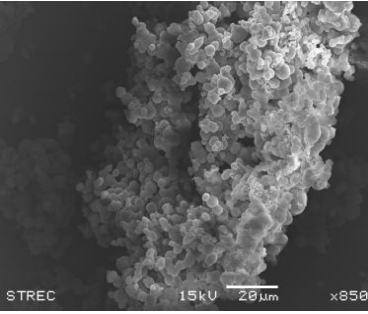
The morphology of MOFs which construction by the same metal ion but using different organic linkers **3A** or **3B** gave different size and shape of particles. For example, the morphology of MOF **M1** that synthesized by using **3A** and  $\text{Zn}(\text{NO}_3)_2$  was rectangular bar shape. A particle size was around  $20 \mu\text{m} \times 200 \mu\text{m}$ . In the case of MOF **M10** synthesized from **3B** and  $\text{Zn}(\text{NO}_3)_2$  with the same condition reaction as MOF **M1**, the morphology was aggregated particles with a particle size around  $5 \mu\text{m} \times 20 \mu\text{m}$ . MOFs **M7**, **M8** and **M9** used **3A** as organic linkers and  $\text{Er}^{3+}$ ,  $\text{Eu}^{3+}$  and  $\text{Tb}^{3+}$  as metal ions respectively. MOFs **M13**, **M14** and **M15** using **3B** as organic linkers and  $\text{Er}^{3+}$ ,  $\text{Eu}^{3+}$  and  $\text{Tb}^{3+}$  as metal ions, respectively. The MOFs prepared from **3A** were bigger and have more well-shaped than MOFs prepared from **3B**. Therefore, different organic linkers play an important role in controlling the structures of MOFs.

**Table 4.1** SEM images of synthesized MOFs and particle size.

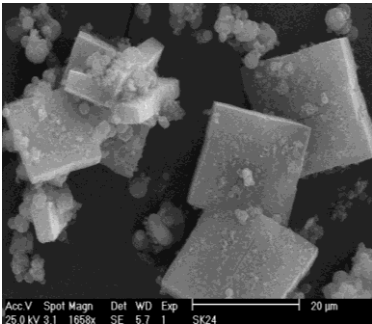
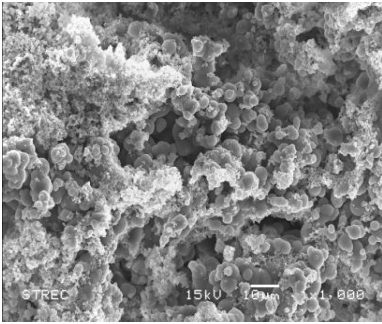
Ligands Metal salts	3A	3B
Code of MOFs/ SEM images		
Zn(NO <sub>3</sub> ) <sub>2</sub>	<p style="text-align: center;"><b>M1</b></p> 	<p style="text-align: center;"><b>M10</b></p> 
Zn(OAc) <sub>2</sub>	<p style="text-align: center;"><b>M2</b></p> 	-
Cu(NO <sub>3</sub> ) <sub>2</sub>	<p style="text-align: center;"><b>M3</b></p> 	<p style="text-align: center;"><b>M11</b></p> 
Cu(OAc) <sub>2</sub>	<p style="text-align: center;"><b>M4</b></p> 	-



**Table 4.1** SEM images of synthesized MOFs and particle size. (Continued)

Ligands Metal salts	3A	3B
	Code of MOFs/ SEM images	
$\text{Ni}(\text{NO}_3)_2$	<p><b>M5</b></p> 	<p><b>M12</b></p> 
$\text{Cd}(\text{NO}_3)_2$	<p><b>M6</b></p> 	-
$\text{Er}(\text{NO}_3)_3$	<p><b>M7</b></p> 	<p><b>M13</b></p> 
$\text{EuCl}_3$	<p><b>M8</b></p> 	<p><b>M14</b></p> 

**Table 4.1** SEM images of synthesized MOFs and particle size. (Continued)

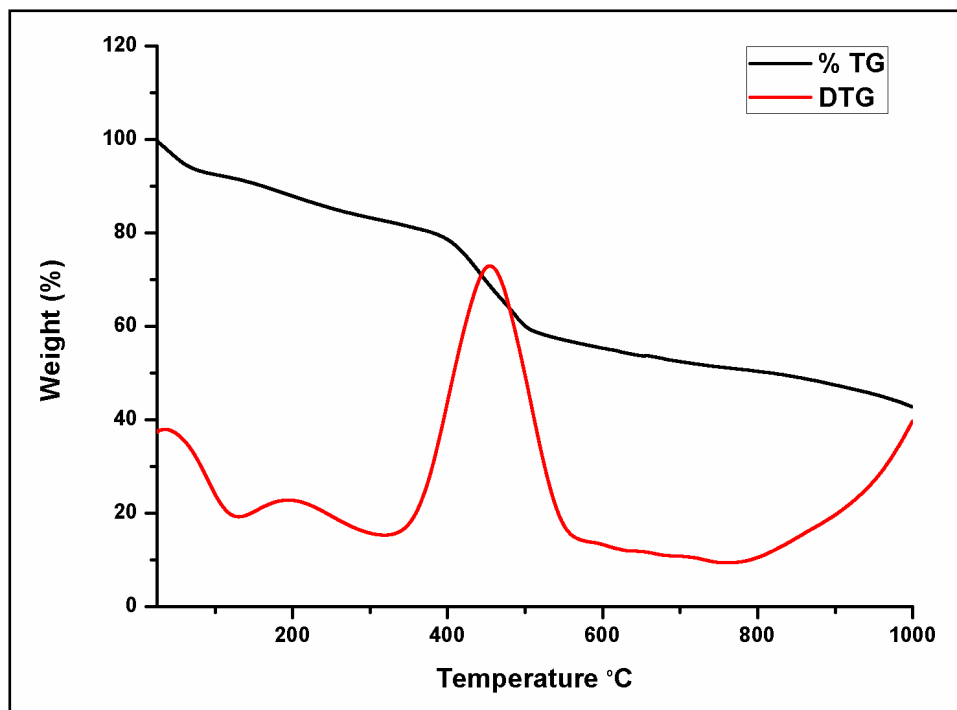
Ligands Metal salts	3A	3B
	Code of MOFs/ SEM images	
Tb(NO <sub>3</sub> ) <sub>3</sub>	<p style="text-align: center;"><b>M9</b></p> 	<p style="text-align: center;"><b>M15</b></p> 

Comparing SEM images and powder XRD patterns of obtained MOFs showed that results were agreeable. In case of MOF **M1**, XRD pattern exhibited amorphous but SEM image showed high crystallinity. These results might due to measurement of powder XRD patterns used bulk sample but morphology was measured from a small part of bulk sample, it does not show overall of the material.

#### 4.2.1.4 Thermal stability

The thermal stability of obtained MOFs were investigated by thermalgravimetric analysis under nitrogen atmosphere. MOF **M1** was used as a candidate. Its thermogram is shown in Figure 4.10 revealed that in the first step was the decomposition of water molecules in the framework. The second step was the decomposition of dimethylformamide (DMF) at about 200 °C and the weight loss of 9%. The third step (350-550 °C) was the decomposition of MOFs.

The samples are used in the N<sub>2</sub> adsorption measurements have to pretreat in order to remove the residual or solvent molecules within the pore of the framework. The result from TGA study reveal that the sample MOFs should be pretreated at 250°C which was the temperature that solvent molecules were completely evaporated.



**Figure 4.10** Thermogram of MOF M1 (3A-Zn).

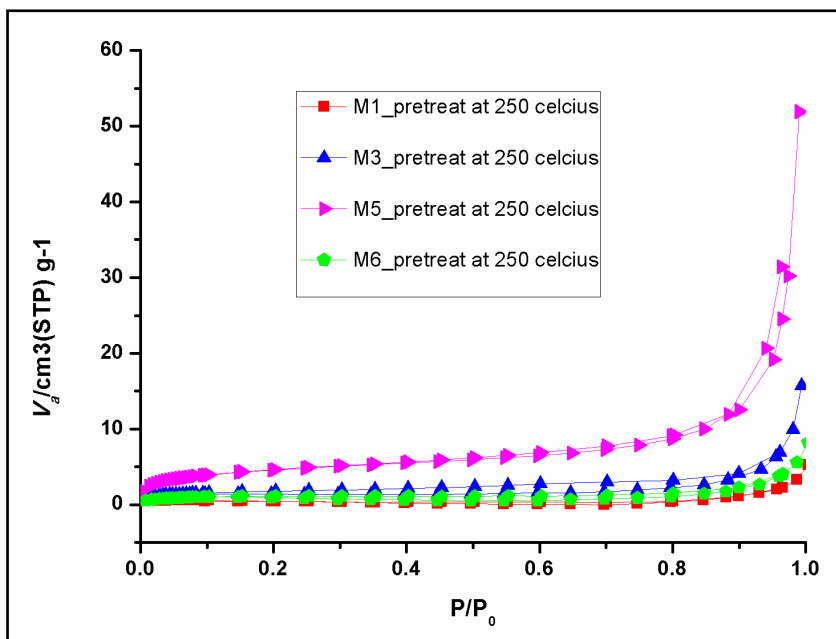
#### 4.2.1.5 Nitrogen Adsorption-Desorption study

The nitrogen adsorption-desorption isotherms of all of 1,3-alternate tetrabenzoic acid calix[4]arene-based MOFs were performed as type III adsorption isotherm of IUPAC classification, which was typical for nonporous material, and the results were illustrated in Figure 4.11-4.15. The BET Surface area of MOFs were shown in Table 4.2. All of the obtained 1,3-alternate tetrabenzoic acid calix[4]arene-based MOFs have a very low surface area comparing with MOF-5 that have surface area around 2,296 m<sup>2</sup>/g. The results implied that the organic linkers used into synthesis MOFs were too large. The MOF cannot be formed in a 3D framework as they might not have a pore. The single crystal structure of MOFs should be characterized.

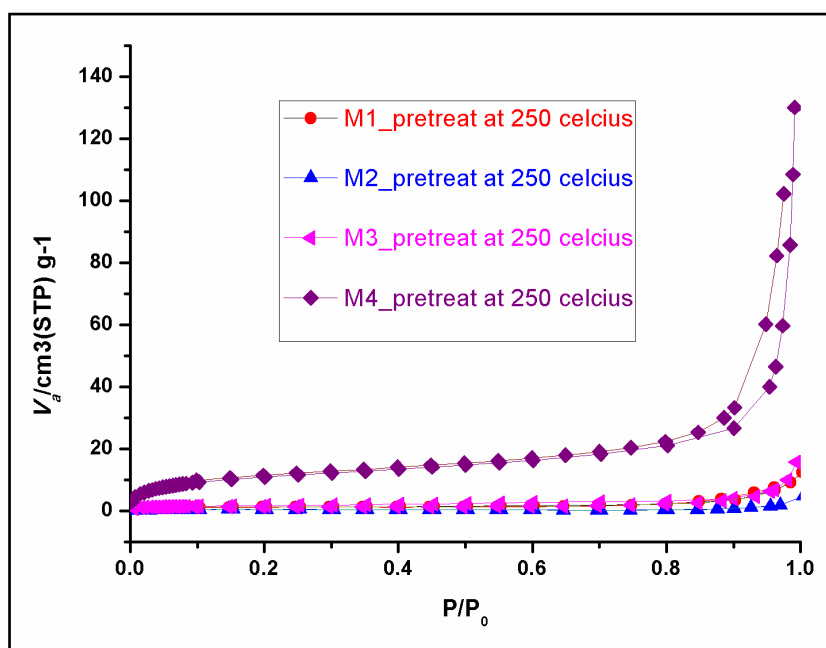
**Table 4.2** Textural properties of synthesized MOFs with pretreatment temperature at 250 °C.

<b>Code of MOFs</b>	<b>Condition</b>	<b>S<sub>BET</sub><sup>a</sup> (m<sup>2</sup>/g)</b>
<b>M1</b>	<b>3A + Zn(NO<sub>3</sub>)<sub>2</sub></b>	5.08
<b>M2</b>	<b>3A + Zn(OAc)<sub>2</sub></b>	1.55
<b>M3</b>	<b>3A + Cu(NO<sub>3</sub>)<sub>2</sub></b>	6.55
<b>M4</b>	<b>3A + Cu(OAc)<sub>2</sub></b>	40.88
<b>M5</b>	<b>3A + Ni(NO<sub>3</sub>)<sub>2</sub></b>	17.15
<b>M6</b>	<b>3A + Cd(NO<sub>3</sub>)<sub>2</sub></b>	-
<b>M7</b>	<b>3A + Er(NO<sub>3</sub>)<sub>3</sub></b>	27.13
<b>M8</b>	<b>3A + Eu(Cl)<sub>3</sub></b>	7.89
<b>M9</b>	<b>3A + Tb(NO<sub>3</sub>)<sub>3</sub></b>	8.90
<b>M10</b>	<b>3B + Zn(NO<sub>3</sub>)<sub>2</sub></b>	2.63
<b>M11</b>	<b>3B + Cu(NO<sub>3</sub>)<sub>2</sub></b>	7.78
<b>M12</b>	<b>3B + Ni(NO<sub>3</sub>)<sub>2</sub></b>	48.75
<b>M13</b>	<b>3B + Er(NO<sub>3</sub>)<sub>3</sub></b>	2.81
<b>M14</b>	<b>3B + Eu(Cl)<sub>3</sub></b>	0.089
<b>M15</b>	<b>3B + Tb(NO<sub>3</sub>)<sub>3</sub></b>	4.79

<sup>a</sup> specific surface area determined by application of the BET-plot method



**Figure 4.11** Nitrogen adsorption-desorption isotherms of MOFs M1, M3, M5 and M6.



**Figure 4.12** Nitrogen adsorption-desorption isotherms of MOFs M1, M2, M3 and M4.

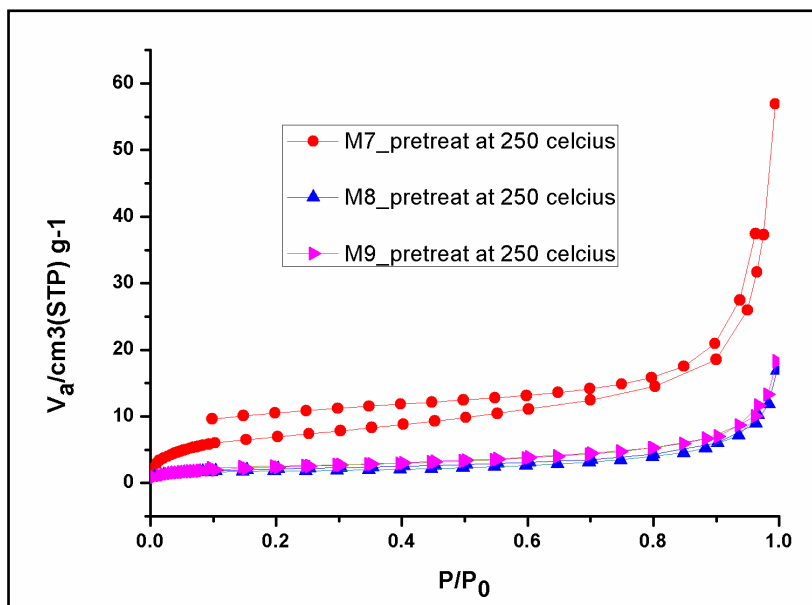


Figure 4.13 Nitrogen adsorption-desorption isotherms of MOFs M7, M8 and M9.

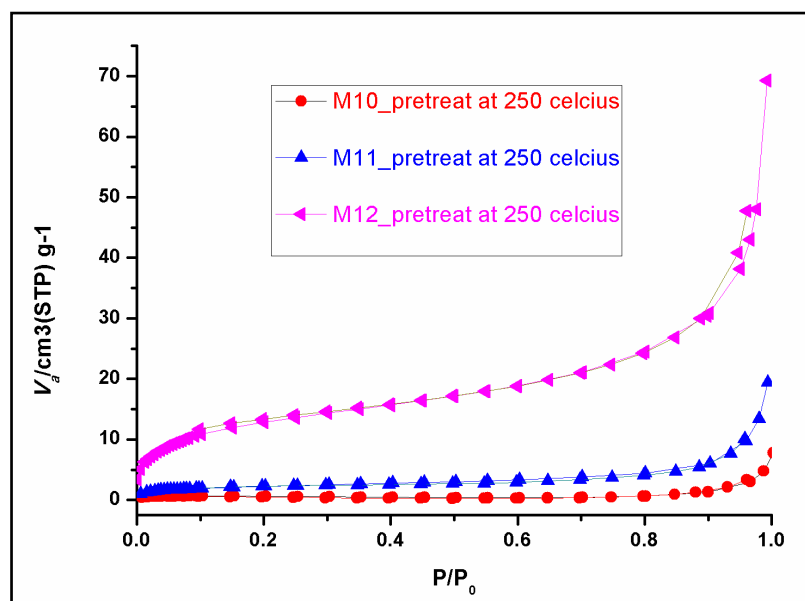
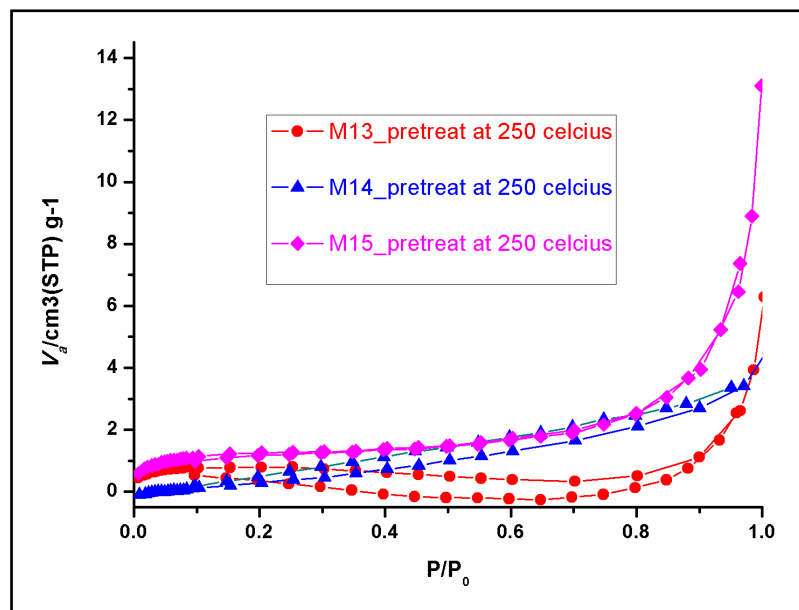


Figure 4.14 Nitrogen adsorption-desorption isotherms of MOFs M10, M11 and M12.



**Figure 4.15** Nitrogen adsorption-desorption isotherms of MOFs **M13**, **M14** and **M15**.

The synthesis MOFs by using solvothermal in conventional heating method is the simple way to synthesize MOFs in a large scale. However, all of the synthesized MOFs via this method exhibited nonporous materials. Furthermore, single-crystals of these MOFs could not be obtained. In order to solve the structure of the 1,3-alternate calix[4]arene based metal-organic frameworks. The single-crystal of synthesized MOFs are require. In the research, the solvothermal method in the small container (seal vial, autoclave) were used for crystalline the MOFs. Fortunately, the single-crystals were obtained.

#### 4.2.2 Preparation of MOFs via solvothermal in seal vials and autoclave

The synthesis of metal-organic frameworks by solvothermal in seal vials and autoclave gave the crystal that is suitable for X-ray diffraction analysis in appropriate conditions. There are 4 MOFs successfully characterized by X-ray technique. The first MOF composed of **3A** and  $\text{Zn}^{2+}$  (Named **CU-SCRU1**). The second MOF obtained from **3B** and  $\text{Zn}^{2+}$  (Named **CU-SCRU2**). The third and the fourth were synthesized by using **3B** and  $\text{Cd}^{2+}$ . They are from the same reaction (Named **CU-SCRU3**, **CU-SCRU4**), but can be fractionally crystallized.

**Table 4.3** Crystallographic Data for **CU-SCRU1** and **CU-SCRU2**

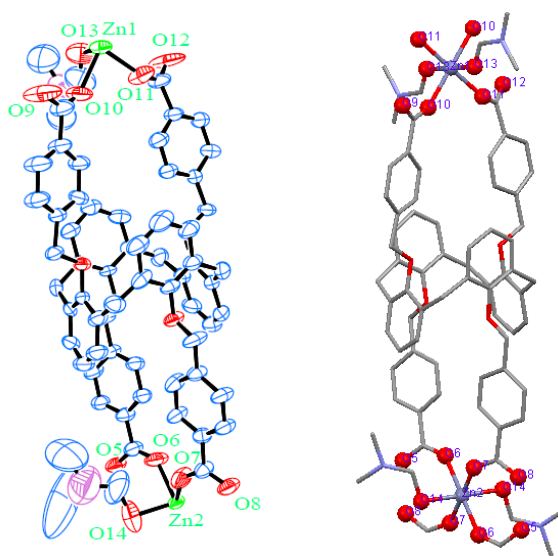
	<b>CU-SCRU1</b>	<b>CU-SCRU2</b>
CCDC deposit no.	928239	928240
formula	C <sub>66</sub> H <sub>58</sub> N <sub>2</sub> O <sub>14</sub> Zn	C <sub>40</sub> H <sub>29.33</sub> O <sub>8.67</sub> Zn <sub>1.33</sub>
fw	1168.51	735.79
temp, K	296(2)	296(2)
cryst syst	Triclinic	Orthorhombic
space group	P-1	Aba2
Z	2	12
a (Å)	12.3045	20.5907
b (Å)	15.7998	25.2533
c (Å)	16.762	29.7148
α (°)	92.890	90
β (°)	92.951	90
γ (°)	97.383	90
V (Å <sup>3</sup> )	3222.0	15451.2
D <sub>x</sub> (g/cm <sup>3</sup> )	1.204	0.949
2θ <sub>max</sub> (deg)	1.22-25.18	1.37-22.26
R <sub>1</sub> , wR <sub>2</sub> [ I > 2σ(I) ]	0.1572, 0.4306	0.1253, 0.3301
R <sub>1</sub> , wR <sub>2</sub> [ all data ]	0.2077, 0.4618	0.1410, 0.3491
Structure determination	SHELXTL 97	SHELXTL 97
refinement	Full-matrix	Full-matrix

#### 4.2.2.1 Crystal structure of CU-SCRU1

A solvothermal reaction of organic linker **3A** with Zn(NO<sub>3</sub>)<sub>2</sub>·6H<sub>2</sub>O in mixed solvents DMF and DEF (1:1, V/V) was placed in 10 mL vial and sealed, the vial was kept at 90 °C in an oven for 48 h, followed by cooling to room temperature over 12 h. Colorless needle-like crystals were obtained and characterized. Single-crystal x-ray diffraction analysis reveals that **CU-SCRU1** composed of two kinds of crystallographically independent Zn(II) ions. Zn<sub>1</sub>(II) ion is in an octahedral coordination geometry with four monodentate carboxylate oxygen

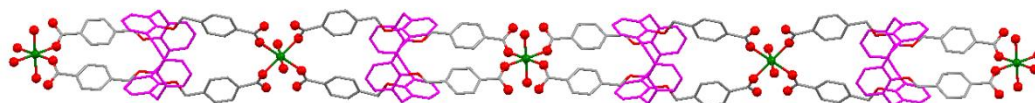


atoms in the equatorial positions and two oxygen atoms from DMF molecules in the axial positions (Figure 4.16). The  $Zn_1$ -O bond lengths are in the range of 2.047-2.128 Å. The coordination environment of  $Zn_2$ (II) ion is same as  $Zn_1$ (II) ion. The  $Zn_2$ -O bond lengths are in the range of 2.040-2.134 Å. The bond angle of octahedral coordination geometries in CU-SCRU1 are close to the ideal bond angle of octahedral as illustrated in Appendix B (Table B-3).

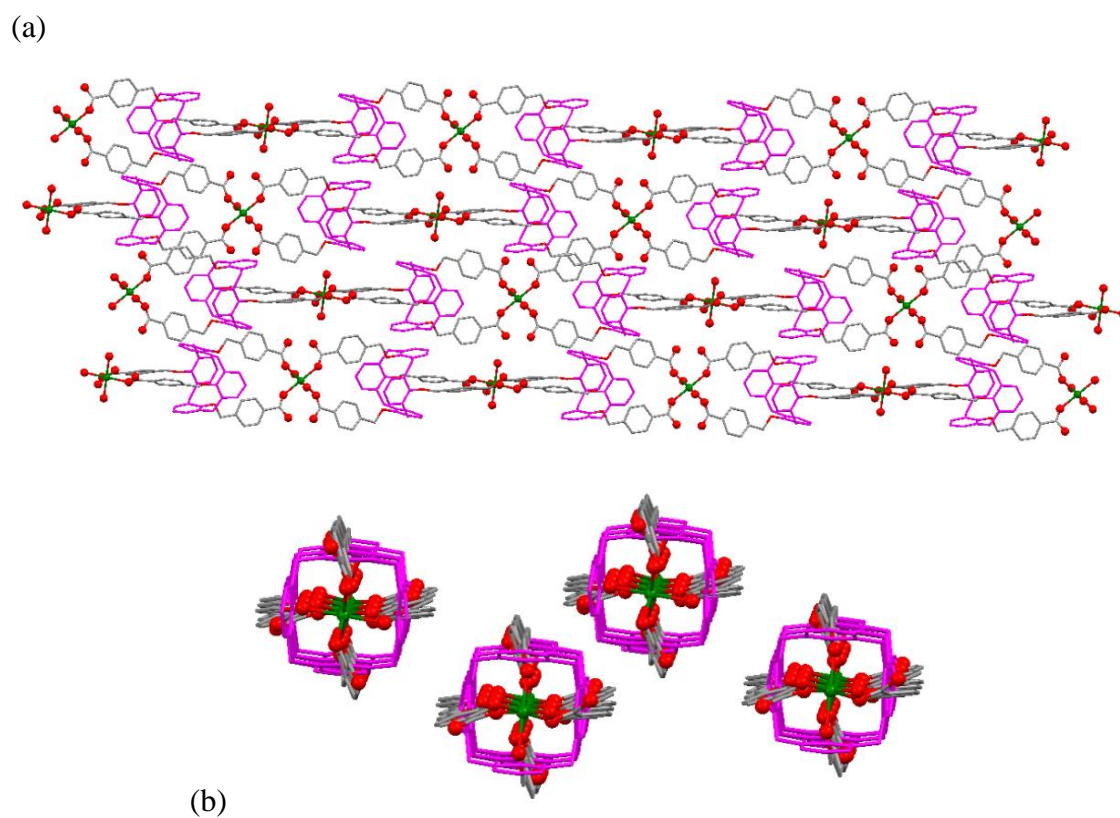


**Figure 4.16** Coordination environment of **CU-SCRU1**; (a) the asymmetric unit and the related coordination atoms are labeled and the hydrogen atoms are omitted for clarity: green, Zn1 and Zn2; red, O; purple, N; blue, C. (b) Zn(II) ion located in octahedral geometry which generated by Mercury.

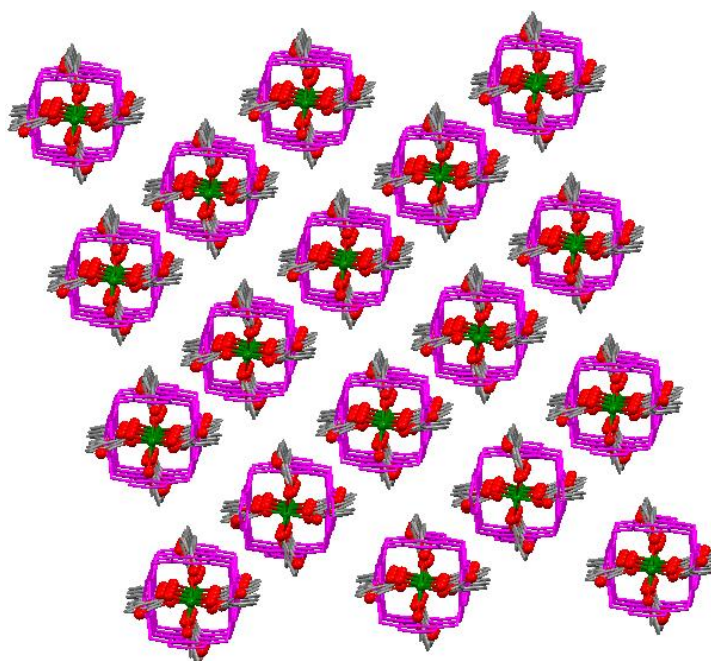
The coordination geometry of  $Zn_1$ (II) and  $Zn_2$ (II) ions are perpendicular to each other. The structure of **CU-SCRU1** extended in 1D linear chain by the coordination bond as display in Figure 4.17. The 2D and 3D structures of **CU-SCRU1** are formed 1D-polymeric chain by weak intermolecular interaction (non-classical H-bonding, Appendix B) as illustrated in Figures 4.18 and 4.19.



**Figure 4.17** Overall 1D polymeric chain of **CU-SCRU1** generated by Mercury.

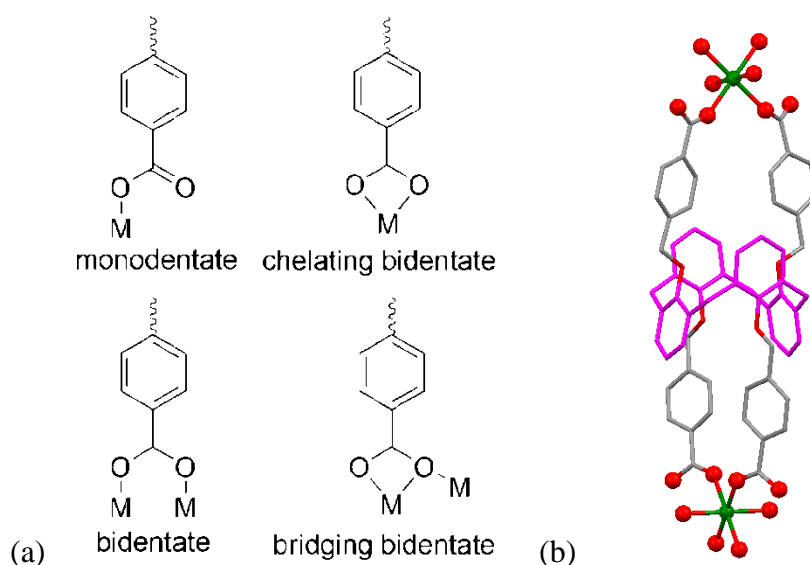


**Figure 4.18** 2D structure of **CU-SCRU1** generated by Mercury. (a) side view, (b) top view.



**Figure 4.19** Top view of the 3D structure of **CU-SCRU1**.

As mentioned previously, the carboxylate donor groups have many modes to chelate with metal ions. Figure 4.20 showed the coordination modes of the multicarboxylate ligand **3A** in the complex of **CU-SCRU1**. There are four carboxylate groups in the ligand **3A**. All carboxylate group are coordinated to Zn(II) ion in a monodentate manner.

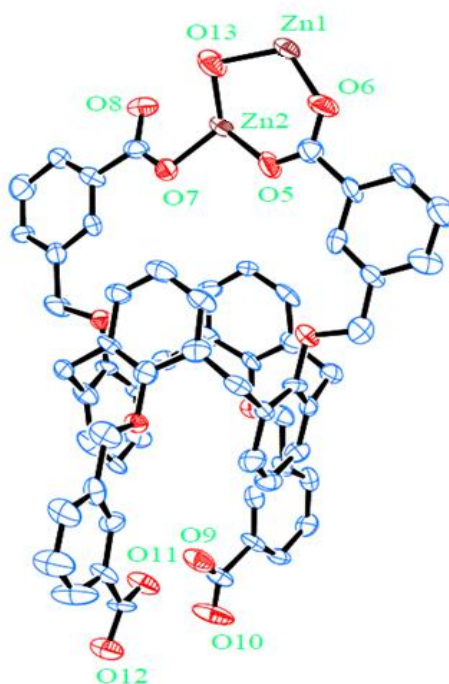


**Figure 4.20** (a) Coordination modes of carboxylate organic linkers, (b) Coordination modes of the tetracarboxylate ligand **3A** with Zn(II) ion in the complex **CU-SCRU1** (Blue, Zn(II); red, O).

#### 4.2.2.2 Crystal structure of CU-SCRU2

A solvothermal reaction of organic linker **3B** with  $\text{Zn}(\text{NO}_3)_2 \cdot 6\text{H}_2\text{O}$  was placed in a 100 mL of Teflon-lined stainless steel with DMF:DEF(1:1, 30 mL). The mixture was heated to 150°C in 6 h and kept to this temperature for 48 h. After cooling to room temperature for 24 h, cubic colorless crystals were obtained and characterized as displayed in Figure 4.21, **CU-SCRU2** composed of two kinds of crystallographically independent Zn(II) ions. Both  $\text{Zn}_1(\text{II})$  ion and  $\text{Zn}_2(\text{II})$  ion are in tetrahedral geometry completed by three oxygen atoms from three carboxylic groups in a monodentate fashion and one oxygen atom bridging between  $\text{Zn}_1(\text{II})$  ion and  $\text{Zn}_2(\text{II})$  ion. For  $\text{Zn}_1(\text{II})$  ion, bond lengths of  $\text{Zn}_1\text{-O}$  are in the

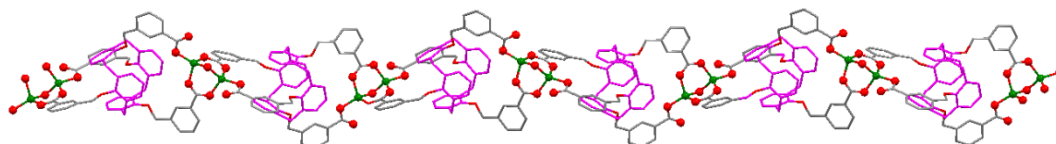
range of 1.938-1.992 Å and the bond angle of tetrahedral geometry are 98.9°-123.2°. In the case of Zn<sub>2</sub>(II) ion, Zn<sub>2</sub>-O = 1.907-2.007 Å and bond angle = 103.9°-115.4° as illustrated in Appendix B (Table B-3).



**Figure 4.21** Coordination environment of **CU-SCRU2**; the asymmetric unit and the related coordination atoms are labeled and the hydrogen atoms are omitted for clarity: green, Zn1 and Zn2; red, O; purple, N; blue, C.

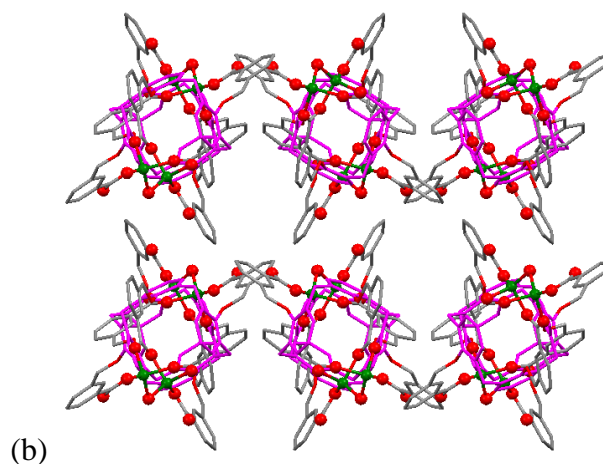
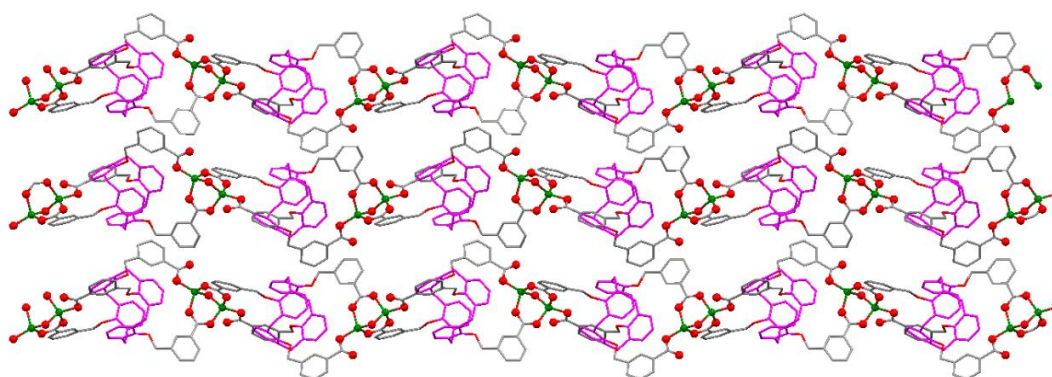
The coordination geometry of Zn(II) ions in the complex of **CU-SCRU1** and **CU-SCRU2** are octahedral and tetrahedral geometry, respectively. This result may be due to the use of different organic linkers which the carboxylic acid group are at the different positions, *para* and *meta* for **3A** and **3B**, respectively. Furthermore, These two compounds were prepared by different synthetic method. As stated above, both the chemical structure of organic linkers and synthesis condition reactions play a vital role in the resulting frameworks.

The structure of **CU-SCRU2** is a 1D zig-zag polymeric chain extending by coordination bonds as shown in Figure 4.22. 2D and 3D structure of **CU-SCRU2** is extended by weak intermolecular interactions as demonstrated in Figure. 4.23.



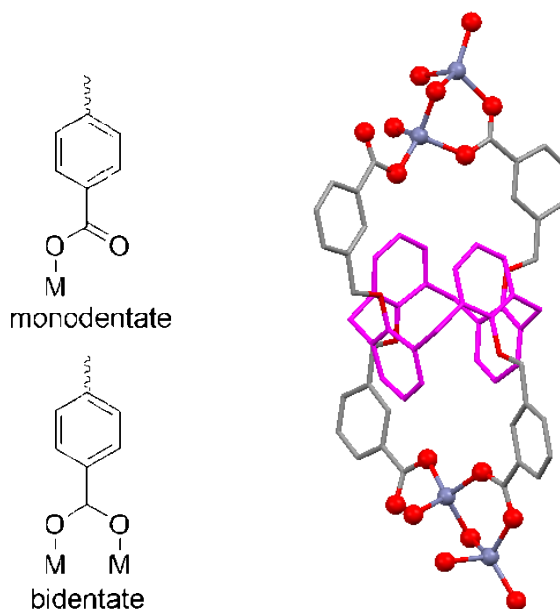
**Figure 4.22** 1D polymeric chain of **CU-SCRU2** generated by Mercury.

(a)



**Figure 4.23** (a) 2D structure of **CU-SCRU2** (Side view) (b) 3D structure of **CU-SCRU2** (Top view), generated by Mercury.

The coordination modes of the ligand **3B** with Zn(II) ion in the complex **CU-SCRU2** are in a monodentate and bidentate fashions as displayed in Figure 4.24.



**Figure 4.24** Coordination modes of the tetracarboxylate ligand **3B** with Zn(II) ion in the complex **CU-SCRU2**.

The result from crystal structures of **CU-SCRU1** and **CU-SCRU2** showed three dimension structure *via* the arrangement of the polymeric coordinated linear chains. These structures do not provide the appropriate pores for capturing gas molecules, and the data from the nitrogen adsorption study reveal that all of obtained MOF which prepared from organic linkers **3A** or **3B** with various metal are nonporous materials.

#### 4.2.2.3 Crystal structure of **CU-SCRU3** and **CU-SCRU4**

A solvothermal reaction of organic linker **3B** with  $\text{Cd}(\text{NO}_3)_2 \cdot 4\text{H}_2\text{O}$  in the mixed solvent DMF and DEF (1:1) (Table 3.5, Entry 1) was placed in a 10 mL vial and sealed. The vial was kept at 90 °C in oven for 48 h, followed by cooling to room temperature over 12 h. Colorless polyhedral crystals

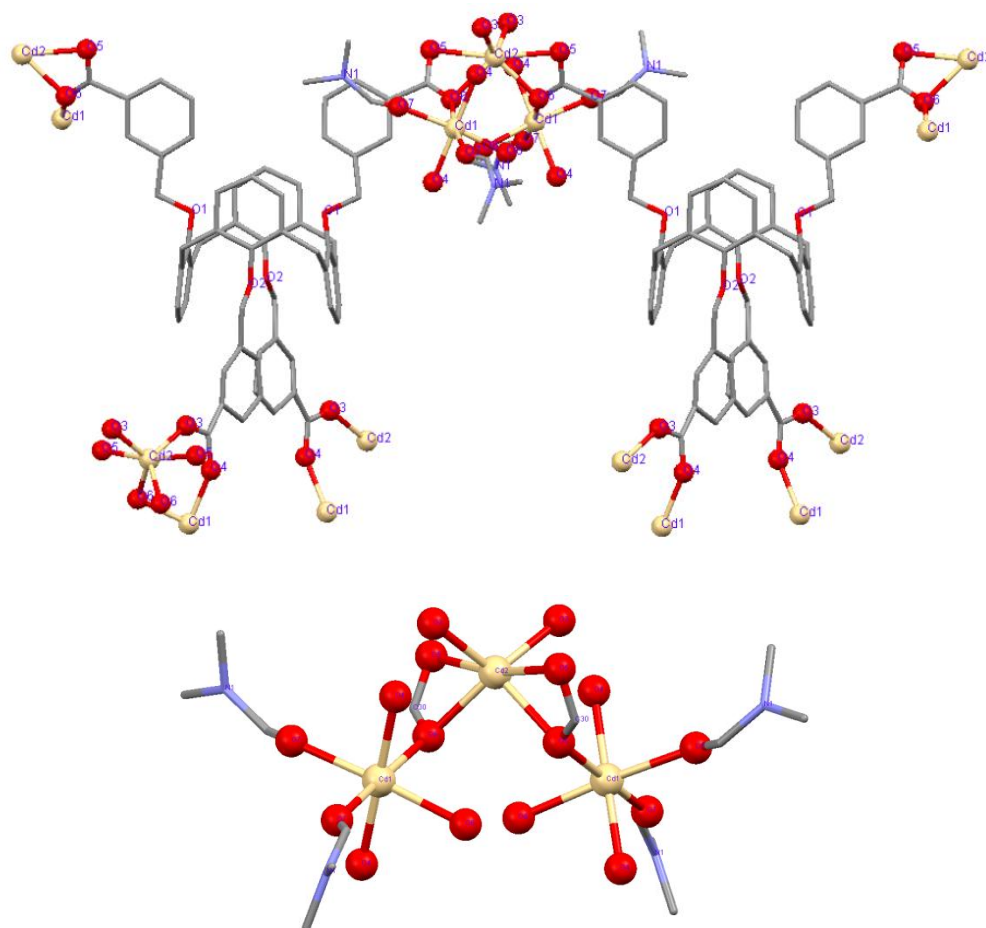
were obtained and characterizes. The crystallographic data for **CU-SCRU3** and **CU-SCRU4** are showed in Table 4.4.

**Table 4.4** Crystallographic Data for **CU-SCRU3** and **CU-SCRU4**

	<b>CU-SCRU3</b>	<b>CU-SCRU4</b>
CCDC deposit no.	922040	916913
formula	C <sub>66</sub> H <sub>58</sub> Cd <sub>2</sub> N <sub>2</sub> O <sub>14</sub>	C <sub>60</sub> H <sub>52</sub> Cd <sub>2</sub> O <sub>16</sub>
fw	1327.94	1253.82
temp, K	296(2)	293(2)
cryst syst	Orthorhombic	Monoclinic
space group	Fddd	C 2/c
Z	32	8
a (Å)	15.5967(11)	15.9438(16)
b (Å)	31.465(3)	32.045(4)
c (Å)	58.253(4)	30.001(4)
$\alpha$ (°)	90	90
$\beta$ (°)	90	105.303(5)
$\gamma$ (°)	90	90
V (Å <sup>3</sup> )	28588(4)	14784(3)
D <sub>x</sub> (g/cm <sup>3</sup> )	1.232	1.127
2 $\theta$ <sub>max</sub> (deg)	22.03	21.14
R <sub>1</sub> , wR <sub>2</sub> [ I > 2 $\sigma$ (I) ]	0.1371, 0.4132	0.1441, 0.4087
R <sub>1</sub> , wR <sub>2</sub> [ all data ]	0.1914, 0.4627	0.1796, 0.4390
GOF	1.814	1.803
data/ restraints/ params	4399 / 0 / 369	7851 / 0 / 704
no. of refines used [ >2 $\sigma$ (I) ]	4399 [R(int) = 0.0687]	7851[R(int)=0.0887]
Structure determination	SHELXTL 97	SHELXTL 97
refinement	Full-matrix	Full-matrix

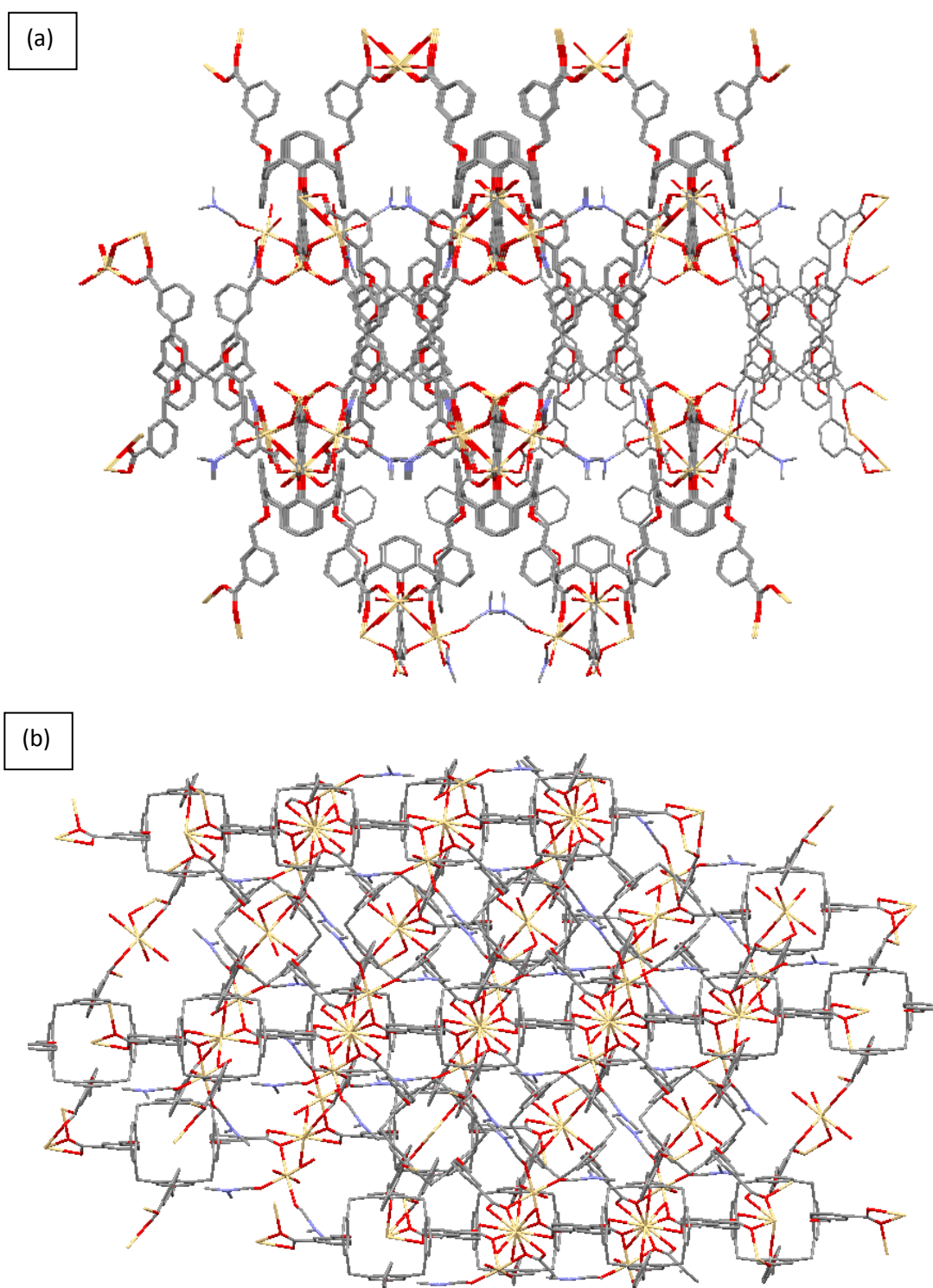
### The crystal structure of CU-SCRU3

As shown in Figure 4.25, two Cd(II) ions showed different coordination environment. Cd<sub>1</sub>(II) ion, which is at the center of a octahedral geometry, is six-coordinated by four carboxylate oxygen atoms and two oxygen atoms from solvent (DMF). However, Cd<sub>2</sub>(II) ion is a six-coordinated twisted octahedral geometry, surrounded by six oxygen atoms from three different **3B** anions. The structure of **CU-SCRU3** features a 3D framework which was generated by Mercury as displayed in Figure 4.26. The selected bond lengths and bond angles of **CU-SCRU3** are illustrated in Appendix B (Table B-4).



**Figure 4.25** Coordination environment of **CU-SCRU3** (H atoms were omitted for clarity).

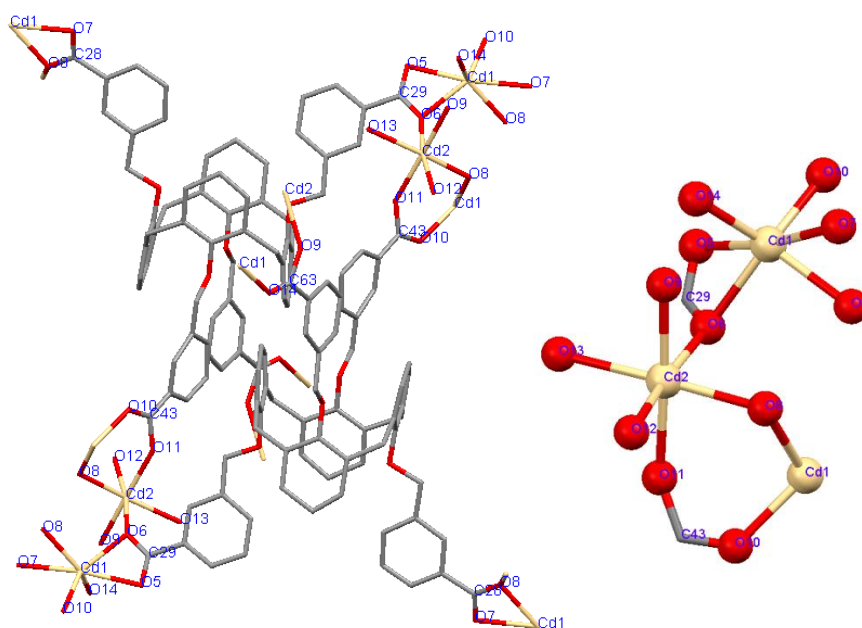




**Figure 4.26** Overall 3D framework of CU-SCRU3 generated by Mercury, (a) view along the *a*-axis, (b) view along the *c*-axis.

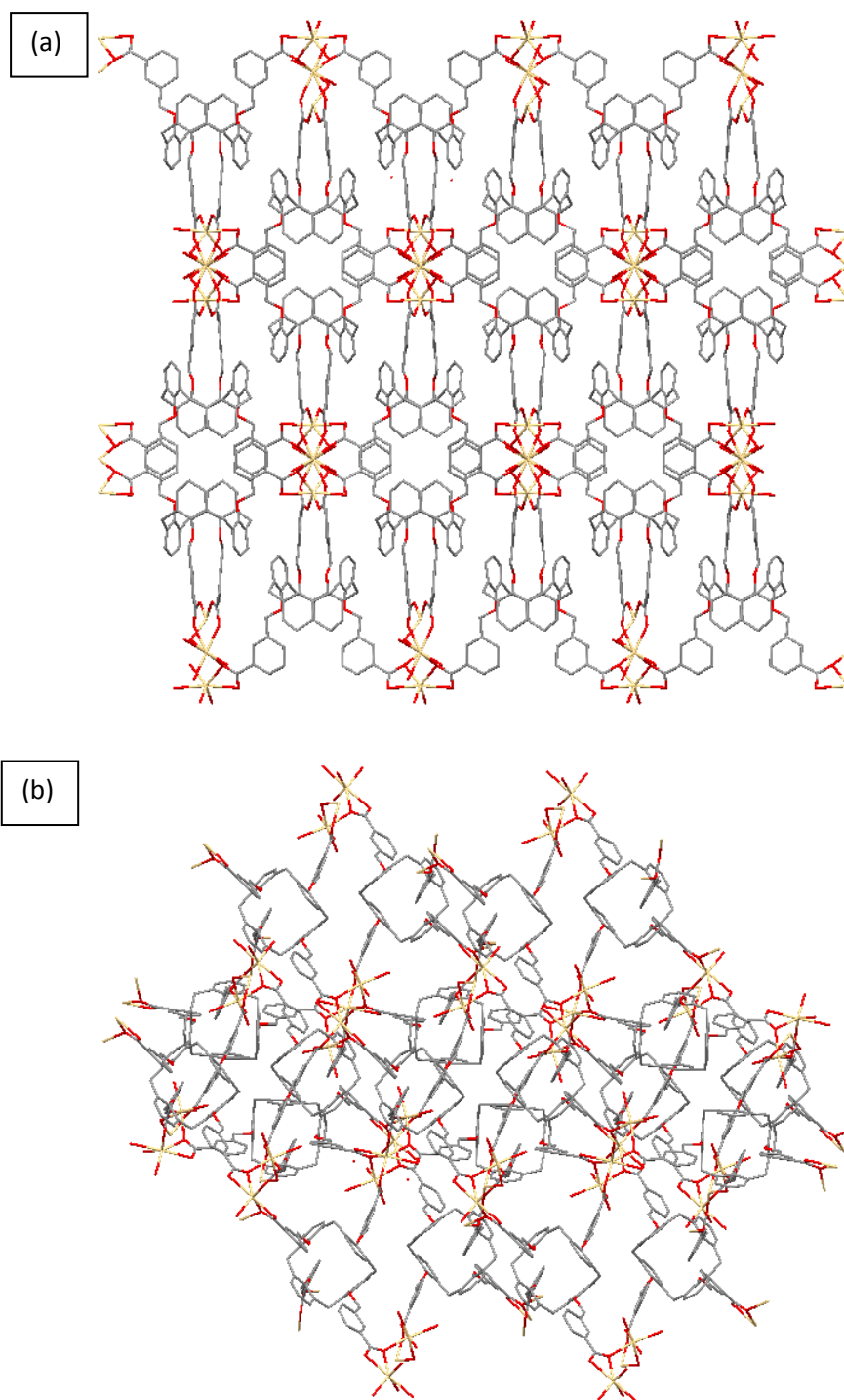
### The crystal structure of CU-SCRU4

The X-ray crystal structure of **CU-SCRU4** as shown in Figure 4.27 which is composed of two kinds of crystallographically independent Cd(II) ions. Cd<sub>1</sub>(II) ion is in a distorted octahedral geometry completed by six oxygen atoms from four carboxylic groups in a chelating/bridging monodentate bidentate and bis-bidentate modes. The coordination environment of Cd<sub>2</sub>(II) is in an octahedral geometry built from two oxygen atoms from water molecules and four oxygen atoms from four carboxylic groups in a chelating/bridging monodentate bidentate and bis-bidentate fashions. The selected bond lengths and bond angles of **CU-SCRU4** are illustrated in Appendix A (Table A-5).



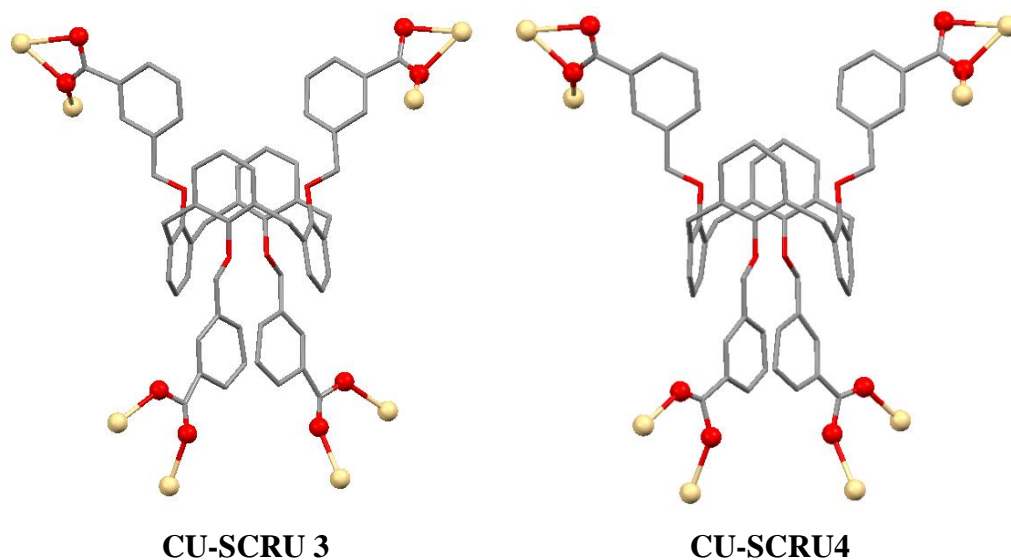
**Figure 4.27** Coordination environment of **CU-SCRU4** (H atoms were omitted for clarity).

The structure of **CU-SCRU4** also exhibited 3D frameworks similar to **CU-SCRU3** which generated by Mercury as displayed in Figure 4.28. It should be noted that the formation of different single-crystals of **CU-SCRU3** and **CU-SCRU4** within the same reaction may be due to the use of a large molecule of organic linker which play important role of the resulting frameworks. The conformation and the flexibility of organic linker provide the different structures.



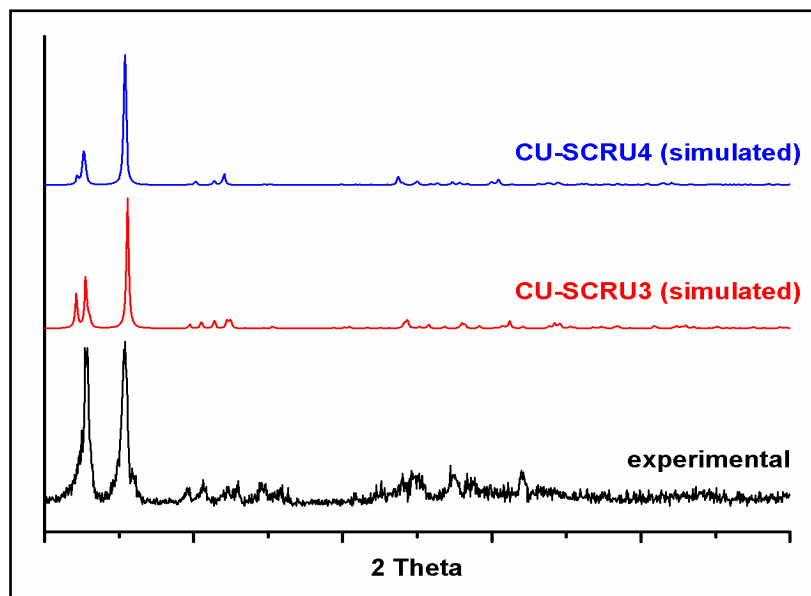
**Figure 4.28** Overall 3D frameworks of **CU-SCRU4** generated by Mercury. (a) view along the *a*-axis, (b) view along the *c*-axis.

Both **CU-SCRU3** and **CU-SCRU4** complex have the same coordination modes of the tetracarboxylate ligand **3B** in monodentate, bidentate and bis-bidentate as displayed in Figure 4.29.



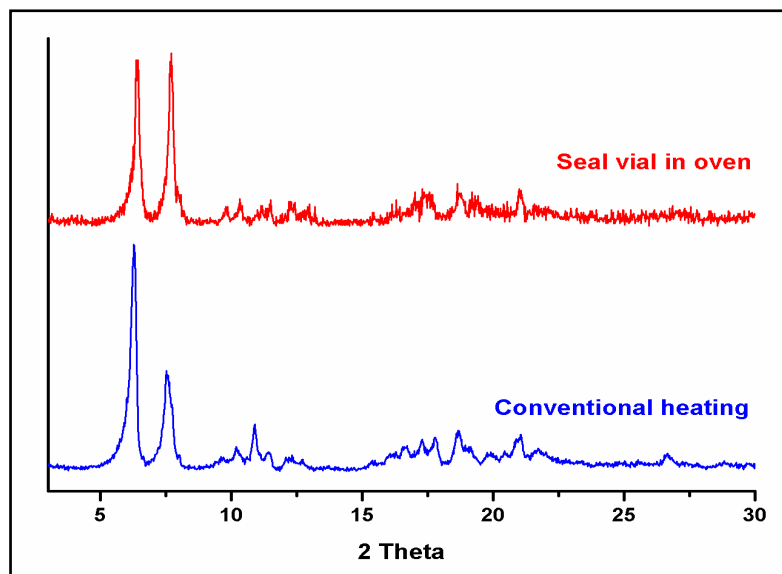
**Figure 4.29** Coordination modes of the tetracarboxylate ligand **3B** in the complex **CU-SCRU3** and **CU-SCRU4**.

Powder X-ray diffraction pattern of the synthesized samples of **CU-SCRU3** and **CU-SCRU4** confirmed that the bulk samples were crystalline and pure. Comparing with the XRD pattern of **CU-SCRU3** and **CU-SCRU4** which simulated on the basis of single crystal structure. Even if, the 2 theta of synthesized sample (6.45, 7.72) are not completely identical with simulated pattern but some peak of synthesized sample match with both **CU-SCRU3** (6.087, 6.451, 6.572, 7.783) and **CU-SCRU4** (6.21, 7.72). This is probably due to a mixture of **CU-SCRU3** and **CU-SCRU4** as illustrated in Figure 4.30. The result indicated that the synthesized sample MOFs can be repeated.



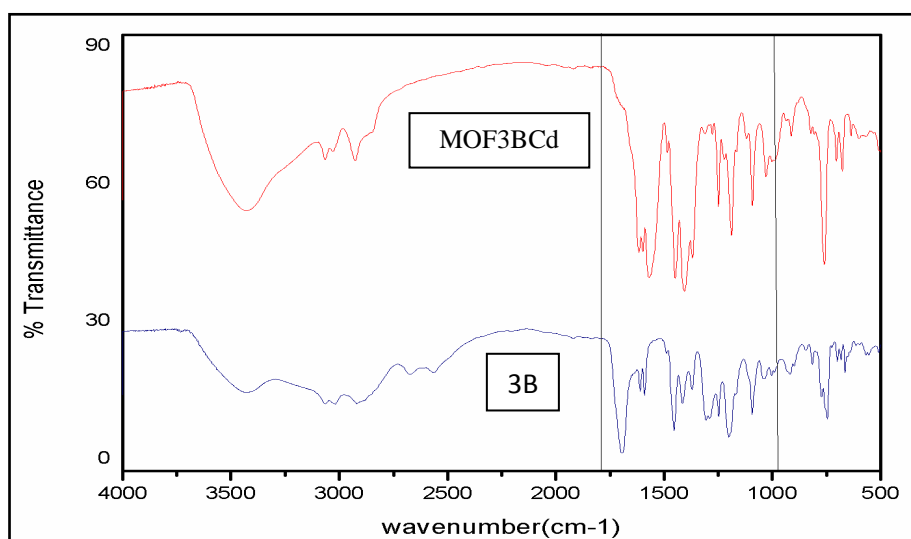
**Figure 4.30** Powder X-ray diffraction patterns of the synthesized sample and the pattern simulated on the basis of the single crystal structure of **CU-SCRU3** and **CU-SCRU4**.

Scale up of the synthesis of MOF can be done by using the optimum reaction condition that gave the appropriate resulting framework. To investigate this point, XRD pattern was used to confirm the product of each method. The XRD pattern of the sample was prepared by synthesizing in a 10 mL vial and conventional method were compared as illustrated in Figure 4.31, indicating that the scale up of the synthesis MOF can be done.



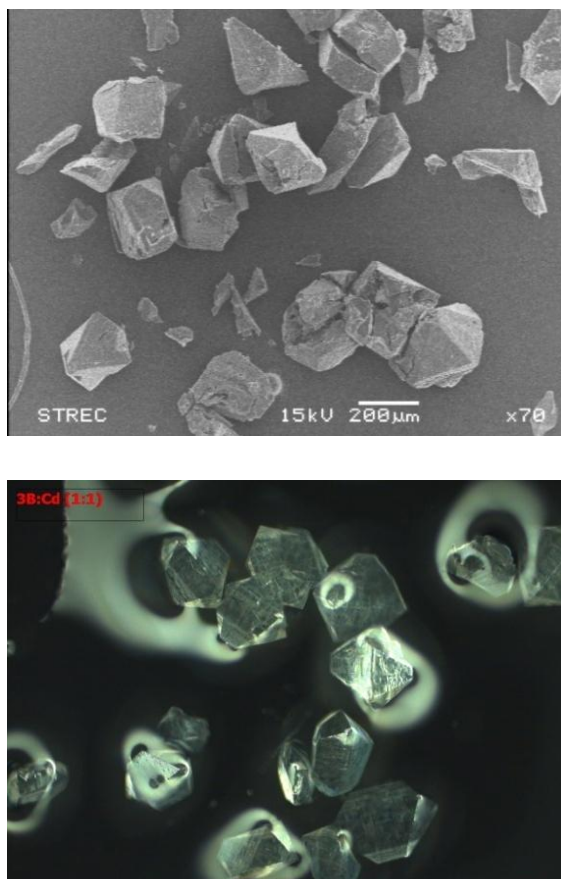
**Figure 4.31** Powder X-ray diffraction patterns of the synthesized sample by the different method.

Comparing IR spectra of organic linker **3B** with MOF3BCd (CU-SCRU3 and CU-SCRU4) (Figure 4.32), the carbonyl (C=O) and C-O stretchings of MOFs 3BCd shifted to lower wavenumber comparing with **3B** due to complexation of carboxylic group with Cd(II) ion as shown in Figure 4.32.



**Figure 4.32** Compared IR spectra of **3B** and MOF3BCd (CU-SCRU3 and CU-SCRU4).

The morphology of MOF **3B**-Cd (**CU-SCRU3** and **CU-SCRU4**) was also studied as shown in Figure 4.33. The SEM image exhibited a semimicro-particle in polyhedral shapes. The average size of particle was around 200  $\mu\text{m}$ . The microscope image showed the single-crystal of MOF **3B**-Cd that was kept in the solvent.



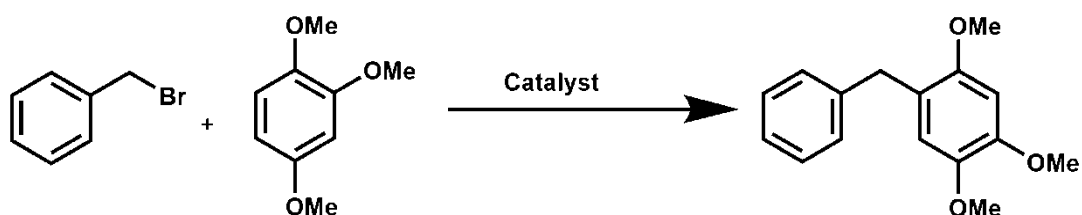
**Figure 4.33** SEM images(top) and microscope images (down) of MOF**3B**-Cd.

In addition, nitrogen-adsorption measurement of the bulk sample reveal that it was nonporous materials. Its adsorption-desorption isotherm was shown in appendix A (Figure A-29).

We would like to use the obtained MOF as gas storage. Unfortunately, the obtained MOFs can not be used as gas storage because they were nonporous materials. As mentioned above, MOFs have many other potential applications. Therefore, we try to explore the catalytic activity of the obtained MOFs.

### 4.3 Study of catalytic activities.

In this part of thesis, we explored the catalytic activity of the obtained MOF. The obtained MOF were tested as solid catalyst in the Friedel-Craft reaction. For initial optimization of the reaction conditions, benzyl bromide and 1,3,5-trimethoxybenzene were chosen as model substrates for the template reaction with selected obtained MOF as heterogeneous catalyst as displays in Scheme 4.3.



**Scheme 4.3** Friedel-Craft alkylation reaction of benzyl bromide and 1,3,5-trimethoxy benzene.

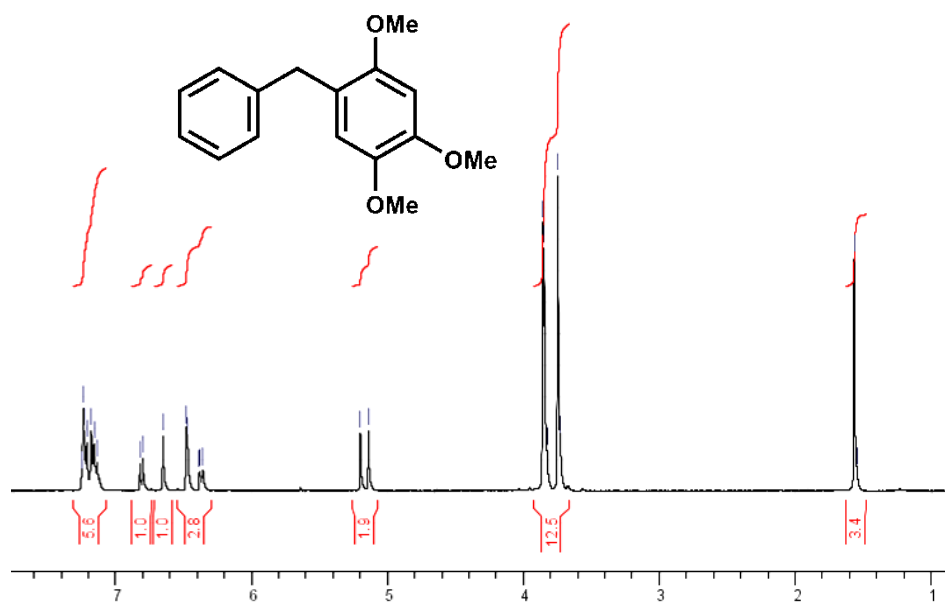
**Table 4.5** Optimized conditions of the Friedel-Craft alkylation reaction.

Entry <sup>a</sup>	Catalysts	Time (hr.)	Conditions	% yield
1	No catalyst	4	Neat, 80 °C	NR <sup>a</sup>
2	M1 (MOF-3AZn)	4	Neat, 80 °C	20
3	M5 (MOF-3ANi)	4	Neat, 80 °C	NR <sup>a</sup>

<sup>a</sup> no reaction.

The result of catalytic activities is shown in Table 4.8, Entry 1, no desired product was observed and starting materials were recovered when the model reaction was carried out in the absence of the catalyst. Using **M5** (MOF-3ANi) as catalyst in entry 3 also did not give the desired product. In the case of **M1** (MOF-3AZn) as catalyst gave the desired product in 20% yield. However, the formation of by product HBr in the reaction destroyed the MOF **M1**. The evidence was confirmed by IR spectrum of the solid MOF **M1** after used in the reaction. This result indicated that MOFs should be used under mild reaction condition. (<sup>1</sup>H NMR spectrum of desired product, Figure 3.44)





**Figure 4.34** <sup>1</sup>H NMR spectrum of desired product.

#### **Future works.**

For the future work, the application of MOF in catalyst field is interest of researcher. We would like to examine the catalytic activities of MOF in other reactions.

## CHAPTER V

### CONCLUSION

In this thesis, metal-organic frameworks of derivatives of 1,3-alternate calix[4]arene as organic linkers were synthesized successfully. The novel organic linkers, 1,3-alternate calix[4]arene tetra-*p*-benzoic acid (**3A**) and 1,3-alternate calix[4]arene tetra-*m*-benzoic acid (**3B**) have been synthesized. They were structural isomers which have the different positions of carboxylic acid groups at the *para* and *meta* sites, respectively. The single-crystal structures of 1,3-alternate tetra-*m*-benzoate calix[4]arene (**2B**) and 1,3-alternate calix[4]arene tetra-*p*-benzoic acid (**3A**) showed the different directions of the carboxyl group which might give different resulting MOF structures.

Metal-organic frameworks were synthesized by using organic linkers **3A** and **3B** with various metal ions and then characterized. Morphologies of MOFs, **M1-M15** were examined by SEM image, which exhibited as micro-particles of MOFs in various uniforms such as needle-like, cubic, rod, polyhedral and platelet shapes. Meanwhile the nitrogen adsorption-desorption isotherms performed as type III adsorption isotherm which was typical for nonporous materials. They had small surface area. These results might be due to the large structure of organic linkers which did not provide the suitable pore for storage of gases. The well understanding of the phenomenon was confirmed by the single-crystal structure of the 1,3-alternate calix[4]arene-based MOFs. The structure of **CU-SCRU1** was prepared from organic linker, **3A** and Zn(II) ion. Its coordinate bonds provided the linear polymeric chains. The geometry of Zn(II) ion was octahedral and its 3D structure occurred by the intermolecular interactions of linear polymeric chains. The pore of this structure did not link together as the pore in the well-known MOF-5. The **CU-SCRU2** structure was synthesized by using **3B** and Zn(II) ion which provided the zig-zag polymeric chain in 1D structure. The packing structure of 1D chain featured in 3D frameworks. The last two structures were obtained under the same reaction which used **3B** and Cd(II) ion. Their unit cells were monoclinic (named **CU-SCRU3**) and orthorhombic

(named **CU-SCRU4**). The adsorption-desorption isotherm of bulk materials was type III which indicated that it was nonporous materials. In addition, we studied the catalytic activity of some MOFs by using the Friedel-Craft alkylation reaction of benzyl bromide and 1,3,5-trimethoxybenzene as a reaction model. We found that in absence of a catalyst, the desired product was not obtained. MOF **M5** as catalyst also did not provide the product. However, when MOF **M1** from the linker **3A** with Zn(II) ion was used as a catalyst, the desired product was obtained in 20% yield. However, **M1** decomposed under this reaction due to the formation of side product, HBr. The result indicates that MOF should be used under milder condition.

## REFERENCES

- (1) Yang, G., Zhou, L., Liu, X., Han, X., and Bao, X. Adsorption, reduction and storage of hydrogen within ZSM-5 zeolite exchanged with various ions: a comparative theoretical study. Micropor. Mesopor. Mat. 161 (2012): 168-178.
- (2) Im, J. S., Yun, J., Kang, S. C., Lee, S. K., and Lee, Y.S. Hydrogen adsorption on activated carbon nanotubes with an atomic-sized vanadium catalyst investigated by electrical resistance measurements. Appl. Surf. Sci. 258 (2012): 2749-2756.
- (3) Assfour, B., and Seifert, G. Adsorption of hydrogen in covalent organic frameworks: comparison of simulations and experiments. Micropor. Mesopor. Mat. 133 (2010): 59-65.
- (4) Li, H., Eddaoudi, H., O'Keeffe, M., and Yaghi, O. M. Design and synthesis of an exceptionally stable and highly porous metal-organic framework. Nature. 402 (1999): 276-279.
- (5) Murray, L. J., Dinca, M., and Long, J. R. Hydrogen storage in metal-organic frameworks. Chem. Soc. Rev. 38 (2009): 1294-1314.
- (6) Xiang, Z., Leng, S., and Cao, D. Functional group modification of metal-organic frameworks for CO<sub>2</sub> capture. J. Phys. Chem. 116 (2012): 10573-10579.
- (7) Senkovska, I., and Kaskel, S. High pressure methane adsorption in the metal-organic frameworks Cu<sub>3</sub>(btc)<sub>2</sub>, Zn<sub>2</sub>(bdc)<sub>2</sub>dabco, and Cr<sub>3</sub>F(H<sub>2</sub>O)<sub>2</sub>O(bdc)<sub>3</sub>. Micropor. Mesopor. Mat. 112 (2008): 108-115.
- (8) Li, J. R., Kuppler, R. J., and Zhou, H. C. Selective gas adsorption and separation in metal-organic frameworks. Chem. Soc. Rev. 38 (2009): 1477-1504.
- (9) Farrusseng, D., Aguado, S., and Pinel, C. Metal-organic frameworks: opportunities for catalysis. Angew. Chem. Int. Ed. 48 (2009): 7502-7513.
- (10) Keskin S., and Kızılel, S. Biomedical applications of metal-organic frameworks. Ind. Eng. Chem. Res. 50 (2011): 1799-1812.

- (11) Allendorf, M. D., Bauer, C. A., Bhakta, R. K., and Houk, R. J. T. Luminescent metal-organic frameworks. Chem. Soc. Rev. 38 (2009): 1330-1352.
- (12) Burrows, A. D. and others. The effect of reaction conditions on the nature of cadmium 1,3,5-benzenetricarboxylate metal-organic frameworks. Inorg. Chim. Acta. 366 (2011): 303-309.
- (13) Kuppler, R. J., and others. Potential applications of metal-organic frameworks. Coordin. Chem. Rev. 253 (2009) : 3042-3066.
- (14) Zhang, P., Niu, Y.-Y., Wu, B.-L., Zhang, H.-Y., Niu, C.-Y., and Hou, H.-W. 2D frameworks of Cu(II) and Zn(II) organo-metallic polymers self-assembled with N,N'-(1,2-phenylene)diisonicotinamide: syntheses, structures, photoluminescence, and thermal properties. Inorg. Chim. Acta. 361 (2008): 2609-2615.
- (15) Hou, Q., Jia, M.-J., Zhao, J.-J., Jin, J., Yu, J.-H., and Xu, J.-Q. Two new 3-D photoluminescence metal-organic frameworks based on cubane Cu<sub>4</sub>L<sub>4</sub> clusters as tetrahedral nodes. Inorg. Chim. Acta. 384 (2012): 287-292.
- (16) Wang, F., and Kang, Y., Unusual cadmium(II)-adenine paddle-wheel units for the construction of a metal-organic framework with mog topology. Inorg. Chem. Commun. 20 (2012): 266-268.
- (17) Perry, J. J., Perman, J. A., and Zaworotko, M. J. Design and synthesis of metal-organic frameworks using metal-organic polyhedra as supermolecular building blocks. Chem. Soc. Rev. 38 (2009): 1400-1417.
- (18) Zhang, J., Liu, R., Feng, P., and Bu, X. Organic cation and chiral anion templated 3D homochiral open-framework materials with unusual square-planar {M<sub>4</sub>(OH)} units. Angew. Chem. Int. Ed. 46 (2007): 8388 - 8391.
- (19) Liu, C.-M., Xiong, R.-G., You, X.-Z., and Chen, W. A two-dimensional square network inclusion compound incorporating guest molecules through both hydrogen bonding and nonionic electrostatic attraction. Crystal structure of [Cd(4,4'-bpy)<sub>2</sub>(H<sub>2</sub>O)<sub>2</sub>](ClO<sub>4</sub>)<sub>2</sub>·1.5(4,4'-bpy)·(C<sub>6</sub>H<sub>4</sub>NO<sub>3</sub>Cl)·H<sub>2</sub>O. Acta. Chem. Scand. 52 (1998): 1353-1358.

- (20) Jeffrey A. Rood. Metal-Organic Frameworks as Functional, Porous Materials. Doctor's Thesis, Graduate program in Chemistry and Biochemistry, University of Notre Dame, Indiana, 2009.
- (21) Tranchemontagne, D. J., Mendoza-Cortés, J. L., O'Keeffe M., and Yaghi, O. M. Secondary building units, nets and bonding in the chemistry of metal-organic frameworks. Chem. Soc. Rev. 38 (2009): 1257-1283.
- (22) Chae, H. K., and others. A route to high surface area, porosity and inclusion of large molecules in crystals. Nature. 427 (2004): 523-527.
- (23) Suh, M.P., Park, H. J., Prasad, T. K., and Lim, D.-W. Hydrogen storage in metal-organic frameworks. Chem. Rev. 112 (2012): 782-835.
- (24) Lee, J. Y., Li, J., and Jagiello, J. Gas sorption properties of microporous metal organic frameworks. J. Solid State Chem. 178 (2005): 2527-2532.
- (25) Su, S., and others. Lanthanide anionic metal-organic frameworks containing semirigid tetracarboxylate ligands: structure, photoluminescence, and magnetism. Cryst. Growth Des. 12 (2012): 1808-1815.
- (26) Wang, G., and others. A porous lanthanide metal-organic framework with luminescent property, nitrogen gas adsorption and high thermal stability. Inorg. Chem. Commun. 13 (2010): 95-97.
- (27) Platero-Prats, A. E., Iglesias, M., Snejko, N., Monge, Á., and Gutiérrez-Puebla E. From coordinatively weak ability of constituents to very stable alkaline-earth sulfonate metal-organic frameworks. Cryst. Growth Des. 11 (2011): 1750-1758.
- (28) Zhao, D., Timmons, D. J., Yuan, D., and Zhou, H.-C. Tuning the topology and functionality of metal-organic frameworks by ligand design. Accounts Chem. Res. 44 (2011): 123-133.
- (29) Du, J.-L., Wei, Z.-Z., and Hu, T.-L. Metal coordination polymers of 2,3-bis(benzimidazol-1-ylmethyl)quinoxaline: syntheses, crystal structures and luminescent properties. Solid State Sci. 13 (2011): 1256-1260.
- (30) Dutta, A., Patra, A. K., and Bhaumik, A., Porous organic-inorganic hybrid nickel phosphonate: adsorption and catalytic applications. Micropor. Mesopor. Mat. 155 (2012): 208-214.

- (31) Lian, Z.-X., Cai, J., and Chen, C.-H. A series of metal-organic frameworks constructed with arenesulfonates and 4,4'-bipy ligands. Polyhedron. 26 (2007): 2647-2654.
- (32) Liu, C.-B., and others. Hydrothermal syntheses and crystal structures of PbII coordination polymers based on a N,O-donor ligand. Inorg. Chem. Commun. 27 (2013): 69-75.
- (33) Rowsell, J. L. C., and Yaghi, O. M. Metal-organic frameworks: a new class of porous materials. Micropor. Mesopor. Mat. 73 (2004): 3-14.
- (34) Xu, L., Choi, E.-Y., and Kwon, Y.-U. Ionothermal Syntheses of six three-dimensional zinc metal-organic frameworks with 1-alkyl-3-methylimidazolium bromide ionic liquids as solvents. Inorg. Chem. 46 (2007): 10670-10680.
- (35) Wang, X.-L., Zhang, J.-X., Liu, G.-C., Lin, H.-Y., Chen, Y.-Q., and Kang, Z.-H. Effect of flexibility of organic dicarboxylates anions on the four 3D metal-organic frameworks constructed from flexible benzimidazolyl-based ligand. Inorg. Chim. Acta. 368 (2011): 207-215.
- (36) Qiu, Y., Liu, Z., Li, Y., Deng, H., Zeng, R., and Zeller, M. Reversible anion exchange and sensing in large porous materials built from 4,4'-bipyridine via  $\pi \cdots \pi$  and H-bonding interactions. Inorg. Chem. 47 (2008): 5122-5128.
- (37) Wu, D.-Y., Huang, W., Duan, C.-Y., Meng, Q.-J. Structure and anion-exchange of a three-dimensional Ag(I) metal-organic framework. Inorg. Chem. Commun. 10 (2007): 1009-1013.
- (38) Hu, J.-S. and others. Syntheses, structures, and characteristics of four new metal-organic frameworks based on flexible tetrapyridines and aromatic polycarboxylate acids. Cryst. Growth Des. 12 (2012): 3426-3435.
- (39) Gao, W.-Y. and others. Porous double-walled metal triazolate framework based upon a bifunctional ligand and a pentanuclear zinc cluster exhibiting selective CO<sub>2</sub> uptake. Inorg. Chem. 51 (2012): 4423-4425.
- (40) Wei, G., Shen, Y.-F., Li, Y.-R., and Huang, X.-C. Synthesis, crystal structure, and photoluminescent properties of ternary Cd(II)/triazolate/chloride system. Inorg. Chem. 49 (2010): 9191-9199.

- (41) Dinca, M., Yu, A. F., and Long, J. R. Microporous metal-organic frameworks incorporating 1,4-benzeneditetrazolate: syntheses, structures, and hydrogen storage properties. *J. Am. Chem. Soc.* 128 (2006): 8904-8913.
- (42) Choi, H. J., Dinca, M., and Long, J. R. Broadly hysteretic H<sub>2</sub> adsorption in the microporous metal-organic framework Co(1,4-benzenedipyrazolate). *J. Am. Chem. Soc.* 130 (2008): 7848-7850.
- (43) Angelova, O., Macicek, J., Atanasov, M., and Petrov, G. Chelating modes of 3-substituted 2,4-pentanediones. Crystal and electronic structure of bis(3-cyano-2,4-pentanedionato)cobalt(II). *Inorg. Chem.* 30 (1991): 1943-1949.
- (44) Fang, C., and others. Synthesis and crystal structures of four pH-dependent Pb(II) and Cd(II)phosphonates based on a novel ligand, 3-phosphono-benzoic acid. *Inorg. Chim. Acta.* 362 (2009): 2101-2107.
- (45) Gándara, F., and others. Rare earth arenedisulfonate metal-organic frameworks: an approach toward polyhedral diversity and variety of functional compounds. *Inorg. Chem.* 46 (2007): 3475-3484.
- (46) Wang, D.-Z., Zhang, Q., Zhang, J.-B., Wua, Y.-G., Cao, L.-H., and Ma, P.-Y. Metal-organic coordination architectures of condensed heterocyclic based 1,2,4-triazole: Syntheses, structures and emission properties. *Polyhedron* 42 (2012): 216-226.
- (47) Eddaoudi, M. and others. Systematic design of pore size and functionality in isorecticular MOFs and their application in methane storage. *Science.* 295 (2002): 469-472.
- (48) Collins, C. S., Sun, D., Liu, W., Zuo, J.-L., and Zhou, H.-C. Reaction-condition-controlled formation of secondary-building-units in three cadmium metal-organic frameworks with an orthogonal tetrakis(tetrazolate) ligand. *J. Mol. Struct.* 890 (2008): 163-169.
- (49) Suh, M.P., Cheon, Y. E., and Lee, E.Y. Reversible transformation of ZnII coordination geometry in a single crystal of porous metal-organic framework [Zn<sub>3</sub>(ntb)<sub>2</sub>(EtOH)<sub>2</sub>].4EtOH. *Chem. Eur. J.* 13 (2007): 4208-4215.



- (50) Jeong, S. and others. Metal-organic frameworks based on unprecedented trinuclear and pentanuclear metal-tetrazole clusters as secondary building units. Inorg. Chem. 50 (2011): 12133-12140.
- (51) Liu, G.-X., and others. Controlled assembly of zero-, one- and two-dimensional metal-organic frameworks involving in situ ligand synthesis under different reaction pH. Polyhedron 27 (2008): 2327-2336.
- (52) Stock, N., and Biswas, S. Synthesis of metal-organic frameworks (MOFs): routes to various MOF topologies, morphologies, and composites. Chem. Rev. 112 (2012): 933-969.
- (53) Xiao, J., Liu, B.-Y., Wei, G., and Huang, X.-C. Solvent induced diverse dimensional coordination assemblies of cupric benzotriazole-5-carboxylate: syntheses, crystal structures, and magnetic properties. Inorg. Chem. 50 (2011): 11032-11038.
- (54) Image of teflon-lined stainless steel autoclave[online]. 2013. Available from: <http://nanotubes.epfl.ch/page-24503-en.html> [2013, March 18]
- (55) Subramanian, M. Standard Operating Procedure (SOP): Use of Autoclaves for Hydrothermal Experiments [online]. 2012. Available from: [http://www.chemistry.oregonstate.edu/blakemore/safety/SOPs/SOP\\_hydrothermal/SOP\\_hydrothermal.html](http://www.chemistry.oregonstate.edu/blakemore/safety/SOPs/SOP_hydrothermal/SOP_hydrothermal.html) [2012, April 28]
- (56) Parnham, E. R. and Morris, R. E. Ionothermal synthesis of zeolites, metal-organic frameworks, and inorganic-organic hybrids. Acc. Chem. Res. 40 (2007): 1005-1013.
- (57) Xu, L., Choi, E.-Y., and Kwon, Y.-U. Ionothermal synthesis of a 3D Zn–BTC metal-organic framework with distorted tetranuclear  $[Zn_4(\mu_4-O)]$  subunits. L. Inorg. Chem. Commun. 11 (2008): 1190-1193.
- (58) Lu, C.-M., Liu, J., Xiao, K., and Harris, A. T. Microwave enhanced synthesis of MOF-5 and its CO<sub>2</sub> capture ability at moderate temperatures across multiple capture and release cycles. Chem. Eng. J. 156 (2010): 465-470.
- (59) Liu, W., Ye, L., Liu, X., Yuan, L., Lu, X., and Jiang, J., Rapid synthesis of a novel cadmium imidazole-4,5-dicarboxylate metal-organic framework

- under microwave-assisted solvothermal condition. Inorg. Chem. Commun. 11 (2008): 1250-1252.
- (60) Yang, H., Orefuwa, S., and Goudy, A. Study of mechanochemical synthesis in the formation of the metal-organic framework  $\text{Cu}_3(\text{BTC})_2$  for hydrogen storage. Micropor. Mesopor. Mat. 143 (2011): 37-45.
- (61) Janiak, C., and Vieth, J. K. MOFs, MILs and more: concepts, properties and applications for porous coordination networks (PCNs). New J. Chem. 34 (2010): 2366-2388.
- (62) Yuan, W., Friscic, T., Apperley, D., and James, S. L. High reactivity of metal-organic frameworks under grinding conditions: parallels with organic molecular materials. Angew. Chem. Int. Ed. 49 (2010): 3916-3919.
- (63) Cohen, S. M. Postsynthetic methods for the functionalization of metal-organic frameworks. Chem. Rev. 112 (2012): 970-1000.
- (64) Burrows, A. D., Frost, C. G., Mahon, M. F., and Richardson, C., Post-synthetic modification of tagged metal-organic frameworks. Angew. Chem. 120 (2008): 8610-8614.
- (65) Xiang, Z., Leng, S., and Cao, D., Functional group modification of metal-organic frameworks for  $\text{CO}_2$  capture. J. Phys. Chem. 116 (2012): 10573-10579.
- (66) Yang, J., Li, P., and Wang, L., Postsynthetic modification of metal-organic framework as a highly efficient and recyclable catalyst for three-component (aldehyde-alkyne-amine) coupling reaction. Catal. Commun. 27 (2012): 58-62.
- (67) Wang Z., and Cohen, S. M. Postsynthetic modification of metal-organic frameworks. Chem. Soc. Rev. 38 (2009): 1315-1329.
- (68) Wu, C.-D., Hu, A., Zhang, L., and Lin, W., A homochiral porous metal-organic framework for highly enantioselective heterogeneous asymmetric catalysis. J. Am. Chem. Soc. 127 (2005): 8940-8941.
- (69) Haneda, T., Kawano, M., Kawamichi, T., and Fujita, M. Direct observation of the labile imine formation through single-crystal-to-single-crystal reactions in the pores of a porous coordination network. J. Am. Chem. Soc. 130 (2008): 1578-1579.

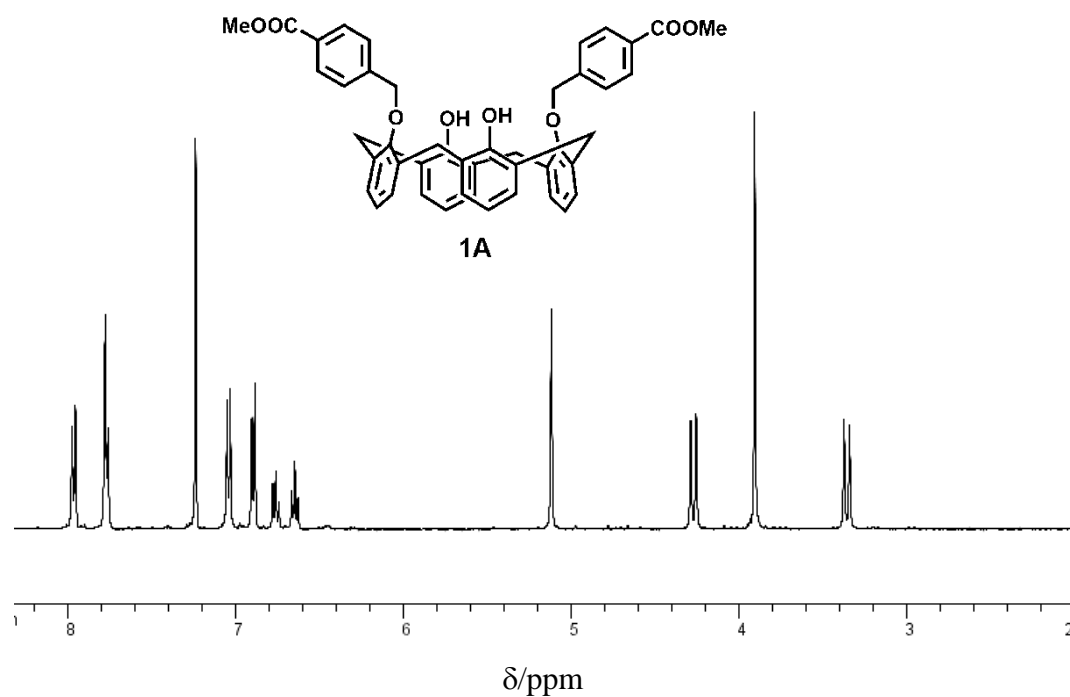
- (70) Savonnet, M. Generic postfunctionalization route from amino-derived metal-organic frameworks. *J. Am. Chem. Soc.* 132 (2010): 4518-4519.
- (71) Wang Z., and Cohen, S. M. Postsynthetic covalent modification of a neutral metal-organic framework. *J. Am. Chem. Soc.* 129 (2007): 12368-12369.
- (72) Kawamichi, T., Kodama, T., Kawano, M., and Fujita, M. Single-crystalline molecular flasks: chemical transformation with bulky reagents in the pores of porous coordination networks. *Angew. Chem. Int. Ed.* 47 (2008): 8030-8032.
- (73) Wang, Z., and Cohen, S. M., Tandem modification of metal-organic frameworks by a postsynthetic approach. *Angew. Chem.* 120 (2008): 4777-4780.
- (74) Morris, W., Doonan, C. J., Furukawa, H., Banerjee, R., and Yaghi, O. M. Crystals as molecules: postsynthesis covalent functionalization of zeolitic imidazolate frameworks. *J. Am. Chem. Soc.* 130 (2008): 12626-12627.
- (75) Image of single-crystal X-ray diffractometer[online]. 2013. Available from: [www.chem.cuhk.edu.hk](http://www.chem.cuhk.edu.hk) [2012, March 8]
- (76) Nguyen, L. T. L., Nguyen, T. T., Nguyen, K. D., and Phan, N. T. S. Metal-organic framework MOF-199 as an efficient heterogeneous catalyst for the aza-Michael reaction. *Appl. Catal. A-Gen.* 425-426 (2012): 44-52.
- (77) Choi, J. Y., Kim, J., Jhung, S. H., Kim, H.-K., Chang, J.-S. and Chae, H. K. Microwave synthesis of a porous metal-organic framework, zinc terephthalate MOF-5, bull. *Korean Chem. Soc.* 27 (2006): 1523-1524.
- (78) Zhang, K.-L., Gao, H.-Y., Pan, Z.-C., Liang, W., and Diao, G.-W. Preparation and characterization of two three-dimensional metal-organic photoluminescent supramolecular networks. *Polyhedron* 26 (2007): 5177-5184.
- (79) Rouquerol, F., Rouquerol, J., and Sing, K. Adsorption by powders and porous solids: principles, methodology and applications. Academic Press: San Diego, 1999.
- (80) Adsorption isotherm [online]. 2012. Available from: <http://saf.chem.ox.ac.uk/Instruments/BET/sorptoptprin.html#ads> [2012, April 28]

- (81) Phan, N. T. S., Le, K. K. A., and Phan, T. D. MOF-5 as an efficient heterogeneous catalyst for Friedel-Crafts alkylation reactions. Appl. Catal. A-Gen. 382 (2010): 246-253.
- (82) Rowsell, J. L. C., and Yaghi, O. M. Strategies for hydrogen storage in metal-organic frameworks, Angew. Chem. Int. Ed. 44 (2005): 4670-4679.
- (83) Lee, J. Y., Farha, O. K., Roberts, J., Scheidt, K. A. Nguyen, S.T., and Hupp, J. T. Metal-organic framework materials as catalysts. Chem. Soc. Rev. 38 (2009): 1450-1459.
- (84) Ma, L., Abney, C., and Lin, W. Enantioselective catalysis with homochiral metal-organic frameworks. Chem. Soc. Rev. 38 (2009): 1248-1256.
- (85) Li, J.-R., Sculley, J., and Zhou. H.-C. Metal-organic frameworks for separations. Chem. Rev. 112 (2012): 869-932.
- (86) Kan, W.-Q., Yang, J., Liu, Y.-Y., and Ma, J.-F. A series of metal-organic frameworks based on 9,10-bis(imidazol-1-ylmethyl)anthracene and structurally related aromatic dicarboxylates: syntheses, structures, and photoluminescence. Polyhedron 30 (2011): 2106-2113.
- (87) Zheng, B., Zhang, D., Peng, Y., Huo, Q., and Liu, Y., Syntheses, structures and luminescence properties of two novel lanthanide metal-organic frameworks based on a rigid tetracarboxylate ligand. Inorg. Chem. Commun. 16 (2012): 70-73.
- (88) Chen, B., Wang, L., Zapata, F., Qian, G., and Lobkovsky, E. B. A luminescent microporous metal-organic framework for the recognition and sensing of anions. J. Am. Chem. Soc. 130 (2008): 6718-6719.
- (89) Horcajada, P. Metal-organic frameworks in biomedicine. Chem. Rev. 112 (2012): 1232-1268.
- (90) Kumar, M., Kumar, R., and Bhalla, V. F<sup>-</sup> Induced 'turn-on' fluorescent chemosensor based on 1,3-alt thiacalix[4]arene. Tetrahedron 65 (2009): 4340-4344.
- (91) Jaime, C., Mendoza, J. D., Prados, P., Nieto, P. M., and Shched, C. <sup>13</sup>C NMR chemical shifts a single rule to determine the conformation of calix[4]arenes. J. Org. Chem. 56 (1991): 3372-3376.

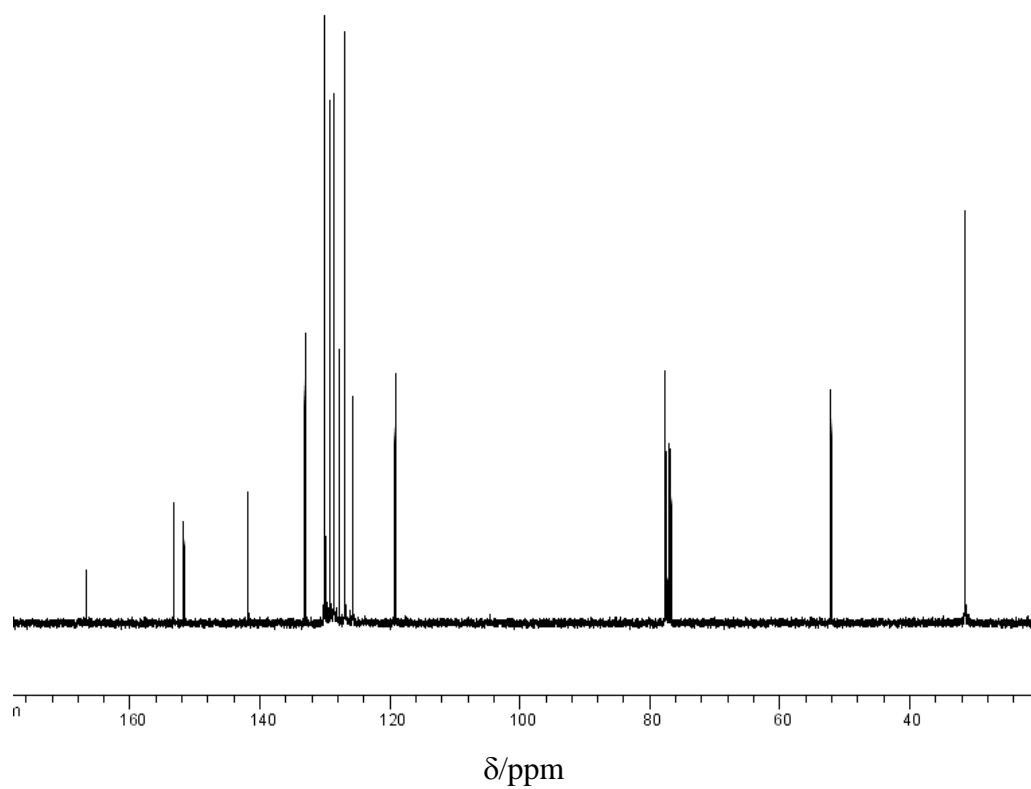
- (92) Yang, Y., Cao, X., Surowiec, M., and Bartsch, R. A. Calix[4]arene-dithiacrown ethers: synthesis and potentiometric membrane sensing of  $\text{Hg}^{2+}$ . Tetrahedron 66 (2010): 447-454.
- (93) Ali, A., Gawali, S. S., Rao, C. P., and Linares, J. A first report of the complexes of 5,11,17,23-tetra-tert-butyl-25,27-diethoxycarboxymethoxy-26,28-dihydroxycalix[4]arene with Mn(II), Fe(III), Co(II), Ni(II), Cu(II) and Zn(II). Inorg. Chem. Commun. 7 (2004): 1298-1301.
- (94) Kim, K., Park S., Park, K. M., and Lee, S. S. Thiacalix[4]arene-based three-dimensional coordination polymers incorporating neutral bridging coligands. Cryst. Growth Des. 11 (2011): 4059-4067.
- (95) Gutsche, C. D., and Levine, J. A. Calix[4]arenes. 6. Synthesis of a functionalizable calix[4]arene in a conformationally rigid cone conformation. J. Am. Chem. Soc. 104 (1982): 2652-2653.

## **APPENDICES**

## **APPENDIX A**

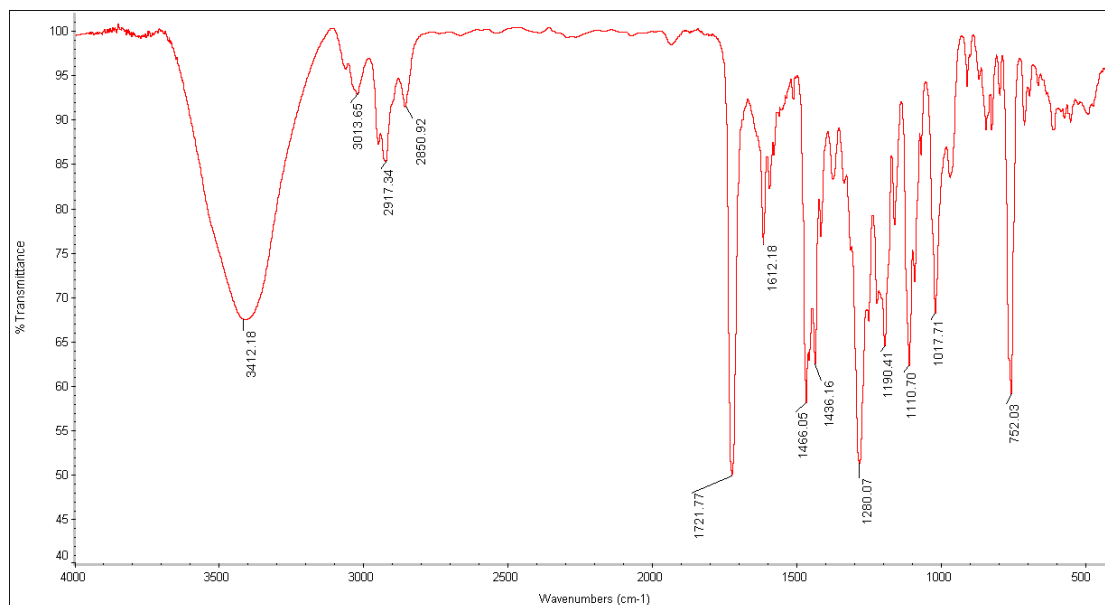


**Figure A-1.** <sup>1</sup>H NMR spectrum of compound 1A.

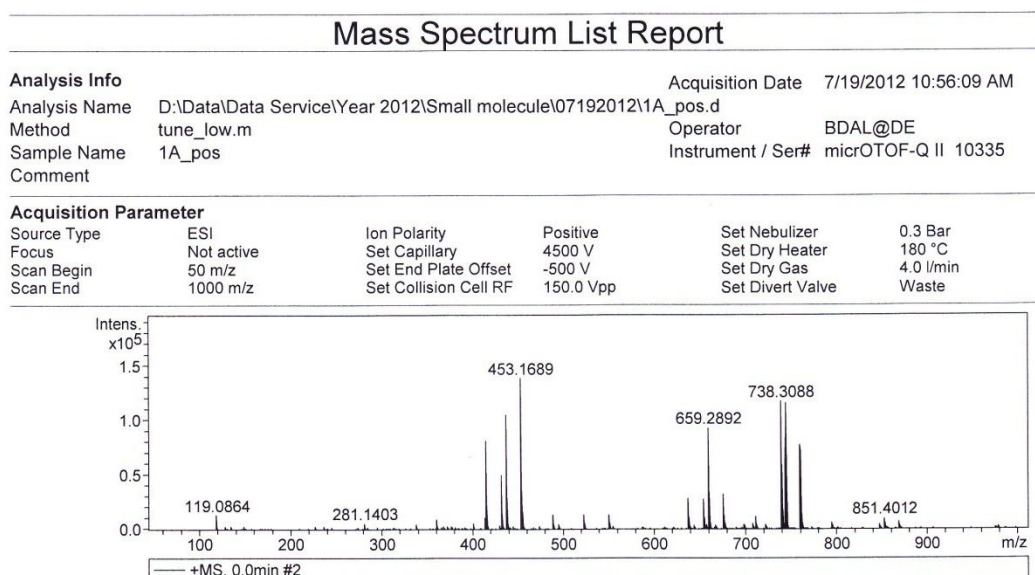


**Figure A-2.** <sup>13</sup>C NMR spectrum of compound 1A.

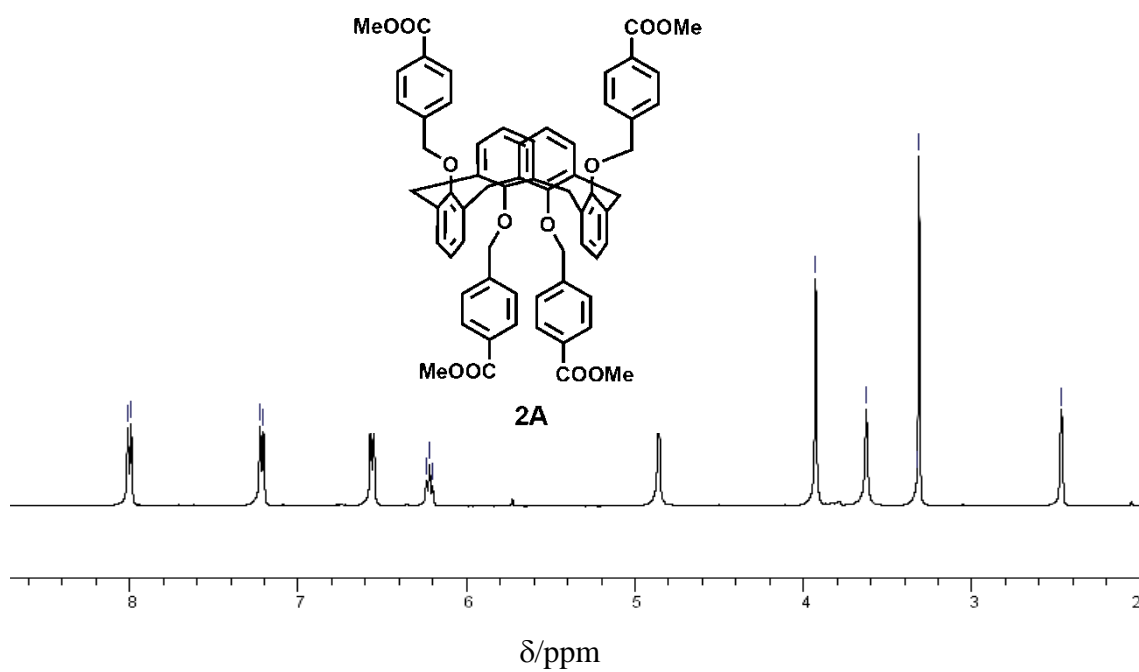




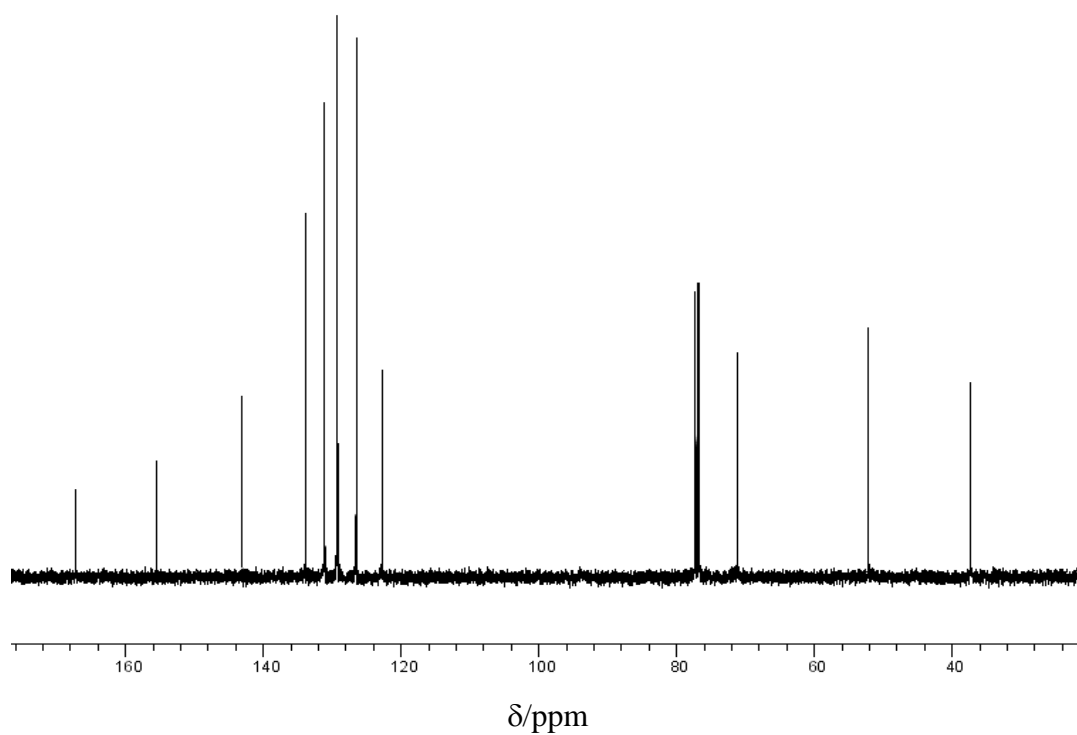
**Figure A-3.** IR spectrum of compound **1A**.



**Figure A-4.** Mass spectrum of compound **1A**.



**Figure A-5.** <sup>1</sup>H NMR spectrum of compound 2A.



**Figure A-6.** <sup>13</sup>C NMR spectrum of compound 2A.

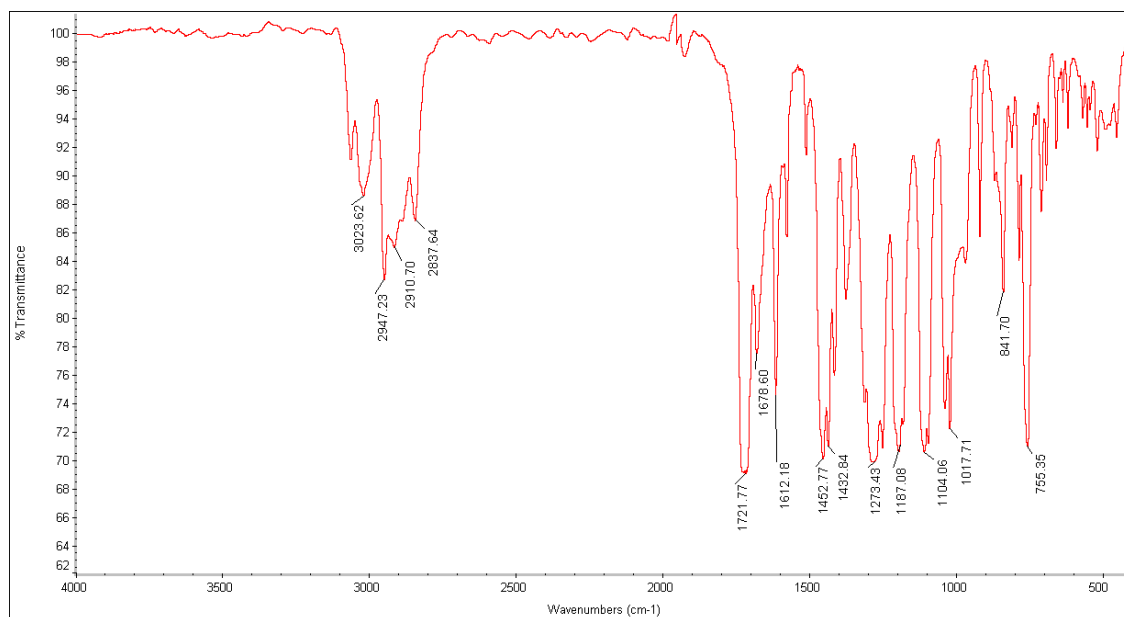


Figure A-7. IR spectrum of compound 2A.

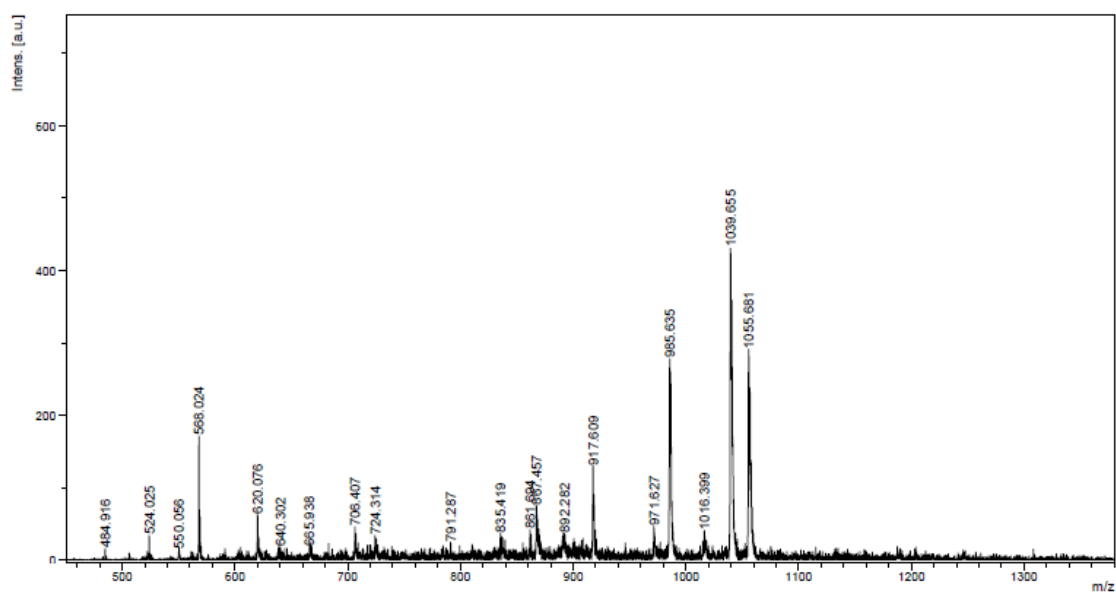
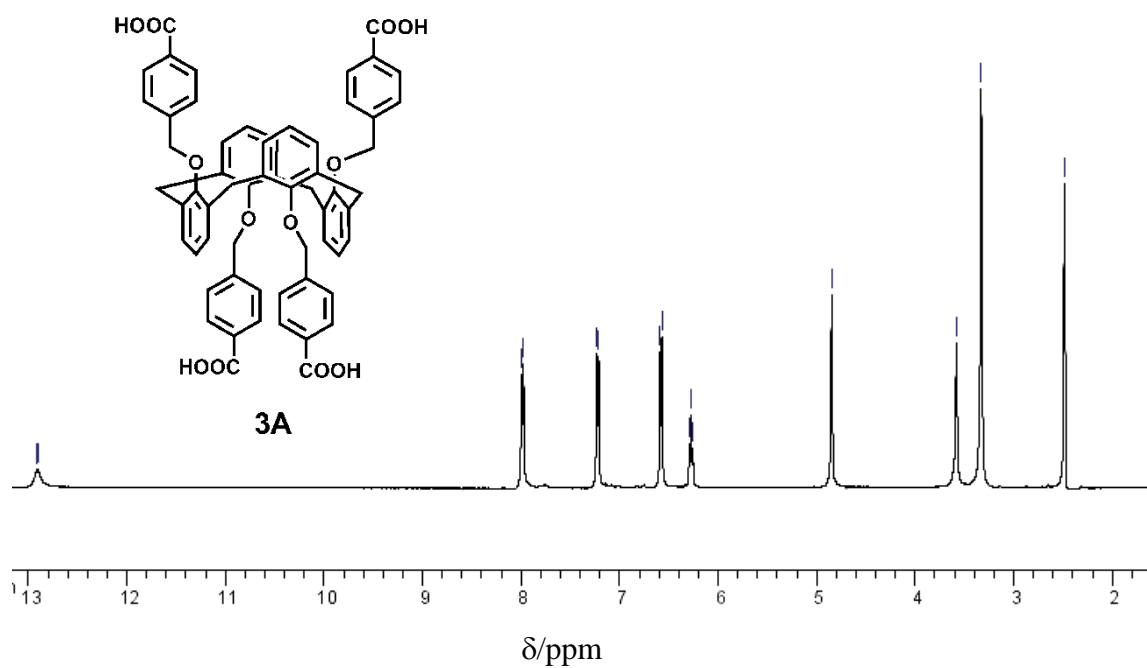
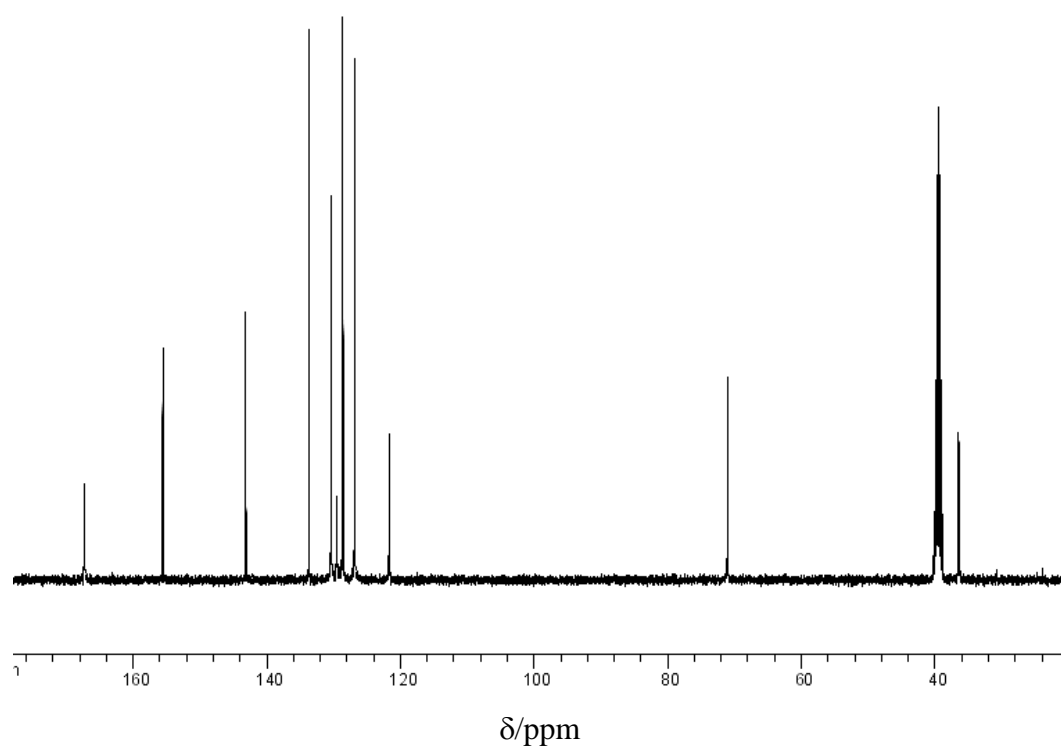


Figure A-8. MALDI-TOF mass spectrum (CCA) of 2A.



**Figure A-9.** <sup>1</sup>H NMR spectrum of compound 3A.



**Figure A-10.** <sup>13</sup>C NMR spectrum of compound 3A.

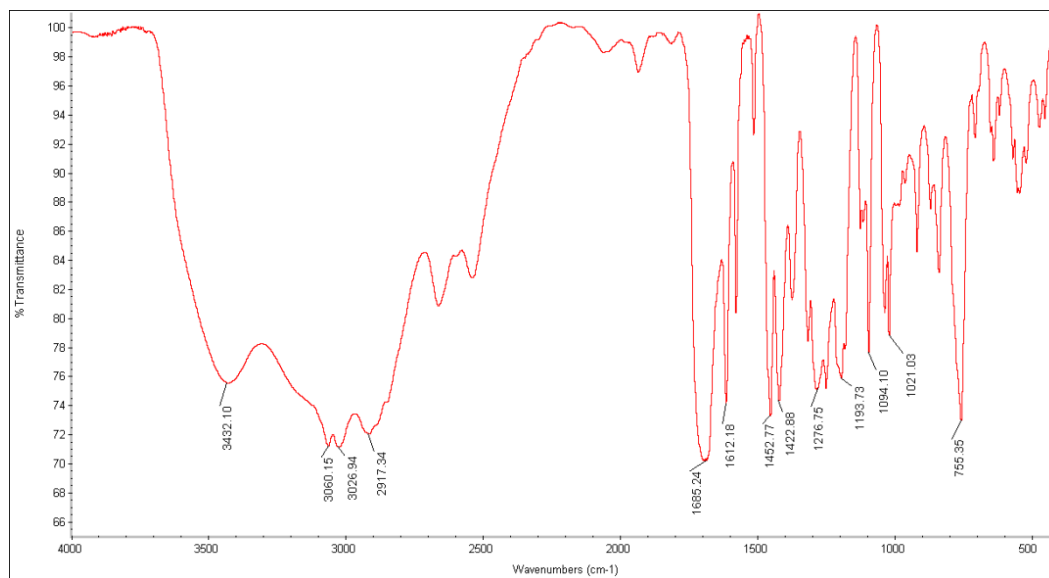


Figure A-11. IR spectrum of compound 3A.

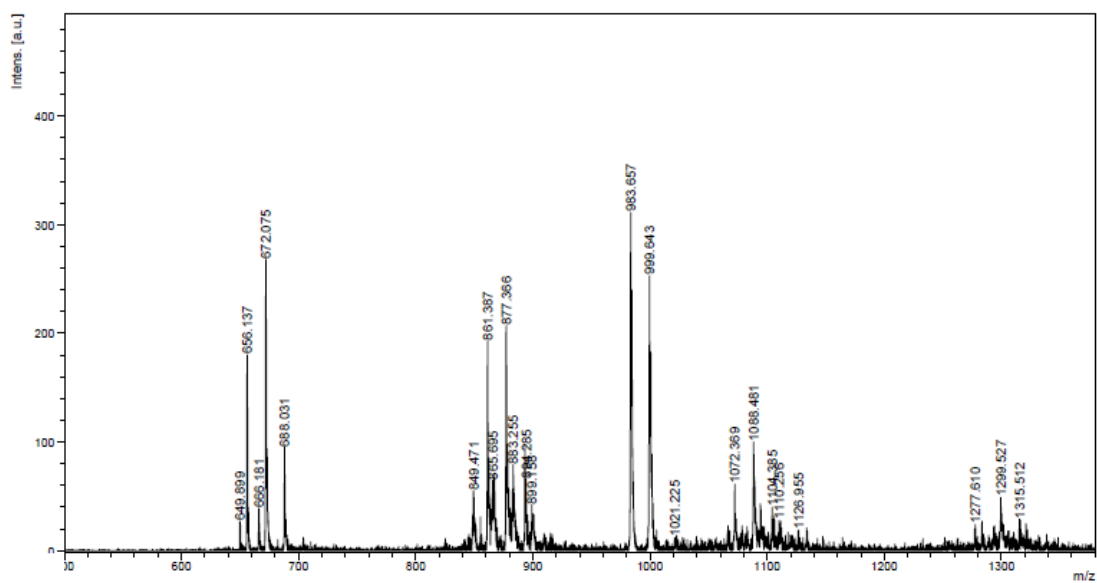
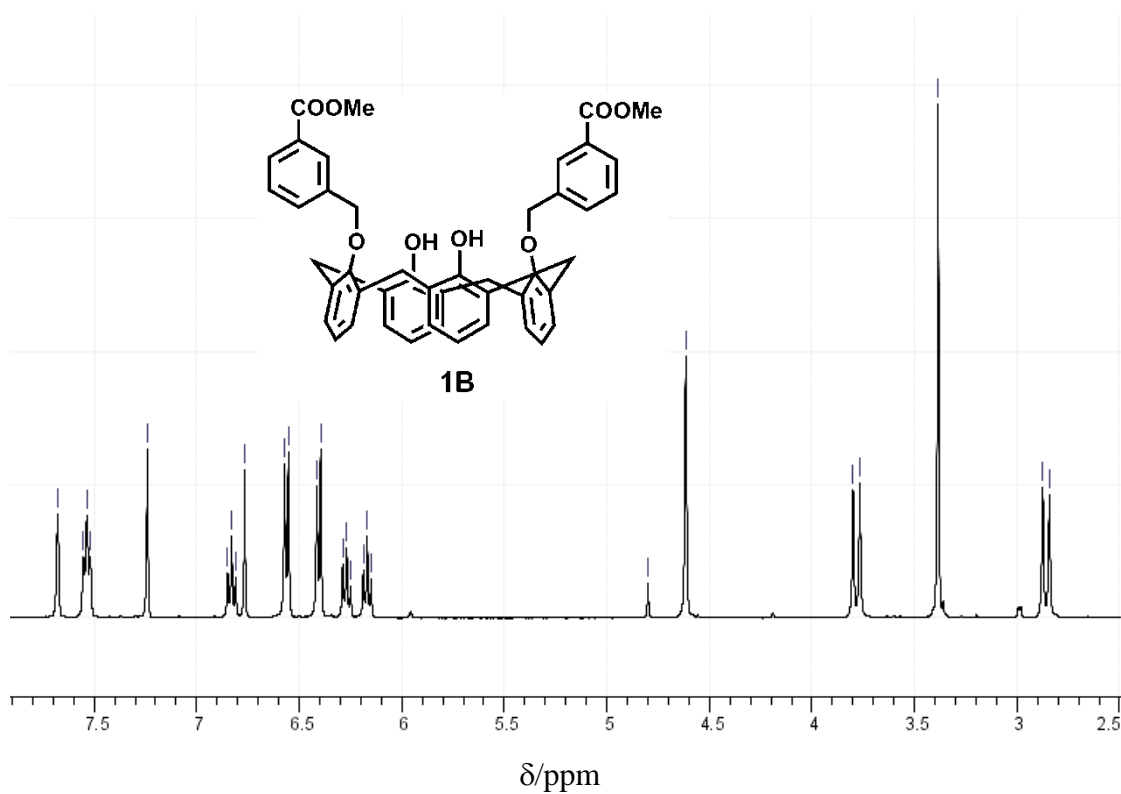
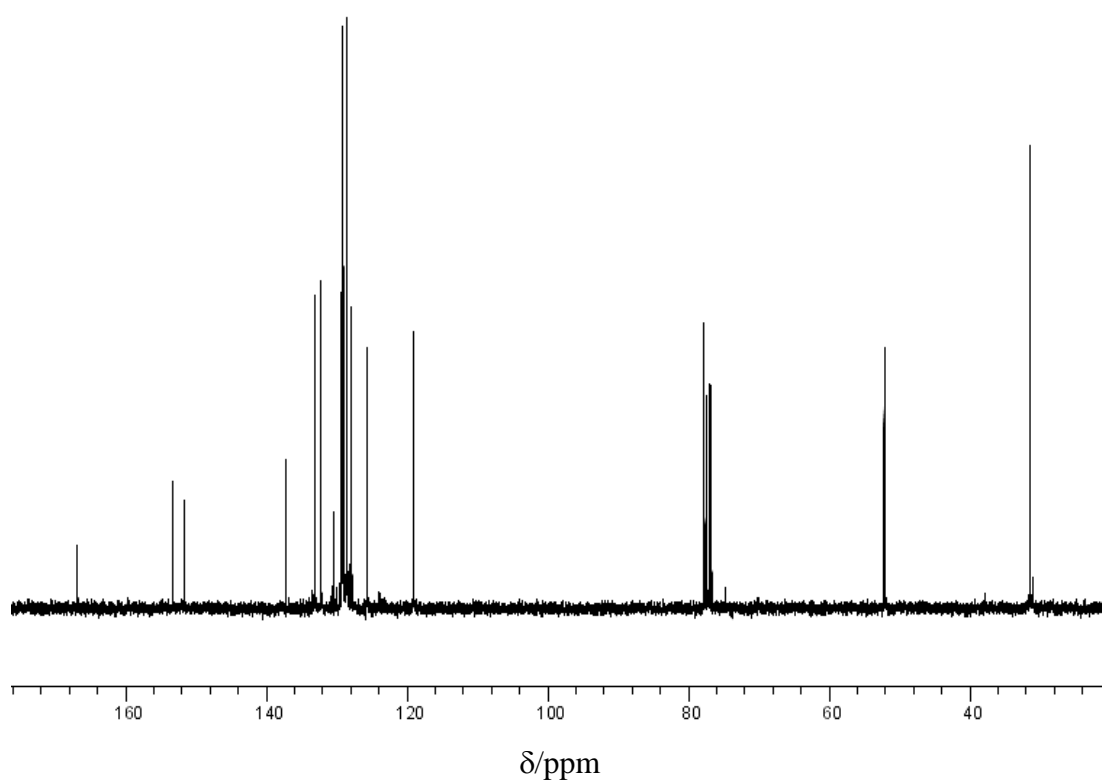


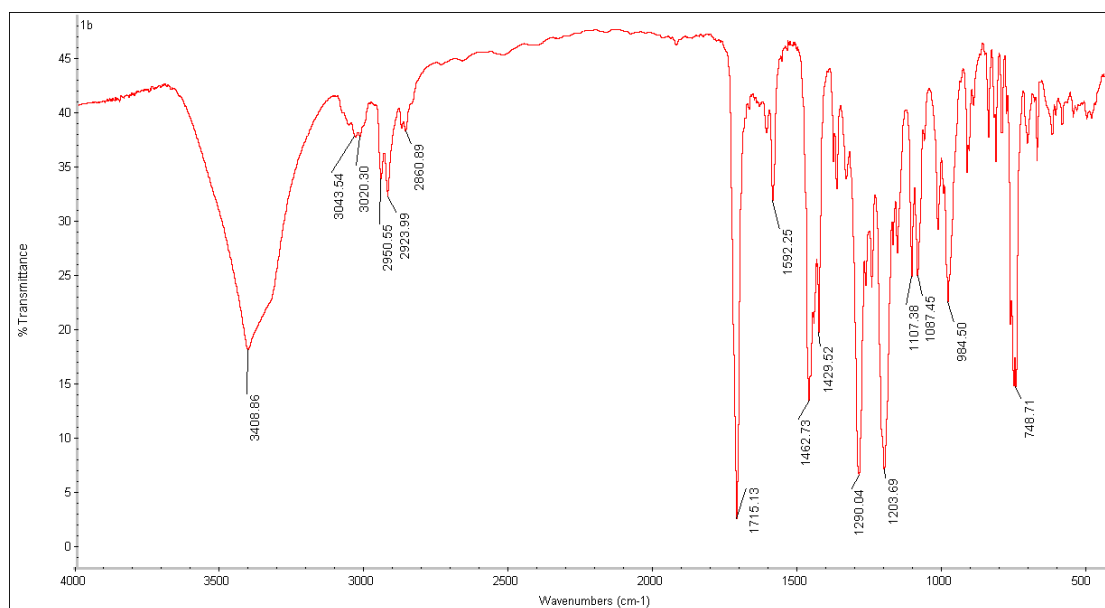
Figure A-12. MALDI-TOF mass spectrum (CCA) of compound 3A.



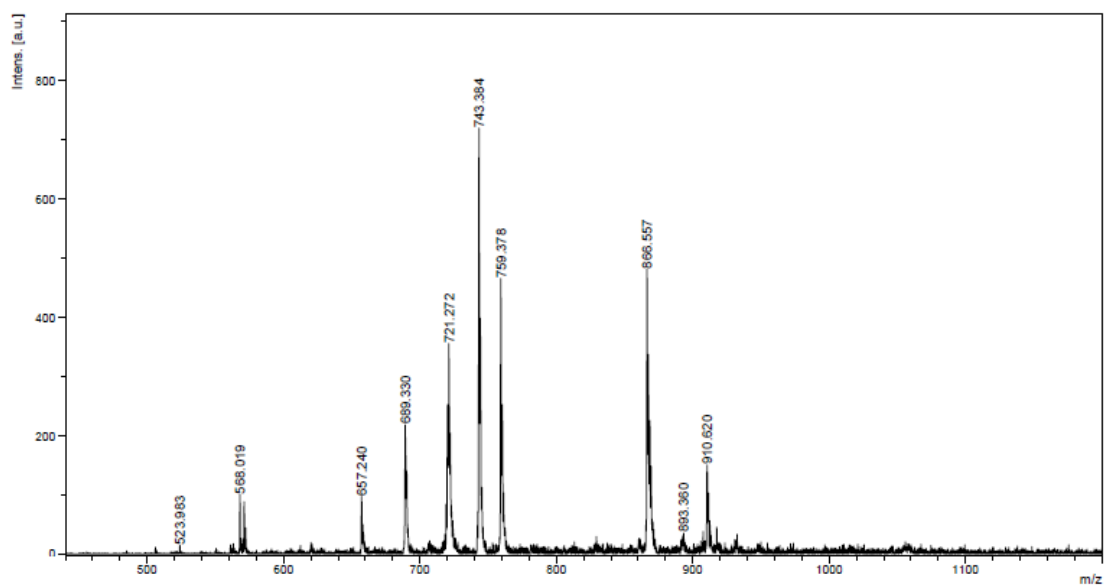
**Figure A-13.** <sup>1</sup>H NMR spectrum of compound **1B**.



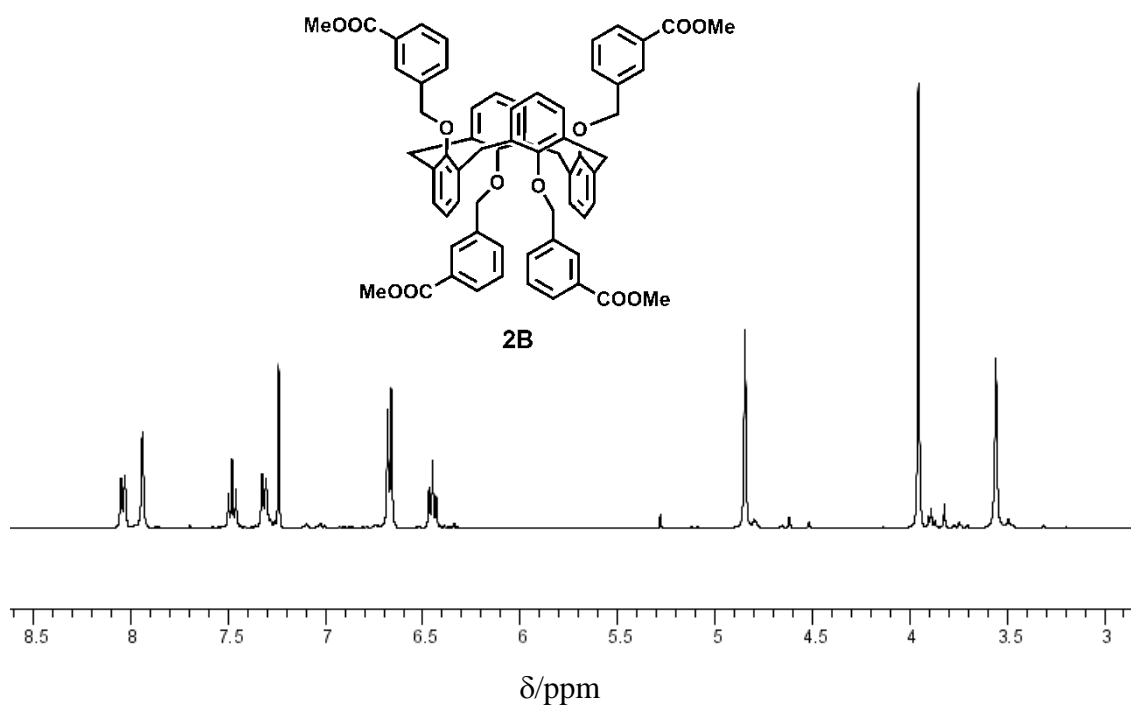
**Figure A-14.** <sup>13</sup>C NMR spectrum of compound **1B**.



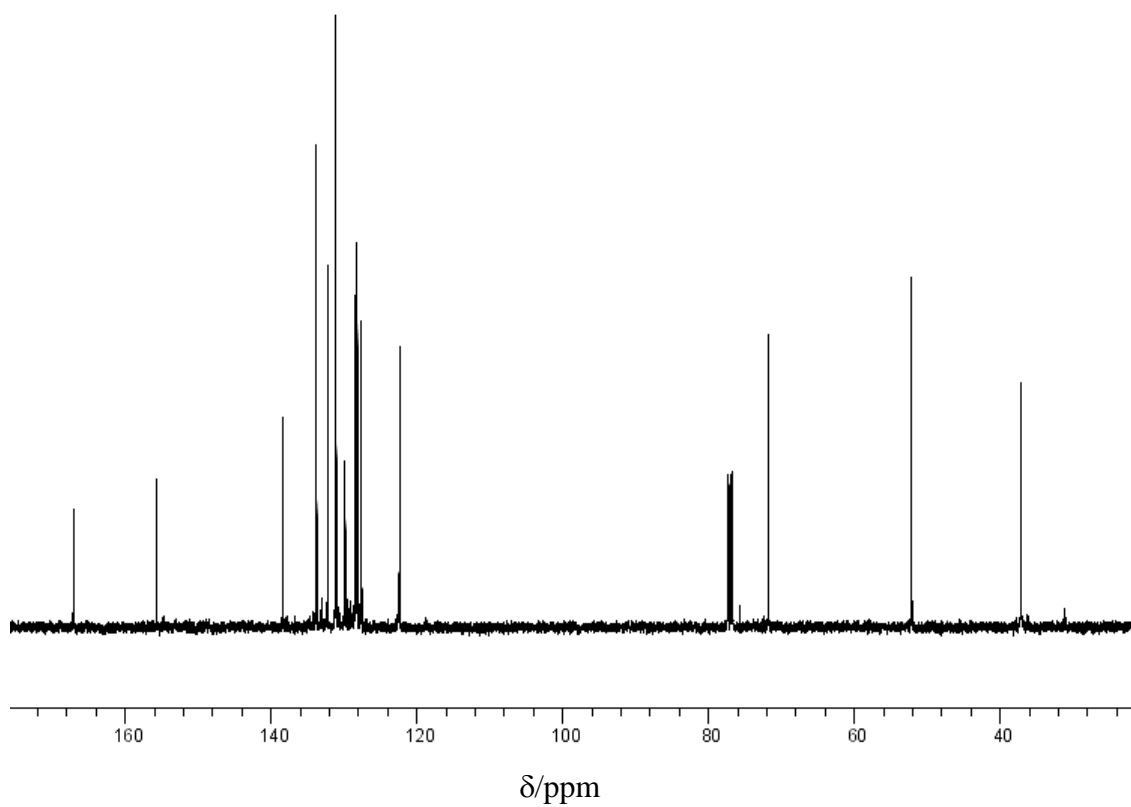
**Figure A-15.** IR spectrum of compound **1B**.



**Figure A-16.** MALDI-TOF mass spectrum (CCA) of compound **1B**.

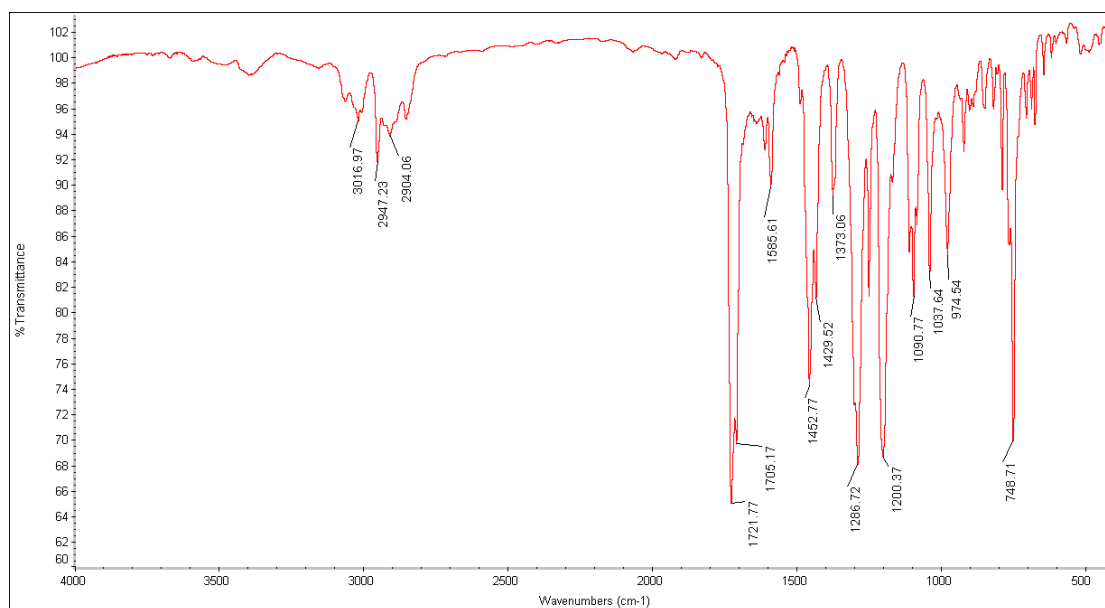


**Figure A-17.**  $^1\text{H}$  NMR spectrum of compound **2B**.

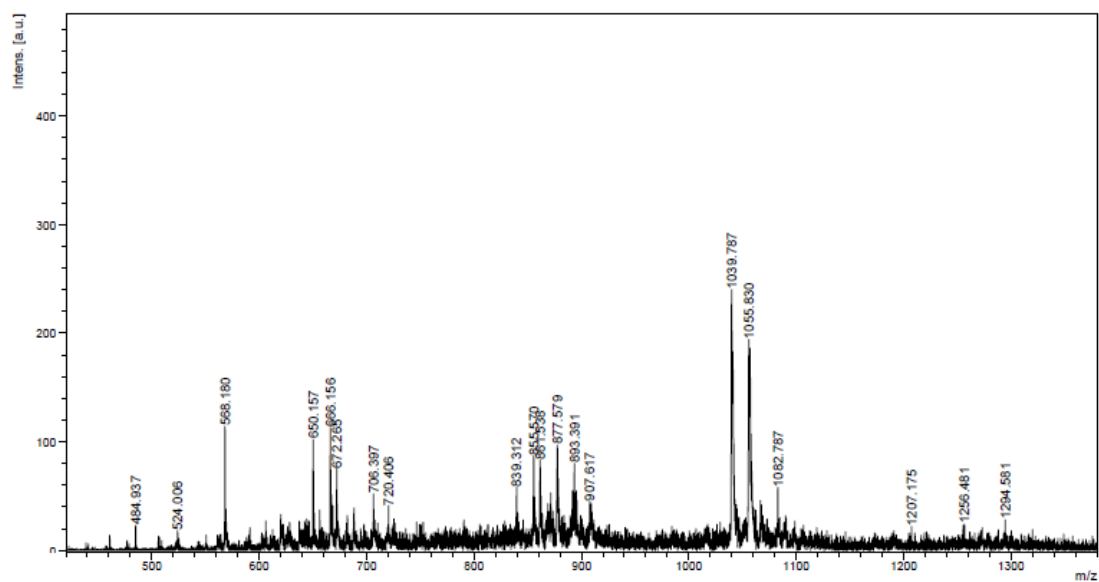


**Figure A-18.**  $^{13}\text{C}$  NMR spectrum of compound **2B**.

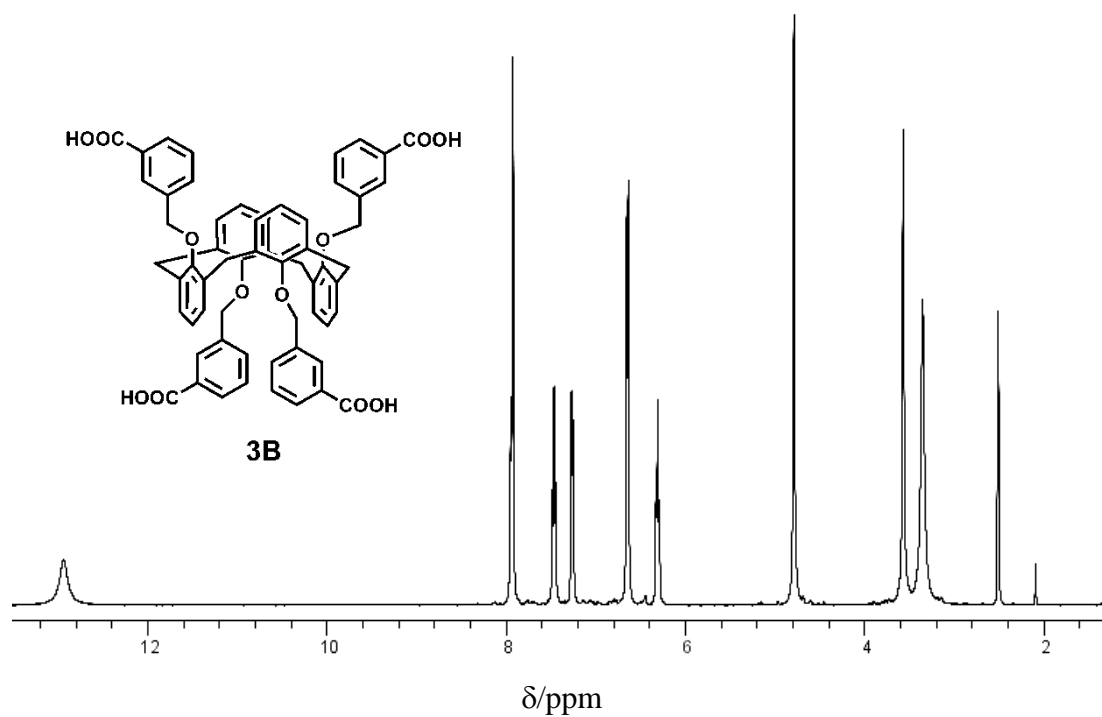




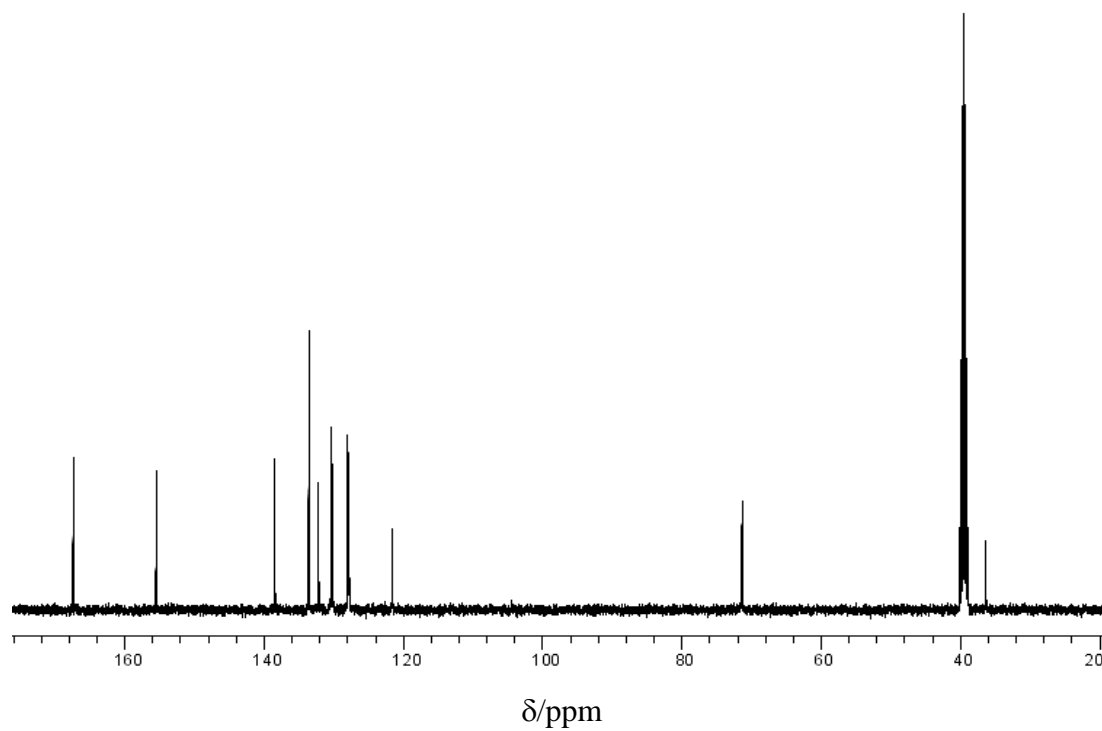
**Figure A-19.** IR spectrum of compound **2B**.



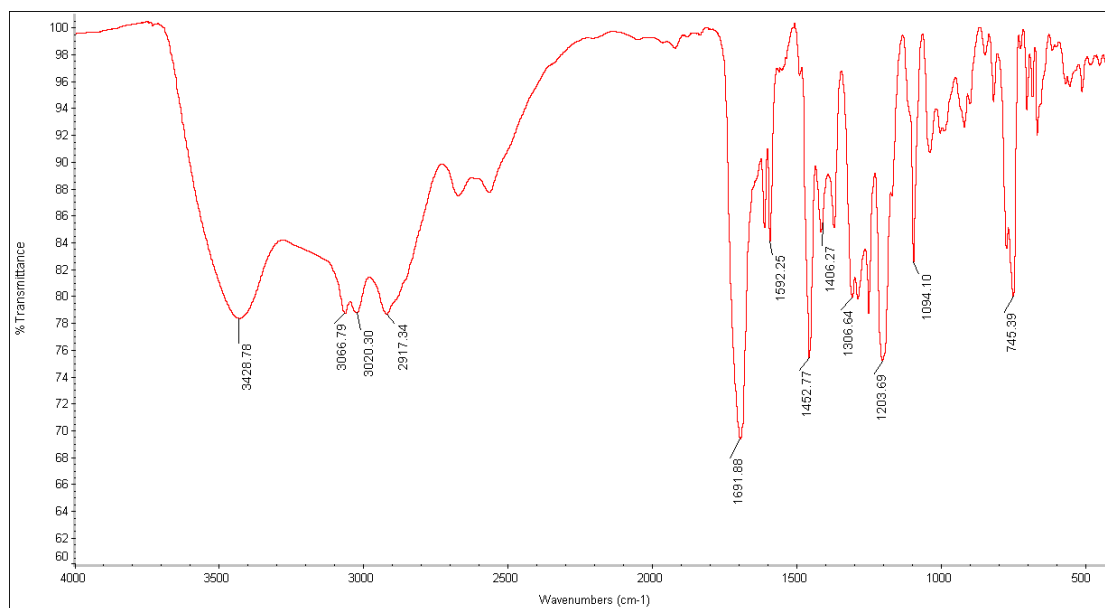
**Figure A-20** MALDI-TOF mass spectrum (CCA) of **2B**



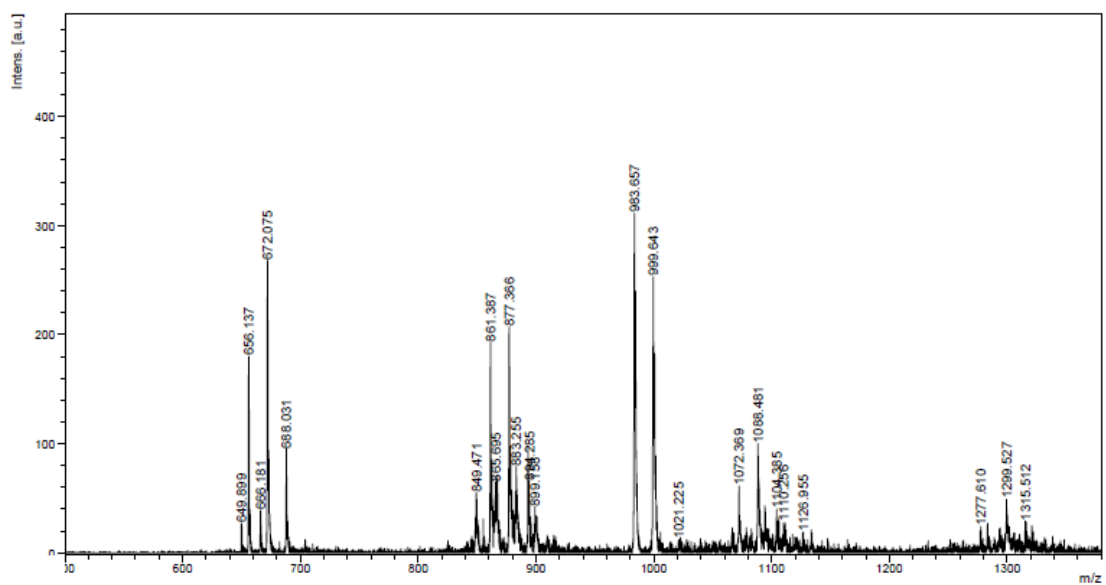
**Figure A-21.** <sup>1</sup>H NMR spectrum of compound **3B**



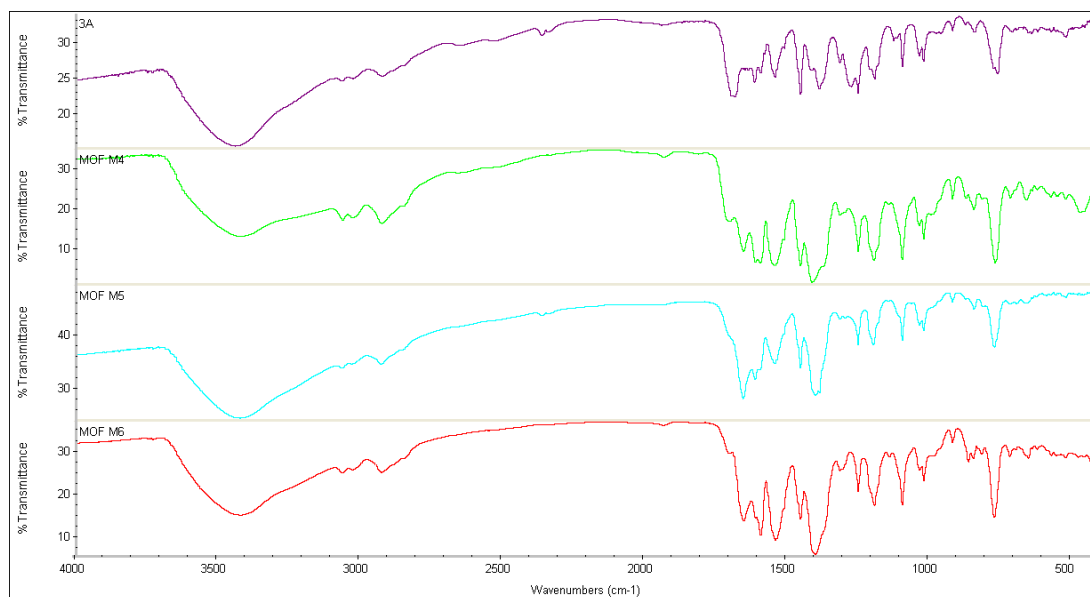
**Figure A-22.** <sup>13</sup>C NMR spectrum of compound **3B**.



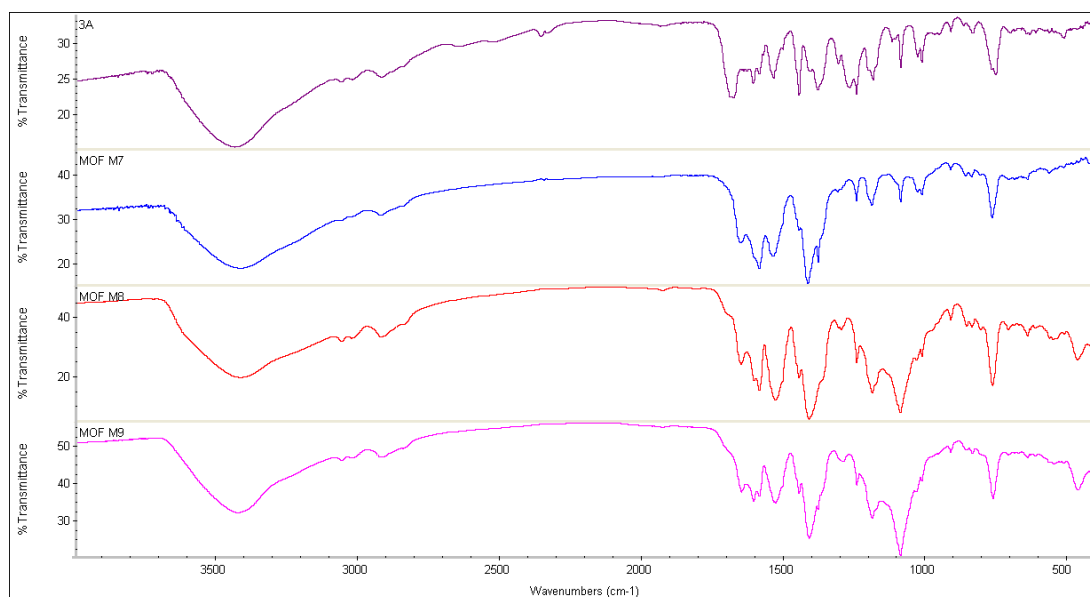
**Figure A-23.** IR spectrum of compound **3B**.



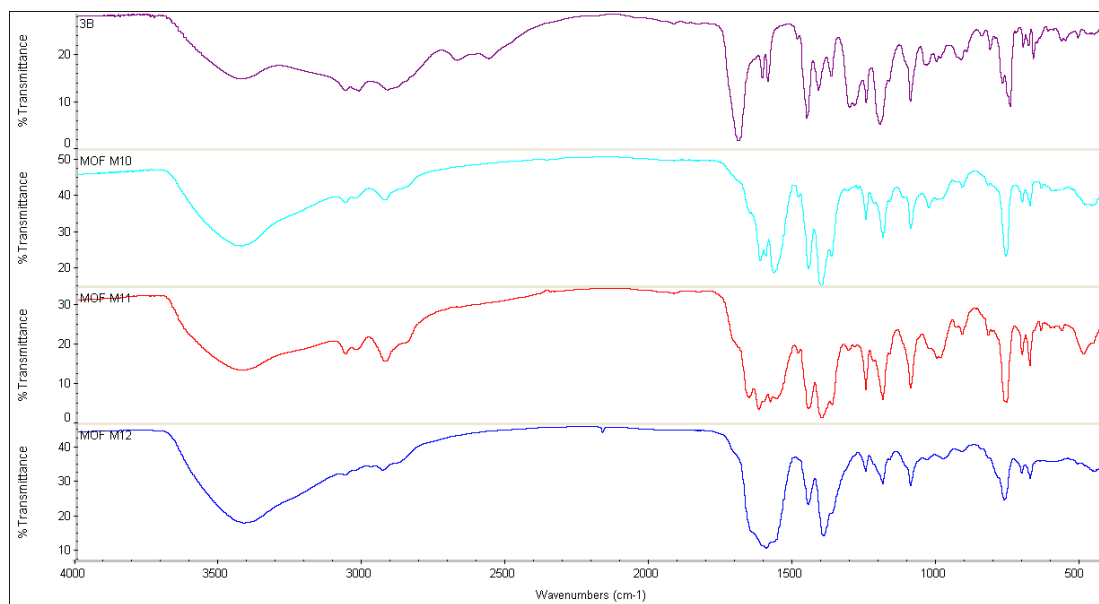
**Figure A-24** MALDI-TOF mass spectrum (CCA) of compound **3B**.



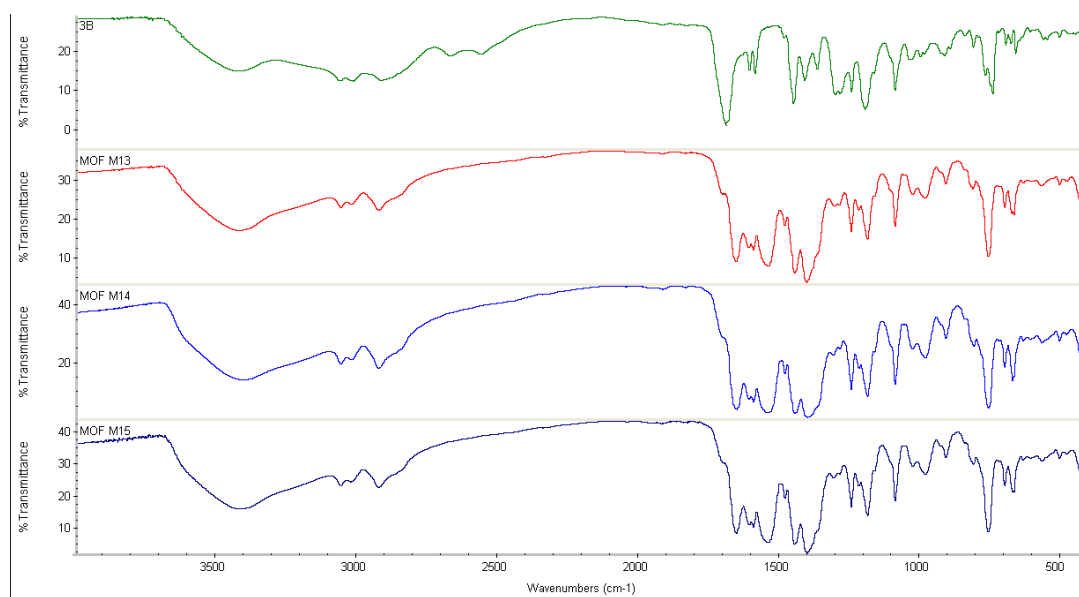
**Figure A-25** Compared IR spectra of **3A**, MOFs **M4** (**3A** + Cu(OAc)), **M5** (**3A** + Ni(NO<sub>3</sub>)<sub>2</sub>) and **M6** (**3A** + Cd(NO<sub>3</sub>)<sub>2</sub>).



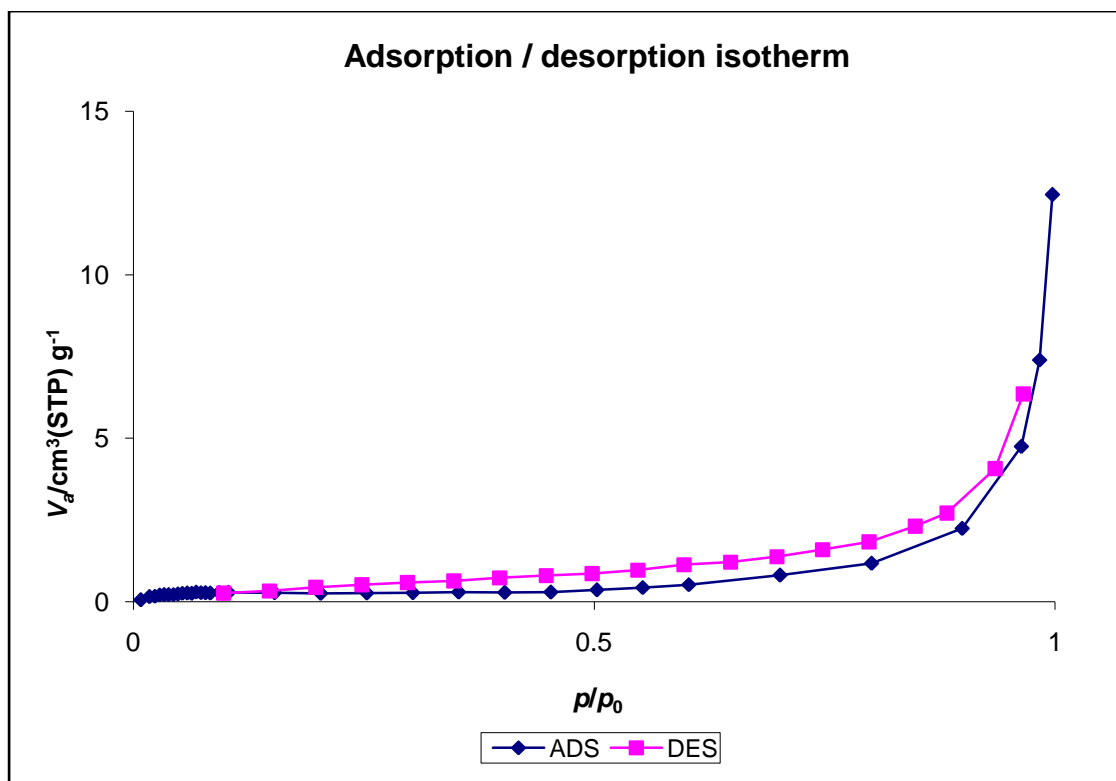
**Figure A-26** Compared IR spectra of **3A**, MOFs **M7** (**3A** + Er(NO<sub>3</sub>)<sub>3</sub>), **M8** (**3A** + EuCl<sub>3</sub>) and **M9** (**3A** + Tb(NO<sub>3</sub>)<sub>3</sub>).



**Figure A-27** Compared IR spectra of **3B**, **M10** (**3B** + Zn(NO<sub>3</sub>)<sub>2</sub>), **M11** (**3B** + Cu(NO<sub>3</sub>)<sub>2</sub>) and **M12** (**3B** + Ni(NO<sub>3</sub>)<sub>2</sub>).



**Figure A-28.** Compared IR spectra of **3B**, MOFs **M13** (**3B** + Er(NO<sub>3</sub>)<sub>3</sub>), **M14** (**3B** + EuCl<sub>3</sub>) and **M15** (**3B** + Tb(NO<sub>3</sub>)<sub>3</sub>).



**Figure A-29.** The nitrogen adsorption-desorption isotherms of bulk MOFs (CU-SCRU3 and CU-SCRU4)

## **APPENDIX B**

**Table B-1.** Crystal data and structure refinement for **2B** compound.

<b>1,3-alternate calix[4]arene tetramethyl-m-benzoate (2B)</b>	
Empirical formula	C <sub>60</sub> H <sub>56</sub> O <sub>12</sub>
Formula weight	969.05
Temperature (K)	296(2)
Wavelength	0.71073 Å
Crystal system, space group	Orthorhombic, Fdd2
Unit cell dimensions	a = 17.9592(6) Å    alpha = 90 deg. b = 43.8686(18) Å    beta = 90 deg. c = 13.1854(5) Å    gamma = 90 deg.
Volume	10388.0(7) Å <sup>3</sup>
Z, Calculated density	8, 1.239 Mg/m <sup>3</sup>
Absorption coefficient	0.086 mm <sup>-1</sup>
F(000)	4096
Crystal size	0.50 x 0.34 x 0.10 mm
Theta range for data collection	1.97 to 25.05 deg.
Limiting indices	-14 ≤ h ≤ 21, -52 ≤ k ≤ 52, -15 ≤ l ≤ 15
Reflections collected / unique	18837 / 4563 [R(int) = 0.0297]
Completeness to theta = 25.05	100.0 %
Max. and min. transmission	0.9915 and 0.9583
Refinement method	Full-matrix least-squares on F <sup>2</sup>
Data / restraints / parameters	4563 / 1 / 336
Goodness-of-fit on F <sup>2</sup>	1.357
Final R indices [I > 2σ(I)]	R1 = 0.1058, wR2 = 0.3000
R indices (all data)	R1 = 0.1253, wR2 = 0.3255
Largest diff. peak and hole	2.631 and -0.422 e.Å <sup>-3</sup>



**Table B-2.** Crystal data and structure refinement for compound **3A**.

<b>1,3-alternate calix[4]arene tetra-<i>p</i>-benzoic acid : 3A</b>	
Empirical formula	C <sub>69</sub> H <sub>69</sub> N <sub>3</sub> O <sub>15</sub>
Formula weight	1180.27
Temperature (K)	296(2)
Wavelength	0.71073 Å
Crystal system, space group	Triclinic, <i>P</i>
Unit cell dimensions	a = 11.1266(8) Å    alpha = 87.095(4) deg. b = 15.1735(10) Å    beta = 78.335(4) deg. c = 18.9294(11) Å    gamma = 83.297(4) deg.
Volume	3107.2(4) Å <sup>3</sup>
Z, Calculated density	2, 1.261 Mg/m <sup>3</sup>
Absorption coefficient	0.089 mm <sup>-1</sup>
F(000)	1248
Crystal size	0.52 x 0.20 x 0.18 mm
Theta range for data collection	1.10 to 25.06 deg.
Limiting indices	-12 ≤ h ≤ 13, -17 ≤ k ≤ 18, -22 ≤ l ≤ 17
Reflections collected / unique	20336 / 10870 [R(int) = 0.0290]
Completeness to theta = 25.06	98.6 %
Absorption correction	None
Max. and min. transmission	0.9842 and 0.9552
Refinement method	Full-matrix least-squares on F <sup>2</sup>
Data / restraints / parameters	10870 / 0 / 806
Goodness-of-fit on F <sup>2</sup>	0.947
Final R indices [I > 2σ(I)]	R1 = 0.0531, wR2 = 0.1375
R indices (all data)	R1 = 0.1245, wR2 = 0.1907
Largest diff. peak and hole	0.349 and -0.224 e.Å <sup>-3</sup>

**Table B-3.** Selected Bond Lengths (Å) and Bond Angles (deg) for **CU-SCRU1** and **CU-SCRU2** (1)

CU-SCRU1 <sup>a</sup>		CU-SCRU2 <sup>b</sup>	
O(10)-Zn(1)	2.128(7)	Zn(1)-Zn(2)	2.936(2)
O(11)-Zn(1)	2.047(8)	O(6)-Zn(1)	1.970(10)
O(13)-Zn(1)	2.068(9)	Zn(1)-O(9)#2	1.938(9)
O(6)-Zn(2)	2.134(6)	Zn(1)-O(11)#2	1.992(9)
O(7)-Zn(2)	2.062(7)	O(13)-Zn(1)	1.957(10)
O(14)-Zn(2)	2.040(9)	O(5)-Zn(2)	2.007(9)
O(11)#1-Zn(1)-O(11)	180.0(7)	O(7)-Zn(2)	1.907(8)
O(11)#1-Zn(1)-O(13)#1	92.9(4)	Zn(2)-O(12)#2	1.999(10)
O(11)-Zn(1)-O(13)#1	87.1(4)	O(13)-Zn(2)	1.927(10)
O(13)#1-Zn(1)-O(13)	180.0(4)	Zn(2)-O(13)-Zn(1)	98.2(5)
O(11)#1-Zn(1)-O(10)	95.6(3)	O(9)#2-Zn(1)-O(13)	123.2(4)
O(11)-Zn(1)-O(10)	84.4(3)	O(9)#2-Zn(1)-O(6)	111.8(4)
O(13)#1-Zn(1)-O(10)	91.5(3)	O(13)-Zn(1)-O(6)	110.8(4)
O(13)-Zn(1)-O(10)	88.5(3)	O(9)#2-Zn(1)-O(11)#2	107.8(4)
O(10)-Zn(1)-O(10)#1	180.0(2)	O(13)-Zn(1)-O(11)#2	100.8(4)
O(14)#2-Zn(2)-O(14)	180.000(3)	O(6)-Zn(1)-O(11)#2	98.9(4)
O(14)-Zn(2)-O(7)#2	90.5(4)	O(7)-Zn(2)-O(13)	123.8(4)
O(14)-Zn(2)-O(7)	89.5(4)	O(7)-Zn(2)-O(12)#2	115.4(4)
O(7)#2-Zn(2)-O(7)	180.000(1)	O(13)-Zn(2)-O(12)#2	105.8(4)
O(14)#2-Zn(2)-O(6)#2	89.9(4)	O(7)-Zn(2)-O(5)	103.9(4)
O(14)-Zn(2)-O(6)#2	90.1(4)	O(13)-Zn(2)-O(5)	106.6(4)
O(7)-Zn(2)-O(6)#2	94.6(3)	O(12)#2-Zn(2)-O(5)	97.9(4)
O(14)-Zn(2)-O(6)	89.9(4)	<sup>b</sup> Symmetry transformations used to generate equivalent atoms: #1 -x+1,-y,-z #2 -x,-y+2,-z+1.	
O(7)-Zn(2)-O(6)	85.4(3)		
O(6)#2-Zn(2)-O(6)	180.000(2)		
<sup>a</sup> Symmetry transformations used to generate equivalent atoms: #1 -x+1,-y,-z #2 -x, y+2,z+1			

**Table B-4.** Selected Bond Lengths (Å) and Bond Angles (deg) for **CU-SCRU3**

Bond Lengths (Å)	O(4)-Cd(1)	2.20(2)	Cd(2)-O(3)#3	2.29(2)
	O(6)-Cd(1)	2.290(15)	Cd(2)-O(3)#4	2.29(2)
	O(7)-Cd(1)	2.09(4)	Cd(2)-O(5)#5	2.505(16)
	Cd(1)-O(7)#3	2.09(4)	O(5)-Cd(2)	2.505(16)
	Cd(1)-O(4)#3	2.20(2)	O(6)-Cd(2)	2.299(12)
	Cd(1)-O(6)#3	2.290(15)	Cd(2)-O(6)#5	2.299(12)
Bond Angles (deg)	Cd(1)-O(6)-Cd(2)	112.2(7)	O(3)#3-Cd(2)-O(3)#4	118.1(19)
	O(7)#3-Cd(1)-O(7)	85(3)	O(3)#3-Cd(2)-O(6)	93.8(7)
	O(7)-Cd(1)-O(4)#3	86.3(16)	O(3)#4-Cd(2)-O(6)	129.6(9)
	O(7)-Cd(1)-O(4)	88.3(13)	O(6)-Cd(2)-O(6)#5	93.8(6)
	O(4)#3-Cd(1)-O(4)	173(2)	O(3)#3-Cd(2)-O(5)	89.5(6)
	O(7)#3-Cd(1)-O(6)	96.5(14)	O(3)#4-Cd(2)-O(5)	85.4(6)
	O(7)-Cd(1)-O(6)	170.4(11)	O(6)-Cd(2)-O(5)	55.0(5)
	O(4)#3-Cd(1)-O(6)	84.2(12)	O(6)#5-Cd(2)-O(5)	133.7(5)
	O(4)-Cd(1)-O(6)	101.2(7)	O(5)-Cd(2)-O(5)#5	170.1(5)
	O(6)-Cd(1)-O(6)#3	84.1(6)		

Symmetry transformations used to generate equivalent atoms:

#1  $-x+7/4, -y+3/4, z$  #2  $-x+2, -y+1, -z$  #3  $x, -y+5/4, -z+1/4$  #4  $-x+5/4, y, -z+1/4$

#5  $-x+5/4, -y+5/4, z$

**Table B-5.** Selected Bond Lengths (Å) and Bond Angles (deg) for **CU-SCRU4**

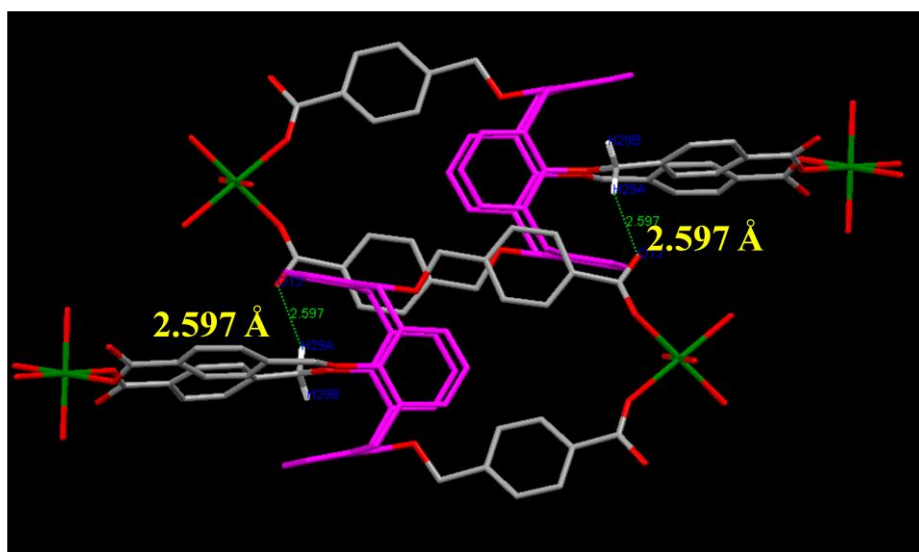
Bond Lengths (Å)	Cd1-O(5)	2.489(14)	Cd2-O(9)#6	2.244(15)
	Cd1-O(6)	2.307(10)	Cd2-O(8)#9	2.263(13)
	Cd1-O(14)#6	2.128(17)	Cd2-O(11)#5	2.276(16)
	Cd1-O(10)#7	2.136(17)	Cd2-O(6)	2.300(14)
	Cd1-O(8)#8	2.291(11)	Cd2-O(12)	2.48(2)
	Cd1-O(7)#8	2.521(14)	Cd2-O(13)	2.44(3)
Bond Angles (deg)	O(5)-Cd1-O(7)#8	172.3(4)	O(9)#6-Cd2-O(11)#5	177.2(8)
	O(6)-Cd1-O(5)	53.0(4)	O(8)#9-Cd2-O(6)	83.8(4)
	O(8)#8-Cd1-O(6)	93.7(4)	O(8)#9-Cd2-O(13)	171.4(6)
	O(8)#8-Cd1-O(7)#8	55.0(4)	O(11)#5-Cd2-O(13)	92.5(8)
	O(10)#7-Cd1-O(5)	88.9(6)	O(6)-Cd2-O(13)	90.3(7)
	O(10)#7-Cd1-O(6)	133.9(8)	O(9)#6-Cd2-O(12)	93.5(8)
	O(10)#7-Cd1-O(7)#8	86.8(6)	O(8)#9-Cd2-O(12)	89.6(6)
	O(14)#6-Cd1-O(5)	88.4(7)	O(6)-Cd2-O(12)	171.5(5)
	O(14)#6-Cd1-O(8)#8	133.4(9)	O(13)-Cd2-O(12)	96.8(9)
	O(14)#6-Cd1-O(10)#7	108.8(11)		

Symmetry transformations used to generate equivalent atoms:

#1  $x+1/2, y+1/2, z$  #2  $-x+1/2, y+1/2, -z+1/2$  #3  $x, -y+2, z+1/2$  #4  $x+1, -y+2, z+1/2$

#5  $-x+1, -y+2, -z+1$  #6  $x, -y+2, z-1/2$  #7  $x-1, -y+2, z-1/2$  #8  $x-1/2, y-1/2, z$

#9  $-x+1/2, y-1/2, -z+1/2$



**Figure B-1.** Non-classical H-bonding between 1D-polymeric chain of **CU-SCRU1**

## VITA

Mr. Suppachai Krajangsri was born on January 22, 1988 in Phang-nga, Thailand. He graduated with a high school diploma from Deebukphang-ngawittayayon School. He got a Bachelor Degree of Chemistry from Faculty of Science at Burapha University, Chonburi in 2010. After that, he has been a graduate student at the Department of Chemistry, Faculty of Science, Chulalongkorn University, Bangkok in 2010 and completed the program in 2012. During the study in Master program, he got scholarships: Teaching Assistant Scholarship from Chulalongkorn University during 2010 to 2012.